MARCH 2018

M.Sc. in Civil Engineering

KAYWAN OTHMAN AHMED

UNIVERSITY OF GAZİANTEP

GRADUATE SCHOOL OF

NATURAL & APPLIED SCIENCES

SIMULATION OF BLOCKAGE EFFECTS ON SCOURING DOWNSTREAM OF BOX CULVERTS UNDER UNSTEADY FLOW CONDITIONS

M. SC. THESIS

IN

CIVIL ENGINEERING

BY

KAYWAN OTHMAN AHMED

MARCH 2018

Simulation of Blockage Effects on Scouring Downstream of Box Culverts Under Unsteady Flow Conditions

M.Sc. Thesis

in

Civil Engineering

University of Gaziantep

Supervisor

Prof. Dr. Mustafa GÜNAL

by

Kaywan Othman AHMED

March 2018

THE REPUBLIC OF TURKEY
UNIVERSITY OF GAZİANTEP
GRADUATE SCHOOL OF NATURAL & APPLIED SCIENCES
CIVIL ENGINEERING DEPARTMENT

Name of the thesis: Simulation of Blockage Effects on Scouring Downstream of Box Culverts Under Unsteady Flow Conditions.

Name of the student: Kaywan Othman AHMED

Exam date: 07.03.2018

Approval of the graduate school of natural and applied science.

Prof. Dr. Ahmet Necmeddin YAZICI
Director

I certify that this thesis satisfies all the requirements as a thesis for the degree of Master of Science.

Prof. Dr. Hanifi CANAKCI
Head of Department

This is to certify that we have read this thesis and that in our consensus opinion it is fully adequate, in scope and quality, as a thesis for the degree of Master of Science.

Prof. Dr. Mustafa GÜNAL
Supervisor

Examining Committee Members:	Signature
Prof. Dr. Mehmet KARPUZCU	.....
Asst. Prof. Dr. MAZEN KAVVAS	.....
Prof. Dr. Mustafa GÜNAL	.....

I hereby declare that all information in this document has obtained and presented in accordance with academic rules and ethical conduct. I also declare that, as required by these rules and conduct, I have fully cited and referenced all material and results that are not original to this work.

Kaywan Othman AHMED

ABSTRACT

SIMULATION OF BLOCKAGE EFFECTS ON SCOURING DOWNSTREAM OF BOX CULVERTS UNDER UNSTEADY FLOW CONDITIONS

AHMED, Kaywan Othman

M.Sc. in Civil Engineering

Supervisor: Prof.Dr. Mustafa GÜNAL

March 2018

108 Pages

Scouring at the downstream of culvert considered as one of the main reasons of culvert failure. Failure of the culvert structure is a catastrophic phenomenon. Studying the causes of scouring will give an idea about the solution probabilities; the blockage and geometry of culvert have a great influence on the local scour. In this study, simulated results that obtained from Flow-3D software of box culvert model and formation of scour at the outlet are compared with laboratory results of (Sorourian, 2015) to evaluate the accuracy of the numerical model. Laboratory box culvert was carried out for two conditions; the non-blocked situation and the partially blocked condition with the blockage ratio of 40%, for this destination used two different sizes of plates and the finer sediment was used in Sayana's study with the median grain size being 0.85 mm and 2.0 mm, the flow conditions in the laboratory were unsteady. It is mean that the flow rates during the time were changed. The performance of the numerical model based on renormalization group (RNG) and k-ε model compared with experimental results. The comparison shows that the RNG results has a good agreement than the k-ε model

Keywords: Box-culvert, Scouring, Unsteady flow, culvert, scour depth

ÖZET

MENFEZ GİRİŞLERİNİN BLOKE OLMASININ MENFEZ ÇIKIŞINDA OLUŞAN YEREL OYULMA ÜZERİNE ETKİLERİNİN DÜZENSİZ AKIM KOŞULLARINDA SİMÜLASYONU

AHMED, Kaywan Othman
Yüksek Lisans Tezi, İnşaat Mühendisliği Bölümü
Tez Yöneticisi: Prof.Dr. Mustafa GÜNAL
Mart 2018
108 Sayfa

Menfez mansabında oluşan oyulma menfez yıkılmalarının ana sebebi olarak görülmektedir. Menfez yapısının bozulması felaket bir fenomendir. Oyulma nedenlerini incelemek, çözüm olasılıkları hakkında bir fikir verecektir; menfezin blokajı ve geometrisi, yerel oyulma üzerinde büyük bir etkiye sahiptir. Bu çalışmada, kutu menfez modelinin Flow-3D yazılımından elde edilen sonuçlar ve menfez çıkışındaki oyulma oluşumu (Sorourian, 2015) tarafından yapılan deneysel çalışmanın sonuçları ile karşılaştırılarak sayısal modelin doğruluğu değerlendirilmiştir. Box culvert modeli iki koşul için gerçekleştirildi; blokaj oranı % 40 olan engellenmiş durum ve kısmen tıkanmış durum, bu hedef için iki farklı ebatta plak kullanılmış ve Sayana'nın çalışmasında ortalama çökelme boyutu 0,85 mm ve 2,0 mm olan kararsız akım koşullarında deneyler yapılmıştır. Yani akım değerleri zamana göre değişmiştir. Renormalizasyon grubuna (RNG) ve k-ε sayısal model performansı deney sonuçları ile karşılaştırılmıştır. Karşılaştırma RNG modelinin k- ε sayısal modeline göre daha iyi sonuçlar vermiştir

Anahtar Kelimeler: Kutu menfez, oyulma, düzensiz akım, menfez, oyulma derinliğ

To

My parents

My beloved wife

My child

Ahmed

ACKNOWLEDGEMENT

I would like to express my special appreciation and thanks to my supervisor Prof. Dr. Mustafa GÜNAL, for all her help, patience, valuable advice, always providing and guiding me in the right direction. I'm very grateful and proudest to work under her academic guidance.

Special thanks to my family. Words cannot express how grateful I am to my father spirit that his words lead me to get certificates and my mother for all of the sacrifices that have made on my behalf. Also to all my sisters. I am greatly indebted to my wife, for their strong encouragement during the years of my study

TABLE OF CONTENTS

Page

ABSTRACT ..... **vi**

ÖZET ..... **viii**

ACKNOWLEDGEMENT ..... **viii**

TABLE OF CONTENTS ..... **ix**

LIST OF TABLES ..... **xiii**

LIST OF FIGURES ..... **xiv**

LIST OF SYMBOLS/ABBREVIATIONS ..... **xvii**

CHAPTER 1 ..... **1**

1 INTRODUCTION **1**

1.1 General Introduction 1

1.2 Study Objective 4

1.3 Outline of thesis 4

CHAPTER 2 ..... **6**

2 LITERATURE REVIEW **6**

2.1 Introduction 6

2.2 What is a culvert? 7

2.3 Culvert hydraulic 8

2.4 Scouring 10

2.4.1 Scour type 10

2.4.2 Condition of sediment transport 11

2.5 Scour mechanism 11

2.6 Influencing factors on scour downstream of culverts 12

2.6.1 Flow condition 12

2.6.2 Sediment characteristics 13

2.6.3 Culvert shape 13

2.6.4 Culvert slope 14

2.6.5 Channel Width 15

2.6.6 Scaling of the culvert 15

2.7 Physical Studies 16

2.8 Numerical Studies 17

2.8.1 Numerical model 18

2.8.2 Numerical method 27

2.9 CFD Modeling 29

CHAPTER 3 34

3 CASE-STUDY 34

3.1 Introduction 34

3.2 Experimental test set-up 34

3.2.1 Flume and its components 34

3.2.2 Culvert model 37

3.2.3 Material properties 38

3.3 Computational Fluid Dynamic (CFD) 39

3.3.1 Flow-3D process 40

3.4 Numerical modeling in Flow-3D 42

3.4.1 Physical options in Flow-3D 43

3.4.2 Geometry 44

3.5 Meshing 45

3.5.1 Boundary Conditions 47

CHAPTER 4 49

4 RESULTS AND DISCUSSION 49

4.1 General introduction 49

4.2 Comparison between numerical and experimental results for first set (d_{50}=0.85 mm) 49

4.2.1 Centerline profiles along horizontal axis 51

4.2.2 Maximum scour depth 54

4.2.3 Location of maximum scour depth 56

4.3 Comparison between numerical and experimental results for Second set (d_{50}=2.0 mm) 57

4.3.1 Centerline profiles along horizontal axis by using empirical equation (RNG) 58

4.3.2 Centerline profiles along horizontal axis by using empirical equation (k-ε) 62

4.3.3 Maximum scour depth 65

4.3.4 Location of maximum scour depth 66

4.4 Water surface profile for both sets 68

4.5 Vortex 70

4.5.1 Effect of vortex on scouring 70

4.6 Scour formation using CFD model 73

CHAPTER 5 75

5 CONCLUSIONS AND RECOMMENDATIONS 75

5.1 Conclusions 75

5.2 Recommendations 77

REFERENCES 79

APPENDICES 89

LIST OF TABLES

Page

Table 2.1 Degree of blockage in culvert (Rigby et al. 2002) 8

Table 2.2 Summary of coefficients proposed by Abt et al. (1985) 14

Table 2.3 Scaled parameters for prototype and culvert 15

Table 2.4 Bed-load transport formulas 26

Table 4.1 Comparison results between numerical and physical model..... 50

Table 4.2 Comparison results between numerical and physical model..... 58

LIST OF FIGURES

Page

Figure 2.1 Various shape of culvert (HEC-RAS culvert shapes and dimensions, 2015)..... 7

Figure 2.2 Blockage of culvert (Rural Ramblings, 2009) 8

Figure 2.3 (a) Type on inlet control (Norman et al. 2001). (b) Type of outlet control (Norman et al. 2001) 9

Figure 2.4 The relationship between maximum scouring depth and flow characteristic, culvert characteristics and bed material properties (Opie, 1967) 13

Figure 2.5 Angle of bed-load transport: β is angle between the normal to bed surface and the gravitational vector, and Ψ is angle between the flow and the upslope direction (Lane, 1953)..... 25

Figure 3.1 Test set up (a) plan (b) section view 35

Figure 3.2 Stepwise hydrograph for tests both in partially blocked and non-blocked conditions; First set: hydrograph for material with d_{50}=0.85 mm, Second set: hydrograph for material with d_{50}=2.0 mm.... 36

Figure 3.3 Electromagnetic Flow meter (Simence, 2015)..... 36

Figure 3.4 Parameters corresponding to the partially blocked culvert and the scour hole. 37

Figure 3.5 Culvert model (a) plan (b) section (c) inlet view 38

Figure 3.6 Sieve analysis of sediment 39

Figure 3.7 In Flow-3D, there are five empirical equations for turbulent model 41

Figure 3.8 Physical options in Flow-3D..... 43

Figure 3.9 Sediment scour option..... 44

Figure 3.10 Culvert geometry in Flow-3D..... 45

Figure 3.11 Representation of the geometry meshing of 3D model 46

Figure 3.12 Type of boundary conditions in Flow-3D..... 47

Figure 3.13 Configuration of boundary conditions 48

Figure 3.14 Stepwise hydrograph for tests in Flow-3D 48

Figure 4.1 Stepwise hydrograph for tests both in partially blocked and non-blocked conditions; First set: hydrograph for material with d_{50}=0.85 mm, Second set: hydrograph for material with d_{50}=2.0 mm..... 51

Figure 4.2 Comparison between CFD model and physical model for scour profile with the first set of fine sediment: (a) Flow rate is 3 Lt/s at 10 minutes (b) Flow rate is 6 Lt/s at 20 minutes (c) Flow rate is 8 Lt/s at 30 minutes (d) Flow rate is 10.4 Lt/s at 40 minutes (e) Flow rate is 7.8 Lt/s at 50 minutes (f) Flow rate is 5.9 Lt/s at 60 minutes (g) Flow rate is 3.1 Lt/s at 70 minutes 54

Figure 4.3 Comparison between CFD model and physical model for evolution of normalized maximum scour depth with time for the first set. 55

Figure 4.4 Comparison between CFD model and physical model for normalized location of maximum scour depth with hydrograph for the first set 57

Figure 4.5 Comparison between CFD model and physical model for scour profile with the second set of fine sediment: (a) Flow rate is 6.6 Lt/s at 15 minutes (b) Flow rate is 8.8 Lt/s at 30 minutes (c) Flow rate is 10.7 Lt/s at 45 minutes (d) Flow rate is 12.8 Lt/s at 60 minutes

(e) Flow rate is 10.7 Lt/s at 75 minutes (f) Flow rate is 8.8 Lt/s at 90 minutes (g) Flow rate is 6.6 Lt/s at 105 minutes 61

Figure 4.6 Comparison between CFD model and physical model for scouring profile with the second set of fine sediment by using RNG and k-ε: (a) Flow rate is 6.6 Lt/s at 15 minutes (b) Flow rate is 8.8 Lt/s at 30 minutes (c) Flow rate is 10.7 Lt/s at 45 minutes (d) Flow rate is 12.8 Lt/s at 60 minutes (e) Flow rate is 10.7 Lt/s at 75 minutes (f) Flow rate is 8.8 Lt/s at 90 minutes (g) Flow rate is 6.6 Lt/s at 105 minutes 64

Figure 4.7 Comparison between CFD model by using (RNG, k-ε) and physical model for evolution of normalized maximum scour depth with time for the second set 66

Figure 4.8 Comparison between CFD model and physical model for normalized location of maximum scour depth with hydrograph for the second set 68

Figure 4.9 Water surface profile for both sediment types: (a) US1B0 (b) US1B40 (c)US2B0 (d) US2B40 70

Figure 4.10 Model set up, top view 71

Figure 4.11 section (A): (a) Case US1B0, flow rate is 10.4 Lt/s (b) Case US1B40, flow rate is 10.4 Lt/s (c) Case US2B0, flow rate is 12.8 Lt/s (d) Case US2B40, flow rate is 12.8 Lt/s (d) Case US2B40, flow rate is 12.8 Lt/s by using k-ε. 72

Figure 4.12 3D Plots of scour formation for both sets (a) case US1B0, flow rate is 10.4 Lit/s (b) case US1B40, flow rate is 10.4 Lit/s (c) case US2B0, flow rate is 12.8 Lit/s (d)case US2B40, flow rate is 12.8 Lit/s (d) case US2B40, flow rate is 12.8 Lit/s for k-ε. 74

LIST OF SYMBOLS/ABBREVIATIONS

B	blockage ratio
ds	scour depth
dsm	maximum scour depth
$d_{sm\,(t=i)}$	maximum scour depth at time i (i = 10,20,…70)
d_{50}	median grain size of bed material
g	gravity acceleration
H_W	headwater depth
hB	height of blockage plate
hd	depth of water at culvert outlet
hu	upstream depth of water
Lt	total scour length
Q	flow rate
t	time of experiment
X	horizontal axis (flow direction)
X_{sm}	location of maximum scour depth along horizontal axis
Xsm(t= i)	location of maximum scour ole in horizontal axis at time i of the test
ρ	water density
σ_g	sediment geometric standard deviation

ω	angle of repose notation of the local critical shear stress
CFD	Computational Fluid Dynamic
RANS	Reynolds averaged Navier-Stokes equations
RNG	Renormalized group
LES	Large-eddy simulation
VOF	volume of fluid
FAVORTM	Fractional Area/Volume Obstacle Representation Method
Vf	volume fraction
Af	area fraction
FVM	finite volume method
US1B0	unsteady flow for sand type one with 0% blockage ratio
US1B40	unsteady flow for sand type one with 40% blockage ratio
US2B0	unsteady flow for sand type two with 0% blockage ratio
US2B40	unsteady flow for sand type two with 40% blockage ratio
Stl	stereo lithography

CHAPTER 1

INTRODUCTION

1.1 General Introduction

The simple hydraulic structure used to determine flow control and flow rate in any free surface flow are called culvert. Generally, the culvert is used to transport tributary drainage via highway embankments and similar forms of drain crossing structures. Passing over many different culverts every day occurred but rarely noticed them especially when they work properly. However, everyone will notice them when they fail. Culverts are a short conduit that usually carries storm-water runoff under a railway, roadway or an embankment. In urban and countryside there are a large number of culverts and culvert size bridges. In the study of New South Wales state in 1997, six types of hydraulic structures had been investigated in about 16.7% of the area of New South Wales (Williams & Watford 1997) such as culverts, causeways, bridges, weirs and flood gates. For the above research purposes, more than 5,300 structures had been inspected; about 1900 and 3000 were bridges and culverts respectively. It means that small bridges and culverts were identified more than 92% of the six different types of structures. In addition, at the Transport Road and Maritime Services website (About Road Projects in Sydney Region' 2012) in the Sydney area, 792 bridges and bridge size projects were reported.

On the other hand, the culverts are a constricted part of the waterway, and during flood events, it is more likely to be fully or partially blocked by debris. As an example, in the city of Wollongong at August 1998, a severe storm was occurred caused by extensive flooding. Many real estates broke down due to the loss of human life and service was interrupted. Examining the waterway where the flood occurred at the following day, it showed that most of the waterways, bridges, and culvert were blocked by debris, causing damage due to the bridges and culverts blockage. Because of this clogging, the flood level increased upstream of roads and railways, and diverted the flow out of its normal stream into overland flow paths, increasing the degree of flood

damage (Rigby et al. 2002). On the functional side, the culverts and bridge blockage at the time of the flood are important issues for Road and Maritime services (RMS) and local councils. The risk of damaging private property and public assets is high (Weeks et al.2013).

Scour is the erosion of bank of channel bed due to the bed erosion or water flow at the downstream of hydraulic structures (Ebrhim and Heydarnejad, 2014). It has been examined that for severe scouring, one of the chief causes for the culvert failure is occurred during the time of great flood events, the formation of scour pit that undermines culvert and foundations appeared at the downstream channel bed. Because scouring is recognized as one of the main causes of collapse of the hydraulic structure, prediction of downstream scouring development has a great significant, not only to ensure safety but also to ensure effective long-term maintenance. Therefore, when designing such a structure scouring should be considered. Moody et al. (2005) studied the erosion occurs when flows exert shear stresses on solid boundaries over a certain threshold, which depends on temperature, soil type, etc. Study the erosion of the riverbed and think it is an important part of the design of transportation system. A rapid increase in shear stress can be caused by a change in flow mode geometric shape (Pitt et al. 2007) or (Wu and Rajratnam, 1996). Protection against scouring is expensive. Therefore, by preventing it when needed, it is necessary to predict the maximum scour depth to minimize the risk of culvert failure.

Scouring that occurs when the open channel flow is composed of different scoring types. The whole process obtained by the addition of the following types:

- General scouring
- Contraction scouring
- Localized scouring

In the design of culvert, it is an important consideration to evaluate the degree and extent of local scouring at the downstream of the structure. However, because of the complexity of the problem at high flow rates, it is difficult to perform field measurements in structures that tend to hide the potential significance of the problem, as holes of scouring can be refilled when the flood peaks are gone. A considerable laboratory survey was done on scouring in certain sorts of culvert structures, but there

is a considerable gap in the data, with an overall understanding. As a result, field data is inconsistent, making it difficult to ascertain the potential scour depth estimates obtained from small laboratory tests. Therefore, most of the design estimates of the scour pit depth and width are based on data obtained from on-site investigations and experiments using physical models (Chen 1970. Smith 1957; and Simons and Stevens 1971). For the observed laboratory tests, several experimental tests with two sediment types and different flow rates were performed on partially blocked and non-blocked culvert. Although the complex nature of scouring phenomena may be overly simplified in various laboratory tests, the best practice is an experimental study that can be used with numerical models, and after examining the model the actual case it can be simulated.

Many experimental studies focus on local scouring downstream of hydraulic structures such as grade-control structures, underflow sluice gates, and culvert structure. In addition, physical models are widely used to design large hydraulic structures before computer technology exists, such as dams and canal designs. In the era of technological development in computers, especially personal computers in homes and workplaces, for engineering design purposes the computational model is now becoming an economical and reliable tool. For predicting bed change various numerical models are used. By comparing numerical models and experimental results, it is necessary to confirm the accuracy of hydrodynamic simulation of numerical models.

In this study, used Flow-3D software and mainly focus on understanding the local scour process by employing the computational fluid dynamics codes. Flow-3D is commercially available CFD software and can be used for various models and multi-purpose simulation. First, by comparing experimental results and numerical results reported in the literature, demonstrate the applicability of codes to predict the shape and depth of local scour pit (Dey and Raikar, 2007) and (Bormann et al.1991). The equation of the turbulence model begins with RNG (renormalized group) and k - ε model and solves two transportation of turbulent kinetic energy in addition to the dissipation factor of eddy viscosity calculation. These empirical formulas were used for complex flow fields in Calvert structure.

1.2 Study Objective

The object of this thesis is to perform a numerical simulation based on an experimental study by (Sayana, 2015) which initially held to investigate the effects of blockage on scouring pattern downstream the box culverts and finding the maximum scour depth, location maximum scour depth and vortex direction. In addition, compare the results with experimental studies to confirm the suitability of Flow-3D software to study wash-off phenomena. The study objective for research purposes is summarized as follows:

1. To determine the extent to which inlet blockage of box culverts aggravates scour at the exit of such culverts.

2. To study the geometry of the scour hole at the outlet of non-blocked culverts and compare it with partially blocked culverts.

3. Understand the scouring mechanism and flow structure in the culvert barrel and at the outlet.

4. To find different block ratio, that minimizes the scouring problem.

5. Also, comparing the results of the laboratory and Flow-3D and confirm the accuracy of the numerical simulation.

1.3 Outline of thesis

This thesis consists of five chapters. A brief outline of each chapter is as follows:

Chapter 1 Introduction:

Presenting a brief history of scouring phenomenon in a culvert, the study object, and outline of the thesis.

Chapter 2 Literature Review:

In this chapter, we will discuss the previous approach, culvert shapes, scour types, mechanism of scour at culvert outlet, sediment transport, empirical equations in the numerical model, numerical methods, a previous study of both physical and numerical methods for scouring at culvert outlet.

Chapter 3 Case study:

This chapter describes the experimental and CFD modeling techniques and procedures for specifying mesh set up, boundary conditions and physical parameters.

Chapter 4 Results and Discussion:

In this chapter, comparison with results of both experimental result and a numerical model is shown. Also discussion of results, analysis of water surface profiles, vortex and scour formation.

Chapter 5 Conclusions and Recommendations:

This chapter briefly presents the most important conclusion for results and recommendation for forthcoming works.

CHAPTER 2

LITERATURE REVIEW

2.1 Introduction

Scientists from around the world use their daily energy. Science and technology continues to evolve, researchers have their own part in the world that discovered that one of the main areas of research is the failure reason of the hydraulic infrastructure, especially failure due to scouring phenomena. Various studies have been conducted to guess the effect of the scour and reduce the harm related to the scour problem. The formulas and methods that can be used to estimate local scour at culvert are primarily based on laboratory studies. These studies mainly focus on the scour hole dimension and maximum scour depth. Only limited success is achieved through computer modeling attempts. In this research used clear water under unsteady condition. The choice of the countermeasure type and the scour hole geometry is essential for economical design and sa

fety of culvert with various flow hydrographs. In fact, empirical relationships can predict scour depth well under similar conditions. In addition, a site survey is necessary to raise the knowledge of the subject.

A better understanding of any research process can be achieved through the combination of physical and computational models (de Vries, 1973). Calculated transport patterns of sediment in the computational field include numerical solutions for the ruling series of governing differential equations, momentum, continuity, and energy in combination with the interaction of fluid and sediment particles. The computational model of sediment transport is a smart tool for studying erosion in various environments such as lakes, coastal areas and rivers studied after the development of computational fluid dynamics with the high-performance

computer. Typically, the benefit of a computational model configured to represent site-specific conditions are that they can be easily implemented by different physical

domains compared to the physical model (Papanicolaou, 2008). In this study, the numerical model simulation of scouring phenomenon at the culvert outlet was studied. The mechanism of scour at the culvert outlet and factors influencing the scour geometry has been reviewed.

2.2 What is a culvert?

A culvert is a hydraulically short conduit which stream flow conveys through a road embankment or transport some other type of flow obstruction**.** Calvert is made from different materials and is available in many various shapes and configurations as shown in Figure 2.1. Selection factors for waterway include channel characteristics, road profile, construction and maintenance costs, flood damage assessment and estimates of service life.

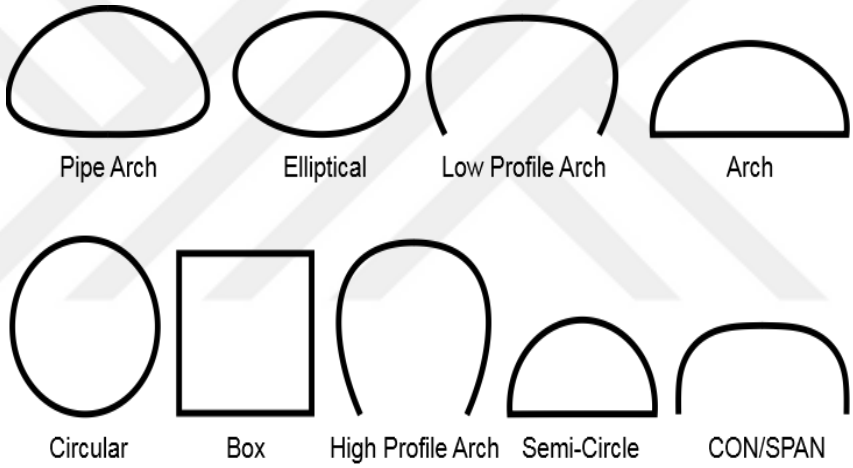

Figure 2.1 Various shape of culvert (HEC-RAS culvert shapes and dimensions, 2015)

In this study, shows that two different investigation fields are important in understanding this topic. These fields are:

- Culvert blockage; and
- Scouring at the culvert outlet.

In these studies, the main focus was the consequences of obstruction and the blockage in the downstream channel. Barthelmess and Rigby (2011) based on the availability, mobility, and transportability of debris, estimated the blockage of culvert and the bridge. Rigby and Barthelmess (2011) they also investigated the mechanisms of blocking culverts as shown in Figure 2.2, and their effect on the behavior of floods.

Figure 2.2 Blockage of culvert (Rural Ramblings, 2009)

Calvert is a place for waterway where contraction to the flood passage happens and therefore some type of blockage is likely to occur (Weeks et al. 2009).

US Department of Transportation Federal Highway (2005) the accumulation of debris at the entrance of culverts may result in erosion at the culvert outlet, increase in local scour at abutments, overtopping and failure of the embankment and the formation of pressure flow scour (Bradley et al. 2005). In most cases, debris racks or trash are placed upstream of culverts to avoid debris from blockage since clogging can result in localized flooding. The blockage is independent of other factors such as material type, land use, stream slope, contributing catchment area, the number of culverts upstream and blockage of upstream culverts. The degree of blockage is the percentage of opening area which closed by debris. Table 2.1 reveals the blockage degrees of culvert, reported in the study by Rigby et al (2002).

Table 2.1 Degree of blockage in culvert (Rigby et al. 2002)

Degrees of blockage %	Percentage of structure blocked during flood events
0-10	5
11-40	14
41-60	2
61-90	21
90-100	58

2.3 Culvert hydraulic

In a culvert, a variety of different flow conditions can happen. Culvert flow is affected by different factors such as roughness, slope, barrel length, outlet and inlet geometry

and also hydraulic conditions including culvert flow rate, water depth, and culvert downstream conditions. In order to systematically analyze culvert flow, based on control section the various types of flow have been analyzed. A control section has a relationship between the ratio of upstream headwater and flow rate (Norman et al. 2001). Based on that culvert flow, it is classified into two main parts, outlet control and inlet control as shown in Figure 2.3 (a, b).

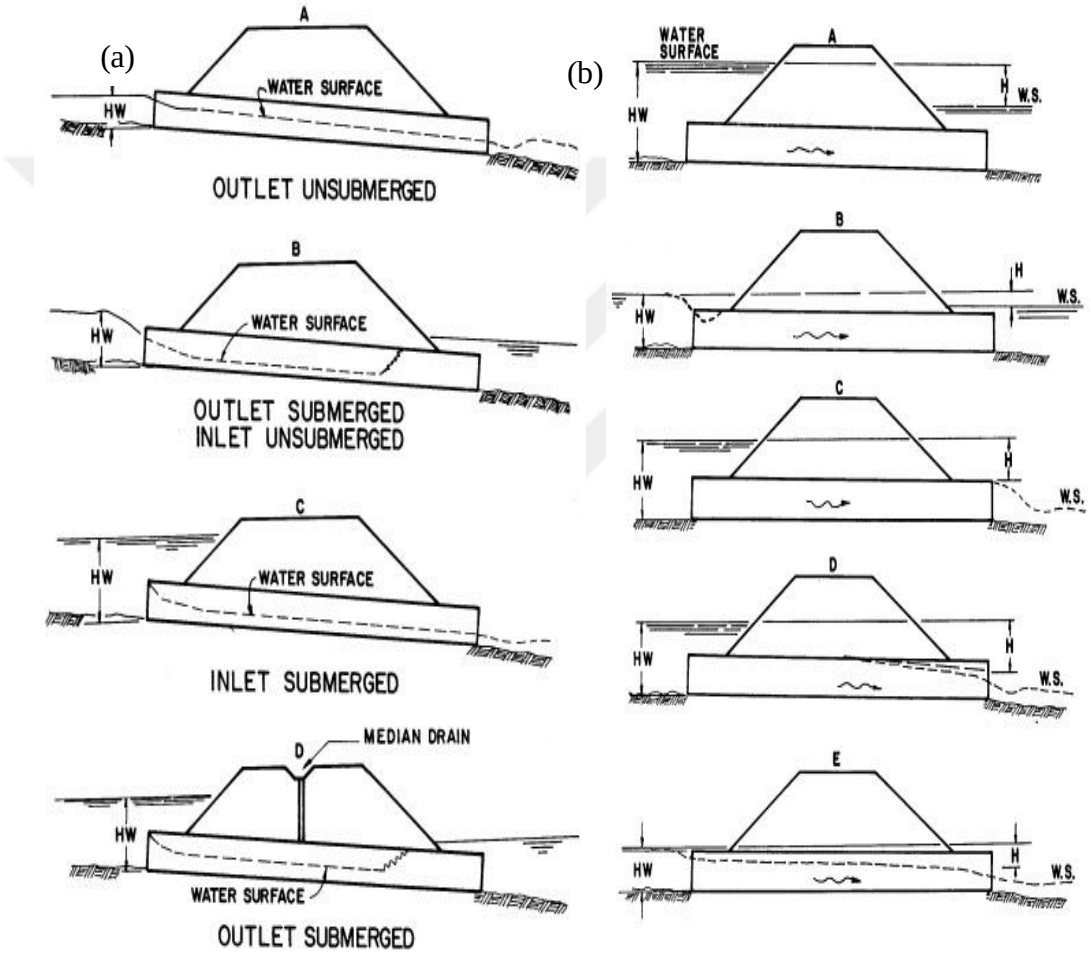

Figure 2.3 (a) Type on inlet control (Norman et al. 2001). (b) Type of outlet control (Norman et al. 2001)

2.4 Scouring

Scouring indicates the erosion of river bed sediment by water and lowering this level. In the following sections, the type of scour, mechanism of scour and influencing factors on scouring at the culvert outlet based on previous studies has been presented.

Scouring can be studied in two different categories

- Based on scour type
- Based on the condition of sediment transport.

2.4.1 Scour type

Scouring has different types. As it was defined by Breusers and Raudkivi (1991), there are three types of scouring that may happen at a structure site which can be classified as:

2.4.1.1 General scour

General scouring happens in streams and rivers due to natural processes, whether or not structures are present (Breusers & Raudkivi, 1991). The general scour function is mainly influenced by the sectional shape of the river valley. When the flow of the flood is confined, it brings about a large change in the height of the water surface, and the scouring power of the flow increases (Raudkivi, 1998).

2.4.1.2 Constriction scour

When the flow area is decreased due to hydraulic structure, the shear stress on the river bed and average velocity of flow increase and also the erosive forces acting the river bed also increase (Ozalp, 2013). the bed marital from the contracting section moved till equilibrium state is reached after erosion increased.

2.4.1.3 Local scour

Local scour happens in non-uniform flow regions, either where the water is accelerated around or through some structures or in regions where vortices or large eddies, produced flow separation or decelerating flow from structures. In this way, local scouring is different from general stream degradation in two aspects: local scour is

confined to a relatively small region associated with the disturbance and the flow in the local scour region is much more non-uniform (Stevens, 1968).

2.4.2 Condition of sediment transport

Based on the different conditions of transport scour can be classified in two groups (Breusers & Raudkivi 1991):

2.4.2.1 Clear water scour

If the upstream shear stress of the structure is not greater than the critical shear stress at the initial of sedimentation movement, the bed material will not move. In this study, the scour happens under clear water condition.

2.4.2.2 Live bed scour

Unlike the clean water condition, in this condition, the critical threshold is smaller than shear stress, and sediments move from upstream of the structure to the scour region. In this study, the flow includes bed material movement. Live-bed scour generally occurs in recirculating flumes and also natural river systems.

2.5 Scour mechanism

Early work on the nature of scouring began with Rouse (1939) and Laursen (1952), which tried to observe the principle of scouring, and described it as a function of discharge, time and material properties. Smith (1957) one of the first researchers who studied scouring below culverts. He studied a relationship between the flow characteristics and the scour hole geometry and also scour development below cantilevered culvert outlets. Smith (1957) related the scour to the energy dissipated at the culvert outlet. Equation (2-1) present the general relationship between the energy of the flow and the scour dimension.

$$\frac{h^*_{100}}{H_b} = a_1 + m\ log\frac{E_0}{{H_b}^2 {W^3}_m \rho} \qquad (2.1)$$

In this equation h_{100} is the cube root of the volume of scour after 100 hours, E_0 is the energy of the jet at the tail water surface, H_b is the height of drop from the upstream

bed level to the bed level downstream, a_1 and m are coefficients, Y is water density and W_m is the mean fall velocity of the particles.

2.6 Influencing factors on scour downstream of culverts

There are many factors that affect downstream scour of a culvert outlet including; flow condition, sediment size, culvert shape, culvert slope, channel width and scale of culvert channel. The following section describes the effect of each of these parameters.

2.6.1 Flow condition

The majority of researchers considered the influence of flow rate in the scour hole formation. Either directly considers the flow discharge in the prediction graph (Chen, 1970 and Opie, 1967).

Opie (1967) was one of the early researcher considered the formulation of flow rate for scour depth. Opie (1967) to obtain a method to predict maximum scouring depth conducted experimental tests on bed material loses. Attempts have been made to tests on culverts with a scale close to field size. Opie (1967) detects that the dimensions of the scour hole have a linear dependence on the variables described hereafter, while the relation may vary with the change in the size of the passage and the material of the bed. Figure 2.4 shows the curve designed which relates between discharge characteristics to maximum scour depth, bed material properties, and outlet characteristics. In this figure, V_m is outlet velocity. Q is flow rate, d_{85} is the sieve diameter of which 84% of sediment is finer by weight, B is the width of the flow at the culvert outlet, ρ is density and $\Delta\gamma_{st}$ Bouyant specific weight of bed material.

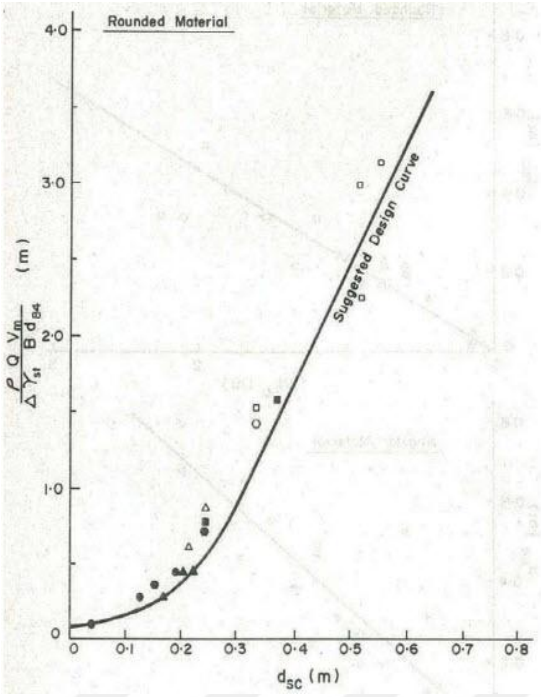

Figure 2.4 The relationship between maximum scouring depth and flow characteristic, culvert characteristics and bed material properties (Opie, 1967)

2.6.2 Sediment characteristics

Sediment characteristics such as density, gradation and sediment size can influence the scour dimension. Chiew and Lim (1996) investigated the influence of the environment on sediment density in scouring at the outlet of circular jets submerged. Tests were done for this purpose in the air and in water. The results presented that the scour hole depth in water is three times smaller than scour hole which forms in the air.

2.6.3 Culvert shape

Numerous cross-sectional shapes are available. The most commonly used shapes, depicted in Figure 2.1, include box (rectangular), circular, semi-circle, pipe-arch, elliptical and arch.

Abt et al. (1987) investigate several experimental tests to obtain the influence of culvert shape on scour hole. The discharge intensity (DI) was changed by a parameter to accommodate different flow geometries associated with the different shapes of culvert as:

$$DI^{*} = \frac{Q}{A(gR_H)^{0.5}} \tag{2.2}$$

where A is a cross sectional area of flow and R_H is the culvert hydraulic radius.

Abt el al. (1987) investigated the influence of culvert shape on outlet scour and developed an equation to correlate the maximum scour depth to modified discharge intensity as:

$$\frac{d_{Sm}}{R_H} = 7.84\left(\frac{Q}{Ag^{0.5}{R_H}^{0.5}}\right)^{0.28} \tag{2.3}$$

R_H the culvert hydraulic radius.

2.6.4 Culvert slope

Abt et al. (1985) the impact of culvert slope to the souring at culvert was investigated and indicate that the maximum depth of scour increase from 10 to 40% over the scour dimensions for sloped horizontal culvert. The maximum scour hole below circular culverts estimated based on this definition as;

$$\frac{d_{Sm}}{D} = a\left(\frac{Q}{g^{0.5}D^{0.5}}\right)^{b} \tag{2.4}$$

The culvert slope which Abt studied varied from 0 to 10%. Table 2-2 summarizes the coefficients of Equation (2.4). In the equation by Abt et al (1986), not considered the effect of sediment size.

Table 2.2 Summary of coefficients proposed by Abt et al. (1985)

Culvert Slope (%)	a	b	R^2
0-2	2.51	0.27	0.59
5	2.68	0.31	0.81
10-Jul	2.82	0.31	0.96

R^2: Coefficient of Determination

2.6.5 Channel Width

Rajaratnam and Diebel (1981), studied that the downstream channel width does not significantly effect on scour depth downstream of culverts. Their results were confirmed by Lim (1995) also noticed that the influence of the downstream channel on scouring process was minimal except when the channel was too narrow.

2.6.6 Scaling of the culvert

In open channel flow, inertial forces and gravitational dominate. Therefore, the best model scaling would be Froude scale which suggests:

$$\frac{F_{rp}}{F_{rm}} = \frac{u_p / \sqrt{gX_p}}{u_m / \sqrt{gX_m}} = 1 \qquad (2.5)$$

Where

F_{rp} and F_{rm} are prototype Froude number and model respectively. X_P and X_m is equal to the characteristic prototype length and model. The u_P is flow velocity in the prototype and X_m is the model velocity. Based on the scaling factor used, laboratory and space equipment, and available laboratory flow, the scale of the culvert was determined as 1:10.

$$\frac{X_p}{X_m} = \lambda = 10 \qquad (2.6)$$

Shown in Table 3.2 are the parameters for prototype and model using Froude scaling ratio and λ is the scaling ratio.

Table 2.3 Scaled parameters for prototype and culvert

Parameter	Scaling ratio	Prototype	Model
Culvert height	10	2 m	200 mm
Culvert length	10	9 m	900 mm
Inlet area	$(10)^2$	4 m^2	40000 mm^2
Flow rate	$(10)^{5/2}$	1.6-3 (m^3/s)	5-25 (Lt/s)
Flow velocity	$(10)^{1/2}$	1.6-6.3 (m/s)	0.5-2(m/s)

2.7 Physical Studies

The physical research was done by conducting experiments on laboratory channels. It is difficult to express rivers in the laboratory's channel so in the laboratory many assumptions are usually incorporated for scouring mechanism, the laboratory studies are still important for understanding basic concepts of sediment transport and river flow. One of the most important problems for researchers is to predict the dimension and shapes of the scour hole near hydraulic structures such as the base of weirs, bridges, open channels, stilling basins and valves due to the both human hazards and financial induced by destruction of the structure. Many studies have been developed empirical methods to express sediment scouring phenomena using data attained in laboratories. By laboratory research, the scour countermeasures can be developed and equations for the maximum scour depth can be improved.

Sorourian, S. at el. (2014) investigate the experimental study is about scouring under unsteady flow condition at the outlet of partially blocked box culverts. Several experimental tests were conducted in the laboratory to investigate the effect of blockage on the scouring pattern. Experimental tests were carried out in both non-blocked and partially blocked states and consequently, the effect of blockage on the scour pattern was investigated. It was obtained that 88% to 98% of the maximum depth of scour happens in the rising limb of the hydrograph. In all steps of hydrograph, the scoured area and maximum scour depth was less in non-blocked condition and the difference was significant at the culvert outlet.

Elsebaie (2013) Investigated the maximum depth of scour and scour pattern along the longitudinal and transverse directions, also discovered that the maximum depth of scour depends on both flow rate and time.

Lanca et al. (2013) investigated the influence of the roughness of the sediment. In their experiments, clear water scour is performed for a long time. Experiments were performed on flow intensity close to the threshold condition of the start of sedimentation movement.

Uymaz (1988) examine the scour phenomenon of non-cohesive soil under the vertical gate. In the case of simultaneous flow under the gate of control structure, the rate of

scour was considered. In experimental work, two different bed materials of homogeneous non-cohesive soil were used.

Experimental studies are limited because of the complexity of expressing actual living conditions. But it helps to understand the basic concepts of rivers and provides a detailed analysis of the parameters relevant to the problem physics. Laboratory studies should be supported by numerical models of scale effects.

2.8 Numerical Studies

Sedimentation is the result of complex natural processes including entrainment, transportation, soil separation, and sedimentation. Not only are the three-dimensional flow and sediment transport equations nonlinear, unknowns are more than the available equations. It causes closure problems necessary for turbulence modeling. On the other hand, solution development is very difficult in generalized three-dimensional cases where both sediment and fluid flow are non-uniform and unsteady. Along with the rapid development of computers, numerical simulation has become an effective research tool. Also, CFD in recent years by researchers has been widely used.

In the early work, because of the high three-dimensional nature of the problem, it should be treated with a three-dimensional model, but the numerical simulation is started from the two-dimensional simulation for practical reasons. According to Morales and Ettema (2012), the 2-D model provides ideas for several limited parameters, these models are based on a reduction in the amount of cell size compared to the 3-D Model, and it is indicating a practical advantage. Morales and Ettema (2012) compared the experimental data with two-dimensional simulation output in the compound channel. The obtained numerical value was investigated and a strong correlation with the experimental data was observed.

Despite some of its advantages, the 2-D model could not answer many questions arising due to the scouring at the hydraulic structure problem. The two-dimensional model requires less processing resources than three-dimensional model. However, in a channel, they gave valuable information related to complex flow physics. The early 3-D CFD model problems of the open channel flow were done by Prinos (1990), Krishnappan and Lau (1986), Pezzinga (1994) and Naot et al. (1993) mainly concerning uniform open channel flow over compound channels. They constructed a

finite element finite difference mixture model that solves the time-dependent nonlinear Navier-Stokes equations.

The outcome is also the first CFD commercial model with the ability to model the local scouring of complex structures without typical limits of structured boundary fitting grids is available from Flow-3D software. A good agreement with measurements described in the literature observed from the results showing that for complex structures the Flow-3D software is a powerful hydraulic design tool. Meanwhile, the computation time required is an important practical limitation of the CFD model and Flow-3D software. When very large grids are required for modeling the structure, computation time is required for long-term scour calculation, so it is much longer than the calculation time required for experimental investigation.

2.8.1 Numerical model

2.8.1.1 Governing equations

The governing equations of flow are the momentum equation and the continuity equation :

$$\frac{\partial \mathrm{u}_i}{\partial x_i} = 0, \tag{2.7}$$

$$\frac{\partial \mathrm{u}_i}{\partial t} + u_j \frac{\partial \mathrm{u}_i}{\partial x_j} = -\frac{1}{\rho}\frac{\partial \mathrm{P}}{\partial x_j} + \frac{\partial}{\partial x_j}\left(2vS_{ij} - \overline{u_i' u_j'}\right), \tag{2.8}$$

$$S_{ij} = \frac{1}{2}\left(\frac{\partial \mathrm{u}_i}{\partial x_j} + \frac{\partial \mathrm{u}_j}{\partial x_i}\right), \tag{2.9}$$

$$\overline{u_i' u_j'} = v_t\left(\frac{\partial \mathrm{u}_i}{\partial x_j} + \frac{\partial \mathrm{u}_j}{\partial x_i}\right) - \frac{2}{3}k\delta_{ij}. \tag{2.10}$$

Where u_i' is the fluctuation of fluid velocity in *i* direction, u_i is the fluid velocity component in *i* direction, P is the pressure, $\overline{u_i' u_j'}$ is the Reynolds stress tensor, ρ is the fluid density, v_t is the turbulence viscosity, S_{ij} is the mean strain rate tensor, v is the fluid kinetic viscosity, k is the turbulent kinetic energy, and $\delta_{ij}$is the Kronecker delta (δ_{ij} =1, *i=j;* $\delta_{ij} = 0$,*i=j).*

2.8.1.2 Turbulent model

Yakhot and Orszag (1986) proposed an improved k - ε turbulence model named RNG (renormalization group) k - ε model whose coefficient cannot be obtained from experimental data, but the theoretical analysis. The RNG k-ε model has better adaptability than the standard k-ε model. For simulate the culvert turbulent flow uses RNG k-ε model in this study. In Flow-3D the governing equations are (1) 3-D Reynolds-averaged Navier-Stokes equations for Boussinesq approximation with fluid flow, (2) the continuity equation and (3) the transport equation. The governing equations are as follows:

(k-ε) model flow was to provide a reasonable approximation for many kinds of flow, additional transport equations for turbulent diffusion are solved, ε_T:

$$\frac{\partial \varepsilon_T}{\partial t} + \frac{1}{V_F}\left(uA_x \frac{\partial_{\varepsilon T}}{\partial x} + vA_y R \frac{\partial_{\varepsilon T}}{\partial y} + wA_z \frac{\partial_{\varepsilon T}}{\partial z}\right) = \frac{CDIS1.\varepsilon T}{k_T}\left(P_{T+CDIS3.G_T}\right) + Diff\varepsilon - CDIS2\frac{\varepsilon_T^2}{k_T} \quad (2.11)$$

$$\frac{\partial \mathrm{k}}{\partial t} + u_j \frac{\partial k}{\partial x_j} = \tau_{ij} \frac{\partial \mathrm{u}_i}{\partial x_j} + \frac{\partial}{\partial x_j}\left[\frac{1}{\rho}\left(\mu + \frac{\mu_t}{\sigma_k}\right)\frac{\sigma_k}{\partial x_j}\right] - \varepsilon \quad (2.12)$$

$$\frac{\partial \varepsilon}{\partial t} + u_j \frac{\partial \varepsilon}{\partial x_i} = C_{1\varepsilon}\frac{\varepsilon}{k}\tau_{ij}\frac{\partial \mathrm{u}_i}{\partial x_j} + \frac{\partial}{\partial x_j}\left[\frac{1}{\rho}\left(\mu + \frac{\mu_t}{\sigma_k}\right)\frac{\partial \varepsilon}{\partial x_i}\right] - C_{2\varepsilon}\rho\frac{\varepsilon^2}{k} \quad (2.13)$$

Here CDIS1, CDIS2, and CDIS3 are all dimensionless user-adjustable parameters and have defaults of 1.44, 1.92 and 0.2, respectively for the ($k-\varepsilon$) model.

The diffusion of dissipation, Diffε is:

$$\text{Diff}\varepsilon = \frac{1}{V_F}\{\frac{\partial}{\partial x}\left(v\varepsilon A_x \frac{\partial_{\varepsilon T}}{\partial x}\right) + R\frac{\partial}{\partial y}\left(v\varepsilon A_y R\frac{\partial_{\varepsilon T}}{\partial y}\right) + \frac{\partial}{\partial z}\left(v\varepsilon A_z \frac{\partial \varepsilon_T}{\partial z}\right) + \xi\frac{v\varepsilon A_X \varepsilon_T}{x}\} \quad (2.14)$$

the rate of turbulent energy dissipation, ε_T, the one-equation model is related to the turbulent kinetic energy K_T

$$\varepsilon_T = CNU\sqrt{\frac{3}{2}}\frac{k_T^{3/2}}{TLEN} \quad (2.15)$$

Where CNU is a parameter (0.09 by default), K_T is the turbulent kinetic energy and TLEN is the turbulent length scale.

In equation (2.12) and (2.13), where k is the turbulent kinetic energy, $k = \frac{1}{2}\overline{u_\iota' u_j'}$, ε is

$$\tau_{ij} = \frac{\mu_t}{\rho}\left(\frac{\partial u_i}{\partial x_j} + \frac{\partial u_j}{\partial x_i}\right) - \frac{2}{3}k\delta_{ij} C\mu = 0.085, C_{1\varepsilon} = 1.42, C_{2\varepsilon} = 1.68, \quad (2.16)$$

$$\sigma_k = 0.7179, \qquad \sigma_\varepsilon = 0.7179$$

the dissipation of turbulent kinetic energy, $\varepsilon = v\overline{\left(\frac{\partial u_\iota'}{\partial x_k}\right)\left(\frac{\partial u_\iota'}{\partial x_k}\right)}$; μ_t is the turbulent eddy viscosity, $\mu = C\mu\rho k^2/\varepsilon$; τ_{ij} is the Reynolds stress,

2.8.1.3 Sediment scour model

Particle dynamics

In previous studies, in order to describe the transport of floating sediments. It is assumed that the inertia of the particles is negligible. Therefore, only the mechanism of advection and diffusion affected the transport of suspended sediment. In the Flow-3D model, incorporating particle dynamics into the code provides a more accurate simulation. The drift velocity of sediment is computed based on fluid-sediment mixture and momentum balances for each sediment fraction given in vector forms as:

$$\frac{\partial \mathrm{u}_{s,i}}{\partial t} + \bar{u}\,.\nabla \mathrm{u}_{\mathrm{s,i}} = -\frac{1}{\rho_{s,i}}\nabla p + F - \frac{k_i}{f_{s,i}\rho_{s,i}}u_{r,i}, \tag{2.17}$$

$$\frac{\partial \bar{u}}{\partial t} + \bar{u}.\nabla \bar{u} = -\frac{1}{\bar{\rho}}\nabla p + F, \tag{2.18}$$

where k_i and $f_{s,i}$, are drag function and volume fraction of sediment respectively, $\mathrm{u}_{\mathrm{s,i}}$ is velocity of sediment fraction i , $\bar{u}$ and ρ are mean velocity and density of fluid sediment mixture respectively, F is ratio of fluid volume to one computational cell (for example, $F = 1$ indicates that the computational cell is filled with fluid), $u_{r,i}$ is relative velocity given by

$$u_{r,i} = \mathrm{u}_{\mathrm{s,i}} - \mathrm{u}_{f.} \tag{2.19}$$

The mean density $\bar{\rho}$ is defined as:

$$\bar{\rho} = \sum_{i=1}^{N} f_{s,i}\rho_{s,i} + (1 - \sum_{i=1}^{N} f_{s,i})\rho_f \tag{2.20}$$

Where N is number of sediment fractions, $\rho_{s,i}$, and ρ_f are densities of sediment fraction i and fluid respectively, Subtracting (2.17) from (2.18) gives

$$\frac{\partial \mathrm{u}_{drift,i}}{\partial t} + \bar{u} \,.\nabla \mathrm{u}_{drift,i} = \left(\frac{1}{\bar{\rho}} - \frac{1}{\rho_{s,i}}\right)\nabla p - \frac{k_i}{f_{s,i}\rho_{s,i}} u_{r,i}. \tag{2.21}$$

The drift velocity $\mathrm{u}_{drift,i}$ is defined as:

$$u_{drift,i} = u_{r,i} - \bar{u}. \tag{2.22}$$

In (2.19), $u_{r,i}$ is computed by assuming that the advection term is very small due to the small gradient in drift velocity and the slow motion of sediment in near-steady state at the scale of the computational time:

$$u_{r,i} = \frac{\nabla p}{\bar{\rho}\, K_i}(\rho_{s,i} - \rho_f) f_{s,i}, \tag{2.23}$$

Where K_i denotes the drag function involving form drag and Stokes drag:

$$k_i = \frac{3}{4}\frac{f_{s,i}}{d_{s,i}}\left(C_{D,i}\|u_{r,i}\| + 24\frac{\mu_f}{\rho_f d_{s,i}}\right), \tag{2.24}$$

Where and μ_f is fluid viscosity, $C_{D,i}$ and $d_{s,i}$ indicate drag coefficient and diameter of sediment species respectively. The mean flow velocity $\bar{u}$ is determined by calculating the velocities of all phases:

$$\bar{u} = (1 - \sum_{j=1}^{N} f_{s,j})u_f + \sum_{j=1}^{N} f_{s,i} u_{s,j}. \tag{2.25}$$

Drift is essentially an additional mechanism of sediment transport in mixed flow with turbulent diffusion advection.

Entrainment

Entrainment involves the process of picking up and re-suspending particles near the bed surface. This needs to be calculated in the saltation region. In the model by using an empirical model can have calculated the entrainment of packed sediment. The entrainment lift velocity of sediment fraction i is the volumetric flux of sediment defined as:

$$u_{lift,i} = a_i n_s d^{0.3} (\tau_{*,i} - \tau_{*c,i})^{1.5} \sqrt{\frac{\|g\| d_{s,i} (\rho_{s,i} - \rho_f)}{\rho_f}}, \tag{2.26}$$

Where $\tau_{*,i}$ is the local Shields parameter on the bed surface, obtained based on the ratio of hydrodynamic forces to the particle submerged weight, given by

$$\tau_{*,i} = \frac{\tau_0}{\|g\| d_{s,i} (\rho_{s,i} - \rho_f)}. \tag{2.27}$$

In the Shields parameter, τ_0 is the local boundary shear stress and d_* is the dimension less mean particle diameter defined as:

$$d_* = d_{50} \left[\frac{\rho_f (\rho_{s,i} - \rho_f) \|g\|}{\mu_m} \right]^{\frac{1}{3}} \tag{2.28}$$

Where μ_m and d_{50} are the viscosity of a mixture and local mean particle size. The critical value of the Shields parameter $\tau_{*c,i}$, Corresponding to the start of the movement of sediment particles. In this model $\tau_{*c,i}$,describes the initial motion on a flat horizontal surface, the Shields-Rouse equation given by:

$$\tau_{*c,i} = \frac{0.1}{{R_{*,i}}^{2/3}} + 0.054\left[1 - \exp\left(-\frac{{R_{*,i}}^{0.52}}{10}\right)\right] \tag{2.29}$$

Where $R_{*,i}$ is the Rouse-Reynolds number, defined as:

$$R_{*,i} = \frac{\sqrt{0.1\rho_f\left(\rho_{s,i} - \rho_f\right)\|g\|{d_{*i}}^3}}{\mu_f} \tag{2.30}$$

In the case of a sloping bed surface, according to the shear force direction and local slope of the bed , $\tau_{*c,i}$, should be modified. In this study the approach suggested by Soulsby (1997), which is similar to the those of Julien (2010) and Brooks (1958), was employed to account for the effect of the bed slope on sediment transport. The adjusted critical Shields parameter is given by

$$\tau'_{*c,i} = \tau_{*c,i}\frac{\cos\psi\sin\beta\sqrt{\cos^2\beta\tan^2\varphi_i - \sin^2\psi\sin^2\beta}}{\tan\varphi_i}, \tag{2.31}$$

where β is the computed angle between bed surface to the normal and the gravitational acceleration vector g, φ_i is the angle of repose of sediment fraction i. The angle of repose equals the sweeping angle of the connected line between the contact point and a particle center of mass which the particle rotates on the bed surface when the particle center revolves on the bed surface, the angle of repose rest on the shape of particle, size of particle and the orientation of the particle on the bed surface of soil when the particle center of mass is perpendicularly above the contact point, and accordingly. Then again, the flowing fluid applies forces, starting the particles motion, on the particles and ψ is the angle between the upslope direction and the flow Figure 2.5. If the flow goes up the slope (i.e. $\psi = 0$), Equation (2.31) then decreases to the formulation of Bormann and Julien (1991):

$$\tau'_{*c,i} = \tau_{*c,i} \frac{\sin(\varphi_i + \beta)}{\sin \varphi_i} \tag{2.32}$$

If the flow goes directly down the slope (i.e. $\psi = 180^\circ$), (2.31) reduces to

$$\tau'_{*c,i} = \tau_{*c,i} \frac{\sin(\varphi_i + \beta)}{\sin \varphi_i} \tag{2.33}$$

When the flow is directed laterally across the slope (i.e. $\psi \pm 90^\circ$), (2.31) becomes equal to the formulation of Lane (1953):

$$\tau'_{*c,i} = \tau_{*c,i} \beta \left(1 - \frac{\tan^2 \beta}{\tan^2 \varphi_i}\right)^{\frac{1}{2}} \tag{2.34}$$

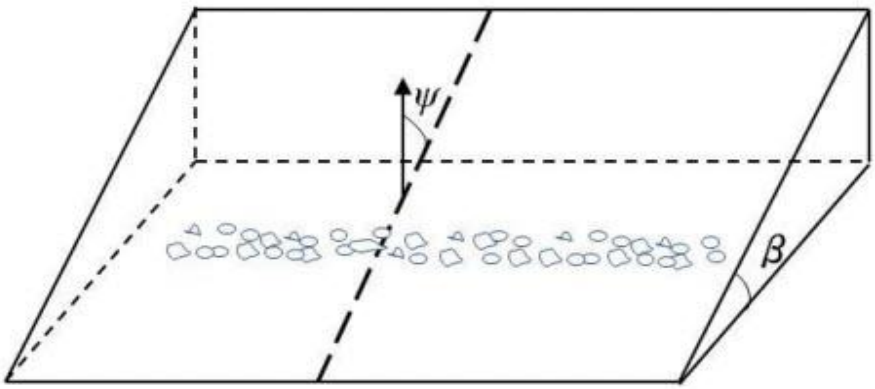

Figure 2.5 Angle of bed-load transport: β is angle between the normal to bed surface and the gravitational vector, and Ψ is angle between the flow and the upslope direction (Lane, 1953)

Bed-load transport

There are two forms of transportation of sediment particles in moving water: suspended load and bed-load. The floating load can be composed of the washing load entrained with the upstream sediment load which deprived the composition and properties of the bed material. There exist three modes of particle motion in the natural circumstances: (a) suspended motion; (b) saltation; (c) rolling and sliding. Non-cohesive bed particles begin to move when the critical shear stress less than shear stress on the bed material. Generally, finer sediment such as clay and silt is easily suspended and entrained, whereas gravel and sand particles slide and roll in the bed load or bed layer. Most of the bed-load transport formulas suggested in the literature was developed empirically. Small scale turbulent numerical modeling that affects bed loading transport requires very fine mesh size and accurate bed survey and it is almost impossible to actually perform in field-scale applications. In order to overcome these problems, empirical formulas can be used to estimate the effect of small-scale turbulence on bed load transport. Table 2.4 shows the bed load formulas (2.35), (2.36) and (2.37) when used for this purpose.

Table 2.4 Bed-load transport formulas

Author	**Formula**
Engelund and Fredsoe (1976)	$q_{*,i} = 18.74\left(\tau_{*,i} - \tau_{*c,i}\right)[{\tau_{*,i}}^{1/2} - 0.7{\tau^{1/2}}_{*c,i}]$
Meyer-Peter and Muller (1948)	$q_{*,i} = 8\left(\tau_{*,i} - \tau_{*c,i}\right)^{1.5}$
Nielsen (1992)	$q_{*,i} = 12\left(\tau_{*,i} - \tau_{*c,i}\right)^{1.5}\sqrt{\tau_{*,i}}$

The bed transport of sediment is quantified by the bed load flux $q_{bv,i}$ that refers to the volume of sediment per unit width per unit time within the bed layer, and is rewritten using the dimensionless bed-load flux $q_{*,i}$:

$$q_{bv,i} = q_{*,i}\sqrt{\left(\frac{\rho_{s,i} - \rho_f}{\rho_f}\right)\|g\|{d_{*i}}^3} \tag{2.38}$$

The Flow-3D model adjusts the time step size so that fluid does not flow to multiple cells in one calculation time step, δt , which is referred to as a Courant stability criterion, defined as:

$$\delta t < 0.45.mm\left(\frac{V_f \delta x_i}{A_x u}, \frac{V_f \delta y_j}{A_y v}, \frac{V_f \delta z_k}{A_z w}\right), \tag{2.39}$$

Where

A and V_f are respectively, area open and fractional volume to flow in the Favor method. If automatic time step is selected in Flow-3D, the model adjusts the time step as much as possible while maintaining the stability criteria.

2.8.2 Numerical method

2.8.2.1 The VOF method

In finite difference numerical simulations several methods have been previously used to approximate free boundaries. The method is described simple but powerful, that is based on the concept of a fractional volume of fluid (VOF). This method has been shown to be more efficient and flexible than other methods for treating complicated free boundary formations.

VOF and FAVOROTM are examples of volume fractions. In these methods, the region has been modeled first subdivides to control volumes or some small grid elements. For elements that contain numerical values, liquid have been retained for each flow variable such as temperature, velocity and presser within the element. Typically, these

values represent some kind of average volumetric of the quantities in the element. All the elements not contain liquid when there are free surfaces. Some elements will be empty and some full. Several elements will be partially filled when those elements contain a free surface. A convenient way of identifying element states is to introduce a quantity of F that registers a fraction of the volume of the element that is filled with liquid. This quantity is called the Volume-of-Fluid (VOF) function. (Flow-3D User Manual, 2012).

This function represents the volume of fluid per unit volume and satisfies the equation:

$$\frac{\partial \mathrm{F}}{\partial t} + \frac{1}{V_F}\left[\frac{\partial}{\partial x}(FA_{xu}) + R\frac{\partial}{\partial y}\left(FA_{yv}\right) + \frac{\partial}{\partial_z}(FA_{zw}) + \xi\frac{FA_{xu}}{x} = \mathrm{F_{DIF}}+\mathrm{F_{SOR}}\right. \quad (2.40)$$

$$\mathrm{F_{DIF}} = \frac{1}{V_F}\left\{\frac{\partial}{\partial x}\left(v_F A_x \frac{\partial F}{\partial x}\right) + R\frac{\partial}{\partial x}\left(v_F A_y R\frac{\partial F}{\partial y}\right) + \frac{\partial}{\partial_z}\left(v_F A_z \frac{\partial F}{\partial z}\right) + \xi\frac{v_F A_{xF}}{x}\right. \quad (2.41)$$

$$V_F\frac{\partial \rho}{\partial t} + \frac{\partial}{\partial x}(\rho u A_x) + R\frac{\partial}{\partial y}\left(\rho_v A_y\right) + \frac{\partial}{\partial_z}(\rho_w A_z) + \xi\frac{\rho_u A_x}{x} = \mathrm{R_{DIF}} + \mathrm{R_{SOR}} \quad (2.42)$$

where:

, ρ is the fluid density, V_F is the fractional volume open to flow, RSOR is a mass source, and RDIF is a turbulent diffusion term. A_x is the fractional area open to flow in the x-direction, A_y and A_Z are similar area fractions for flow in the y and z directions, the velocity components (u, v, w) are in the coordinate directions (x, y, z) or (r, RSOR, z) respectively. The coefficient R depends on the choice of coordinate system in the following way.

2.8.2.2 The FAVOR method

Another volume fraction technique is the FAVORO^{TM} method. Only in this case, which is used to define geometry. Just as the fractional volume of liquid in each grid element has been used to locate the surface of the fluid, another fraction volume of quantity can be used to determine the solid surfaces. In practice, the free volume of fraction Vf of the element that is not blocked by the solid is maintained. It is also useful to store open fractions on each surface of the element. In any case, regardless of

whether store an open or blocked part of an element, the same technique will be used in the VOF method and can be used to locate solid boundaries cutting through a fixed grid. This information has been used to determine the boundary conditions of the walls, which must be consistent with the flow.

Since the boundary geometry of the flow is usually stationary, there is no need to move or update the volume fraction Vf and the area fraction Af in the flow. The fractional volume of liquid F is defined to be the fraction of the open volume of an element, Vf, not the fraction of the total element volume when the FAVORO^{TM} method has been combined with the VOF method. In other word, if G is the volume of an element, then the actual volume of liquid in this element is (FVf) G not (F) G.

2.9 CFD Modeling

Mehnifard et al. (2015) investigated the potency test of the numerical model for local scour due to the submerged horizontal jets the results of laboratory analysis were compared with numerical simulation results from Flow-3D three-dimensional model. In this research, measured maximum depth of scour for six different types and in two states with different depth of tail water and valve openings per different flow rates. Comparing this result shows an error of about 11% of the Flow-3D numerical model associated with the experimental model considered good results by considering the deposition and complexity of scour phenomena. By compared with the other turbulence models, RNG turbulence model provides better results. In the calculation of maximum scour depth, the smallest error was observed when investigated the result of the experimental model with the result numerical simulation model. In other words, in the numerical model Flow-3D, the depth of scour is calculated with higher precision than the other parameters.

Lang et al. (2013) simulated a three-dimensional flow and a local scour by using Flow-3D software. The Finite Volume Method (FVM) are solved with Navier-Stokes equations. RNG κ-ε model and the bed-load transport model was selected in turbulence model based on the Shields number. in Flow-3D the volume of fluid (VOF) method was employed, which tracks the fluid-fluid interface or fluid-air. Simulated results of turbulence and mean flow for fixed bed case include the distribution of velocity, dissipation, backflow length and turbulent energy. Analysis of the flow field distribution reveals that the formation of the scoured surface is mainly affected by

horseshoe vortex and submerged flow. In main scour stage, the scour pit depth increased accordingly because of horseshoe vortex and intensity of submerged flow increased rapidly. As the depth of the scour pit increases, the flow velocity decreases, the strength of the submerged flow and the horseshoe vortex decreases until the water flow velocity decreases, and the sediment cannot be removed.

Richardson et al. (1998) studied the simulated equations by using RNG k-ε model with Flow-3D package program and scouring around piers. By solving the 3D Navier-Stokes equations the scouring phenomenon was simulated. Without sediment transport modeling, the depth of equilibrium was estimated simply by Lagrangi particle tracking analysis. Finally, compared experimental results with numerical results and comparison had a good agreement.

Olsen and Melaaen (1993) used k-ε turbulence model for simulate the sediment scour around circular piers. In this research, based on the convection-diffusion equation constructed their sediment scour model. The transient terms in the model and bed load formulas with modeled the sediment motion have been neglected. the scour depth value calibrated in experimental study by repetitions and after that process, the geometry of scour hole fitted well with the experimental one. Olsen and Kjellesvig (1998) have developed the earlier analysis by counting the transient terms. In this part, investigate the scour around a circular pier and used the same methodology to measure the sediment scouring and compared the results of the maximum scour depth with the empirical equations. They attained agreement results with some of the empirical methods.

Zhang et al. (2005) have been modeled the scour around spur dikes and also simulated the flow through numerous of spur dikes. The performance of the numerical model by selecting k-ε turbulence model was evaluated. Semi-empirical equations based on mass conservation of sediments were used when dealing with sediment scour. By modified bed load equations, sediment motion within the scour hole was defined. A reasonable agreement obtained when the results of scour profiles and flow fields compared with the experiment results.

Olsen and Kjellesvig (1998) carried out under the local scour of a current survey steady by three-dimensional flow, in addition to sediment transport model to compute fluid behavior besides the scour development. Also, in order to investigate the local scouring phenomenon in detail, Olsen and Melaaen (1993) conducted a similar study similar to the previous one. Roulund et al. (2005) in the research to evaluate the comparison used three-dimensional model with k-ε turbulent model. The results of the simulation model agreed well with the experimental results. VOF system and three-dimensional numerical model Liu and Garcia (2008) studied local scouring using free water surface. A well agreement has been obtained from the results with laboratory observation.

Olsen and Melaaen (1993) and Olsen and Kjellesvig (1998) predicted sediment transport model and local scour simulating three dimensional flow. Solved the Reynolds equation with averaged Navier-Stokes equations (RANS) and the k-ε model for turbulence closure using the finite volume method (FVM). Also tested the results with experimental data found to be close to each other. Since the transient term of the RANS equation was ignored in the simulation, the calculated flow field did not capture the complexity observed in the experimental flow field around the model pier.

Olsen (2003) for simulated sediment and water flow used the SSIIM model (Sediment simulation of multi-block intake). The SSIIM model is a software numerically used for simulating flow equations and sediment. It has ability to analyze complex shapes of river beds. based on Unsteady Reynolds Average Navier-Stokes (URANS) equations with k-ε model SSIIM model solves three dimensional Navier Stokes differential equations. Esmaeili (2009) used flow hydrograph for calculate maximum scour depth in the SSIIM model.

Köken and Göğüş (2010) investigated the effect of abutment length on the horseshoe vortex system and the bed shear stress, by using DES model. Köken and Constantinescu (2011) have studied the flow and turbulence characteristics of the scour hole around spike dikes and discussed the mechanism of scour hole development.

The study of partial two-phase flow model was done by Asano (1991). By using empirical formulations and equations examined the vertical velocity of particles. The solutions of the governing equations gave less accurate solutions than the empirical equations. Li (1995) expanded the previous research to formulate a complete set of two-phase flow equations. Ali et al. (1997) showed that the renormalization group (RNG) k-ε model gives a good estimation of the bed shear stress and velocity field.

Wu and Wang (1999) and Dou (1997), Jia et al. (2001) by using a numerical model in three dimensional flow conditions analyzed the mechanism of local scour at bridge piers. Empirical formula used to calibrate sediment transport within the scour hole. Wang and Jia (1999) by using CCHE3D simulated the evolution of the scour hole around the bridge pier. The comparisons were quite well-matched.

Teklemariam, et al. (2002) began applying Flow-3D in hydraulic engineering applications. As a result of studies, for advanced hydraulic engineering projects, CFD analysis provide a significant design support. To provide insight into the planned physical models, the CFD models were also used.

Kumcu, S. Y. (2016) flow depth, pressure and discharge data have been documented for different flow conditions. A major change was made in experimental research on the original project. According to evaluate the performance of CFD in modeling spillway flow, these results obtained from computational fluid dynamics (CFD) simulation and physical model were compared. Solving the Reynolds Average Navier-Stokes (RANS) equation by using a commercially available CFD program, it modeled the numerical model set-up by defining cells that are partially or completely restricted in computational space. To compare the results of the physical model and the numerical model, the velocity pattern, the discharge rate curve and the pressure were used. For the flow properties reasonably good agreement was shown between the numerical model and the physical.

Sharifi and Amiri (2014) used two-equation (k-e) turbulence model in Flow-3D software, Shahheydari et al. (2015) used Flow-3d software and RNG k-ε model was applied as the turbulence model, Gacek, J. D. (2007) Used Flow-3D and Reynolds-averaged Navier-Stokes equations in combination with the standard K-s eddy-viscosity and Mazen Tabbara et. Al (2005) used ADINA software and k–e flow model,

in all researchers have been obtained a good agreement when compared with a physical model.

Julien et al. (2015) investigated the local scour at the downstream of an apron caused by submerged jets issuing from a sluice gate by using Flow-3D computational fluid dynamics code. The performance of the numerical model based on the large-eddy simulation (LES) technique and renormalization group $k-\varepsilon$ turbulence scheme has been evaluated by comparison with laboratory experiments. The simulation results show considerable numerical discrepancies between the LES closure scheme and the renormalization group $k-\varepsilon$. In comparison, a better description of deposition and scour has been achieved using the LES technique, which successfully reproduces the results from the experiment for sediment deposition and scour hole formation.

Lang et al. (2013) studied numerical simulation results present that the numerical method and mathematical model used in this study can better simulate the dynamic procedure of scouring. Development of scour hole with time had been observed and divided into three stages of the initial stage, the main scouring stage, and the equilibrium stage

Mehnifard et al. (2015) examined numerical 3-D model researches on local scour with free surface has been done by Lieu Garcia (2008). In the research used VOF (volume of fluid) method to simulate k-ε model for turbulence and free surface water flow. Comparison of the experimental model results with numerical model results suggests the accuracy of the numerical method for predicting the scour

CHAPTER 3

CASE-STUDY

3.1 Introduction

In this chapter, a 3D numerical model of sediment scours simulated based on an experimental study by Sayana (2015). The experiment was done in UTS hydraulics Laboratory of the University of Technology Sydney. The experimental setup with details of the channel, the physical model features, the measuring facilities and the properties of the bed materials are described. The numerical models were simulated by using Flow-3D software version 10.1. The following section includes a complete detail of performed work.

3.2 Experimental test set-up

3.2.1 Flume and its components

Figure 3.1 shows the plan and sectional view of this physical model was set-up by Sayana (2015). The locate of the experimental set-up in UTS hydraulics Laboratory of the University of Technology Sydney. Experimental tests associated with this study were carried out in a scour testing facility. The tests were done in the recirculating concrete flume and it has the following dimensions 19 m long with a depth and width of 600 mm and 605 mm. The flume had a constant slope of 0.001. The location of test section was in 9m from the inlet of the flume to ensure a fully developed flow reached the test area. The test section was a 5 m long, 150 mm deep sand basin with the same width as the flume. Water was supplied to a static tank from the storage tank. The water, in turn, enters the flume through a valve which controls the water flow rate, and then it runs through the box-culvert. In the experimental program clear water was used throughout the tests under unsteady conditions. To make an unsteady flow, a hydrograph was designed for each set to be conveyed by the culvert. Figure 3.2 shows the hydrograph stepwise for two bed materials. Each set run in non-blocked and partially blocked conditions. For controlling the flow rate measurement in the flume,

the inline electromagnetic flow meter, Siemens MAG 5000, has been used in the laboratory as shown in Figure 3.3, and for dimensions of the scour hole were measured by an Acoustic Doppler Velocimetry known as Micro-ADVP. The position of the flow meter was set-up between the inlet section of the flume and the outlet of the constant head tank as shown in Figure3.1.

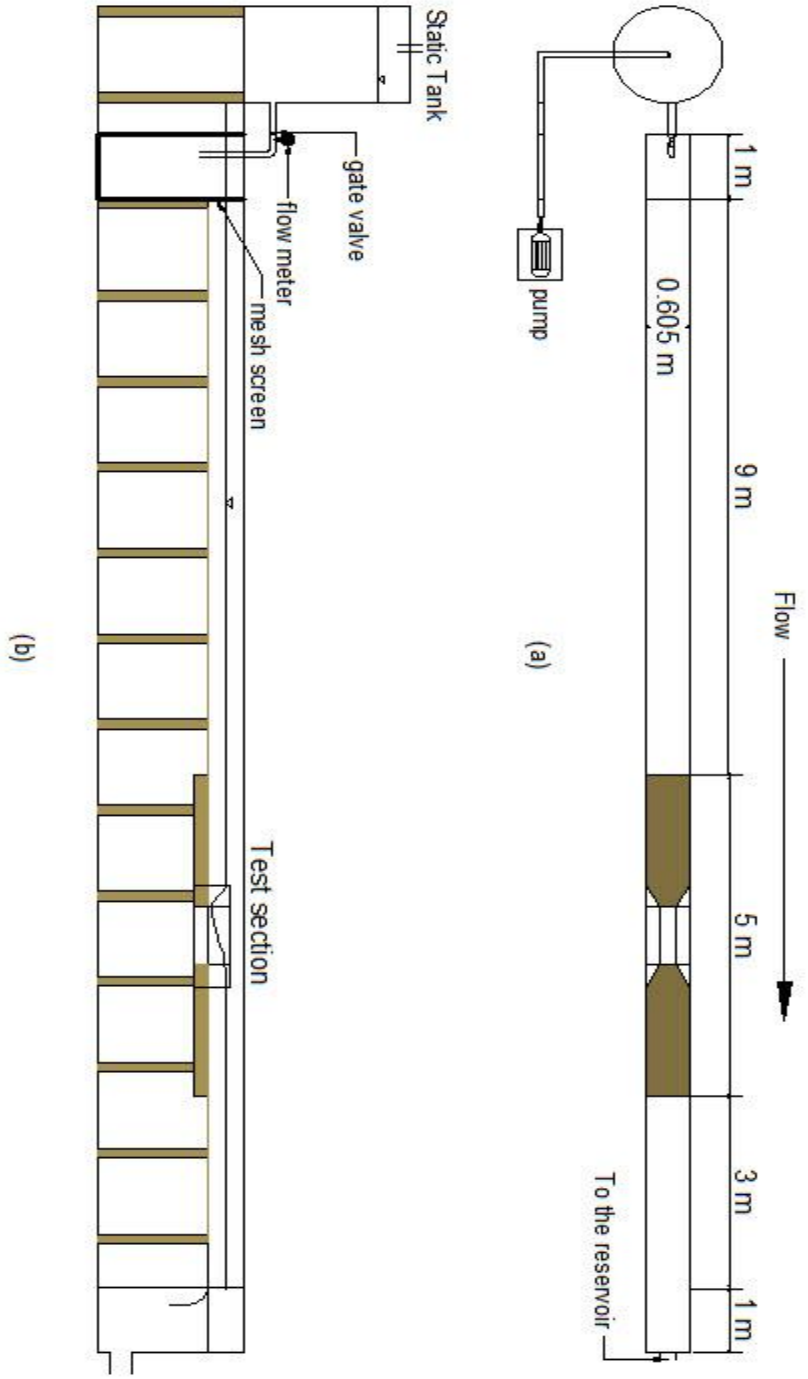

Figure 3.1 Test set up (a) plan (b) section view

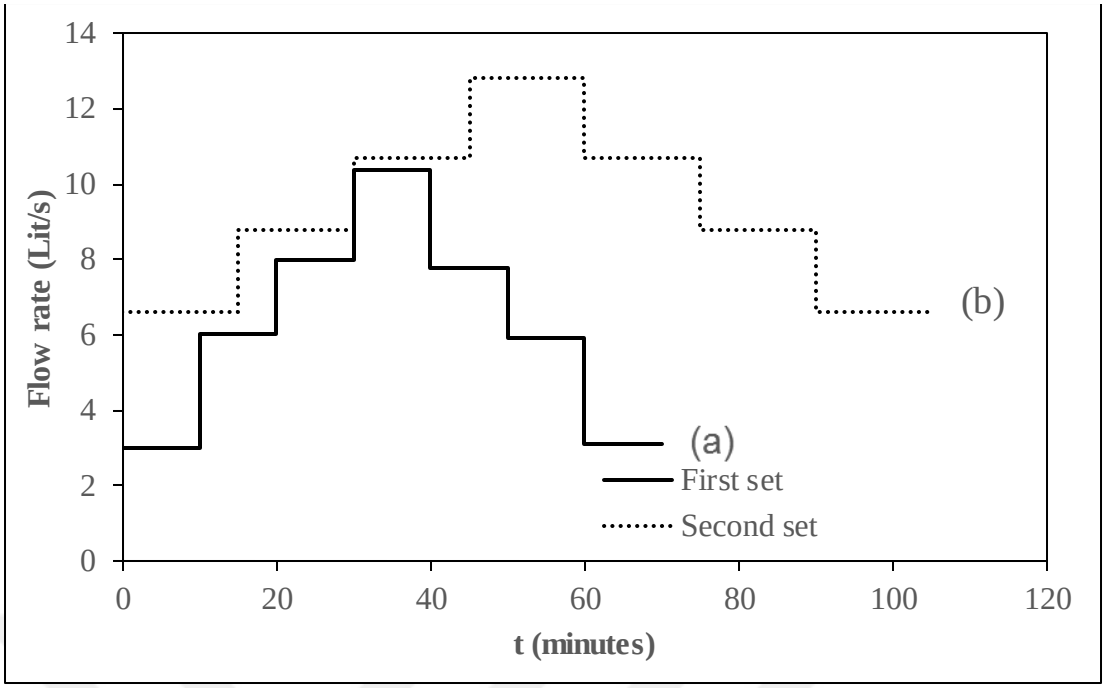

Figure 3.2 Stepwise hydrograph for tests both in partially blocked and non-blocked conditions; First set: hydrograph for material with d_{50}=0.85 mm, Second set: hydrograph for material with d_{50}=2.0 mm

Figure 3.3 Electromagnetic Flow meter (Simence, 2015)

3.2.2 Culvert model

The box-culvert model being tested was placed in the flume on a sand bed. The details of culvert model are shown in Figure 3.4. The culvert opening is 200×200 mm and the length of the culvert barrel is 900 mm. There are transitions with 30° flare at the inlet and outlet of the culvert. The benefit of these transitions are to avoid unnecessary scour hole. To indicate blockage at the inlet, a plate was installed at the culvert opening. Two sizes of plates (200×80 mm and 200×120 mm) were used to attain different blockage ratios in the experimental tests and in all tests level of water passed under the blockage plate and it did not overflow the plate. The outlet culvert's wall was glued to the flume's bed. Although, to seal the model, the transition and both culvert sides were glued to the flume's walls. For all tests two conditions were used:

a) Partially blocked condition: Two different size of plates were used to simulate 40% blockage at the inlet of culvert. The free space between top of culvert to the bottom of plate was 40 mm as shown in Figure 3.5.
b) Non-blocked condition

The most common obstruction is made up of the type of mixed material that is vegetation, urban materials are found in about 70% of cases, typically blocking the culvert from the top down (Rigby et al., 2002). Figure 3.4 shows the parameters corresponding to the partially blocked culvert and the scour hole.

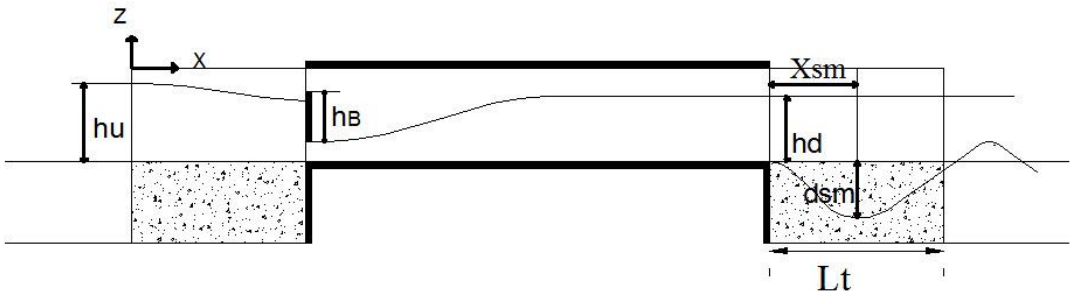

Figure 3.4 Parameters corresponding to the partially blocked culvert and the scour hole.

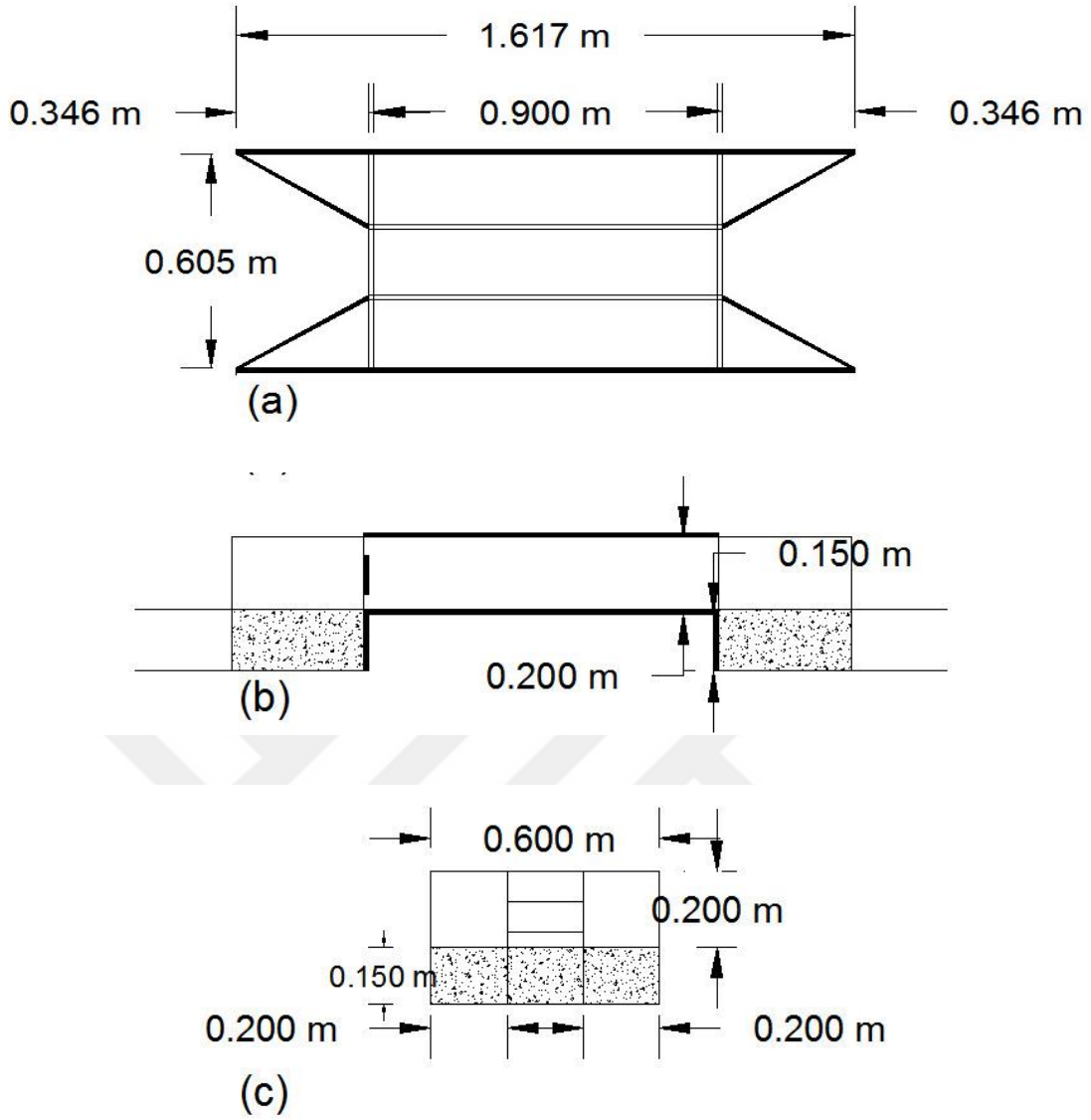

Figure 3.5 Culvert model (a) plan (b) section (c) inlet view

3.2.3 Material properties

In this research that is done by Sayana (2015), for experimental tests two different sediment sizes were used. The finer sediment with the median grain size being (d_{50}= 0.85 mm) with standard deviation σg=1.37, (d_{50}= 2.0 mm) with σg=1.23 and the specific gravity 2.65 (g/cm^3) was used. The sieve analysis for all sediment types were performed and shown in Figure 3.6. Previous to each test, the bed at the inlet and outlet was levelled to the elevation of the culvert invert. Before the tests were begun, the sediment was slowly saturated from the upstream and downstream sides of the culvert.

The sand bed saturated gradually to avoid any air voids and obtained constant density. The tests were performed under an open channel. Each single run is identified by the sand type (S), the blocking condition (B), unsteady flow conditions (U), and the trial number for each set. For example, S1 represents sand type 1 (d_{50} =0.85 mm) and S2 represent sand type 2 (d_{50}= 2 mm). B0 is used for tests in non-blocked condition and B40 used for partially blocked conditions.

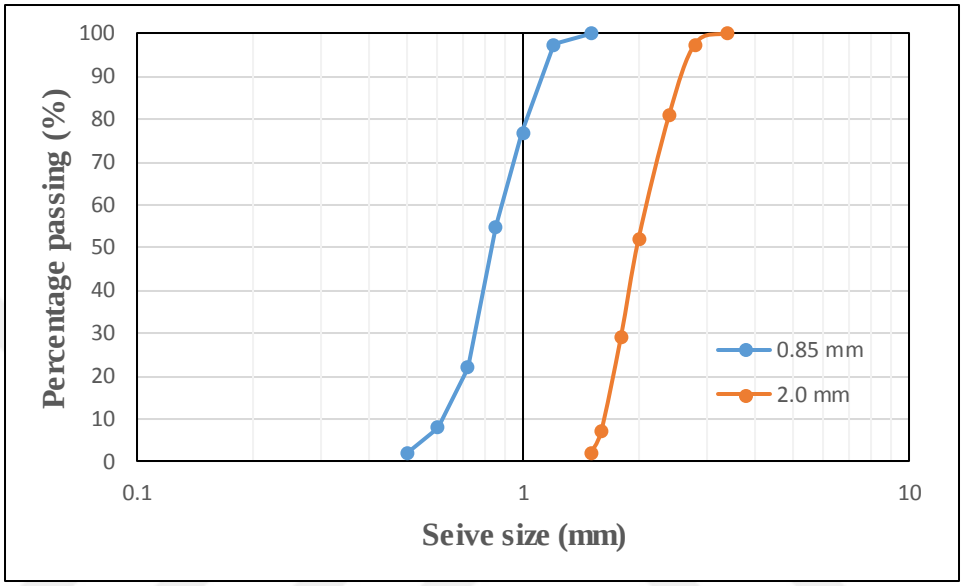

Figure 3.6 Sieve analysis of sediment

3.3 Computational Fluid Dynamic (CFD)

It takes little more than a brief look around to recognize that fluid dynamics is one of the most important of all areas and especially for physics-life as known it would not exist without fluids, and without the behavior that fluids exhibit. Fluid dynamics is the branch of applied science that is concerned with the movement of liquids and gases. These movements are generally referred to as flow and a concept that describes how fluids behave and they interact with their surrounding environment. Generally, Fluid flow is commonly studied in one of three ways; experimental fluid dynamics, theoretical fluid dynamics or numerically computational fluid dynamics (CFD).

Computational fluid dynamics CFD is the science of predicting fluid flow, heat transfer, mass transfer, chemical reactions, and related phenomena by solving the mathematical equations which govern these processes using a numerical process. Also, CFD is a method of simulating a flow process in which standard flow equations such

as the Navier-Stokes and continuity equations are capable of displaying turbulent solutions and solved for each computational cell, these equations are the basis for essentially all CFD codes. the CFD simulations of the flow field were accomplished after searching for the optimum turbulence model and mesh size for the problem. In short, turbulence cannot be ignored in numerical flow modeling. Using CFD software is in many ways similar to setting up an experiment. If the experiment is not correctly set up to simulate a real-life situation, then the results will not reflect the real-life condition and vice versa. The user must decide what things are important and how they should be represented. It is essential to ask a series of questions, including: It is important to ensure that the problem being modeled represents the actual physical situation as closely as possible. CFD is quickly becoming the dominant technique of flow analysis, especially when used for comparison with experimental work. However, it has more significant in aspect measuring scour hole in culvert shape numerically and the advantage CFD is:

- Substantial reduction of lead times and costs of new designs.
- Ability to study systems where controlled experiments are difficult or impossible to perform.
- Ability to study systems under hazardous conditions at and beyond their normal performance limits.
- Practically unlimited level of detail of results.

In this study, by Flow-3D software a numerical modeling was created, which developed by Flow Science Incorporation to simulate a numerical model and compare with experimental results. Flow-3D software simulation worked as the other software in CFD.

3.3.1 Flow-3D process

To analyze the scour formation in the outlet of box culvert, physical modeling is the best method because of that experiments are generally done by reducing the size of the setup. However, it is very costly and required a considerably long time. An alternate way to analyze the flow field is to apply simulations under experimental conditions. Flow-3D software-based simulation model can be used as an analysis tool for computing the scour hole under unsteady flow conditions (Pati, V. V. R. 2010)

In Flow-3D, there are five turbulence models to solve turbulence. These are; Prandtl's mixing length model, one-equation (k) model, two-equation (k-ε) model, Renormalized group (RNG) model and Large Eddy Simulation (LES) model as shown in Figure 3.7. In this section, two of these models were used for turbulence modeling. The RNG model is a development model of the standard k-ε model (Yakhot and Orzsag, 1986). The model is based on Reynolds averaging. The RNG model uses equations similar to the equations for the $k-\varepsilon$ model. However, the equality constants empirically found in the standard k - ε model are explicitly derived in the RNG model. Generally, the RNG model has wider applicability than the standard $k-\varepsilon$ model in particular, it is known that the RNG model more accurately describes flows with low intensity turbulence and a stronger shear region (Flow-3D User Manual, 2012).

This is a result from different studies which revealed RNG which is a good selection model for prediction of the average flow field of the turbulence model and close to the observed result (Anu and Jennifer, 2011).

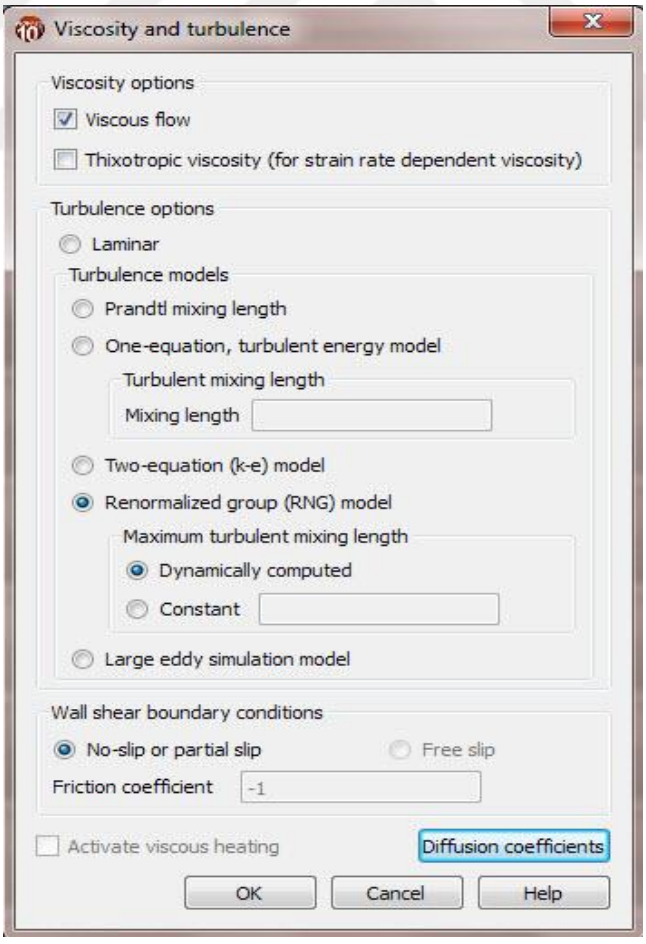

Figure 3.7 In Flow-3D, there are five empirical equations for turbulent model

The RNG k - ε model was derived by extending the hard statistical method (it is called renormalized group theory). It is officially related to the standard k - ε model, but the subsequent improvement:

- In ε equation the RNG theory has additional term that greatly improves the accuracy for speedily strained flows.
- The influence of vortices on turbulence contributes to the RNG model, improving the accuracy of the swirling flow.
- The RNG model implements the analysis method of the turbulent Prandtl number, and the standard k-ε model is a user defined constant value
- The standard k-ε model is a high Reynolds number model, but the RNG model implements an active viscosity analytic differentiation method with low Reynolds number effect.

The above features make the RNG k - ε theory more accurate and reliable for a wide variety of flows compared to the flow of the standard k - ε model (Flow-3D User Manual, 2012).

Flow-3D is a commercial CFD package with special modules intended for hydraulic engineering applications. Despite using a structured orthogonal grid, by the application of the fractional area/volume method (FAVOR), it can model complex geometries, which allows a rectangular computational cell to be partially blocked by an obstacle. By the Volume-of-Fluid (VOF) method Sharp free surface is modeled. Flow-3D has also unique capabilities to model local scour, as detailed by (Hirt, et al. 1981).

3.4 Numerical modeling in Flow-3D

Flow-3D program is the best software simulation to expressing the flow and what happens to the scour formation, representing a study of the program efficiency and flow corresponds to the reality of true expression and its ability in represent of flow and study its properties has been applied to some laboratory models (Abdelnasser, 2015). The scour equations based on experimental data and the scour prediction methods data do not necessarily give rational results with regard to site conditions (Mueller, D. S. et al. 2002), and also similarly for comparing between numerical and experimental work. Results from an earlier study using Flow-3D by Abdelaziz et al (2010), Overall results had a reasonable agreement between predicted results and the

scour bed profile, the maximum scour depth and the maximum deposition measurements after several minutes of the simulation time.

3.4.1 Physical options in Flow-3D

Figure 3.8 present the various physical option in Flow-3D software. there are three important parameter involved with this study for simulating the numerical model and getting accurate data for scour formation.

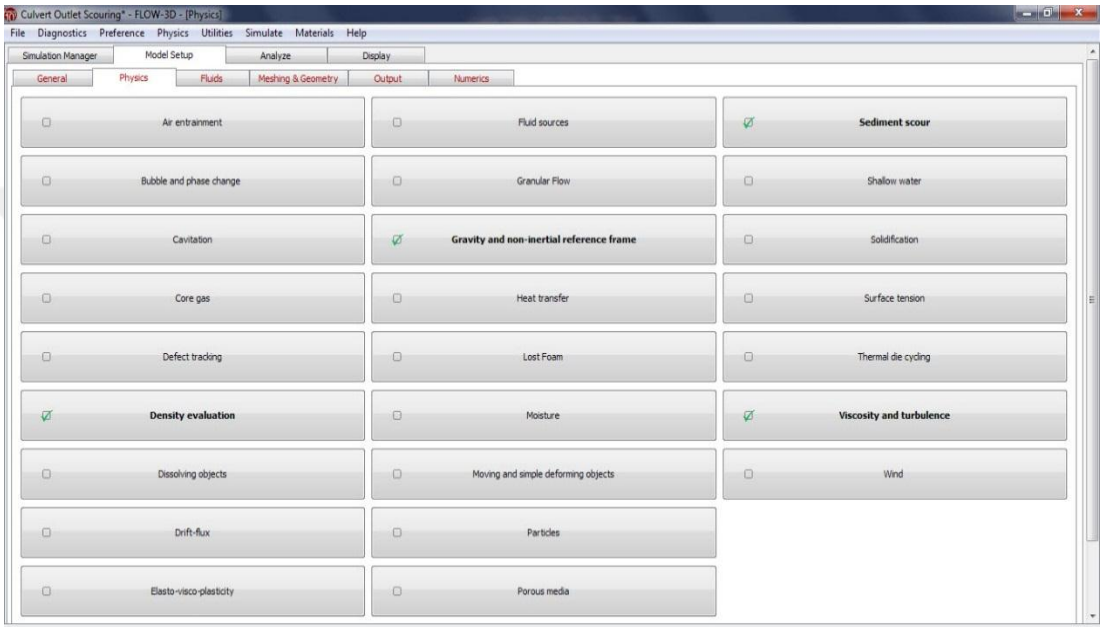

Figure 3.8 Physical options in Flow-3D

The gravity option activated with the vertically downward or z-direction gravitational acceleration component set to negative value 9.81 m/s^2.

The sediment scour option was activated as shown in Figure 3.9. The sediment scour option several parameters, in this study, the inputted parameters were the sediment martial used with two different median grain size (d_{50}=0.85 mm) and (d_{50}=2.0 mm with mass density 2650 kg/cm^3, drag coefficient 0.5, entrainment coefficient 0.018, bed load coefficient 8.0, angle of repose 30 degree, several inputted parameters depend on (Flow-3D user manual, 2012).

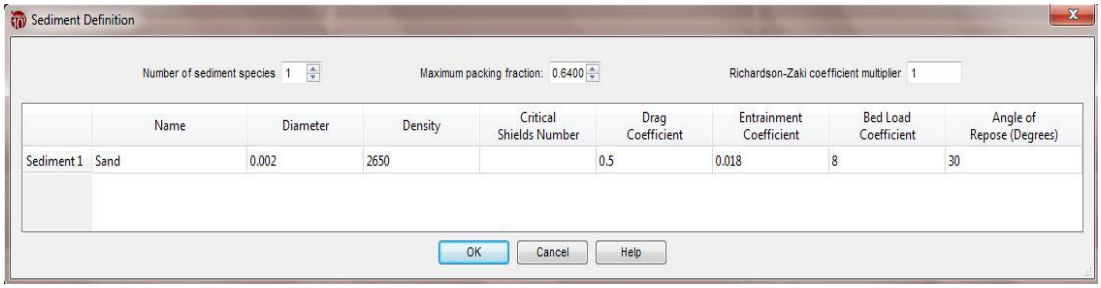

Figure 3.9 Sediment scour option

Finally, the viscosity and turbulence options were also activated. In this study, two different empirical equations RNG and $k-\varepsilon$ ware selected as shown in Figure 3.7.

3.4.2 Geometry

For obtained accurate simulated data in Flow-3D, it must be designed exact geometry model fit to the physical model and imported to the Flow-3D. Flow-3D geometry model was an element of a numerical model. Simple geometry model can be designed by Flow-3D software directly but when complex model consists of subcomponents, Subcomponents can be thought of as building blocks of geometry. They represent the holes, complements and solid objects that may be combined in various ways to describe more complex forms. Properties are typically not defined at the subcomponent level; only the geometry. Subcomponents may be defined using stl files in Flow-3D. in this study, the model designed in Auto-Cad software in 2D with a detail dimensions and extrude to 3D then, exported as a stereolithographic (stl) format. The stl file was directly imported into the Flow-3D, but the coordinates of the original point should be known in Auto-Cad or other software as shown in Figure 3.10.

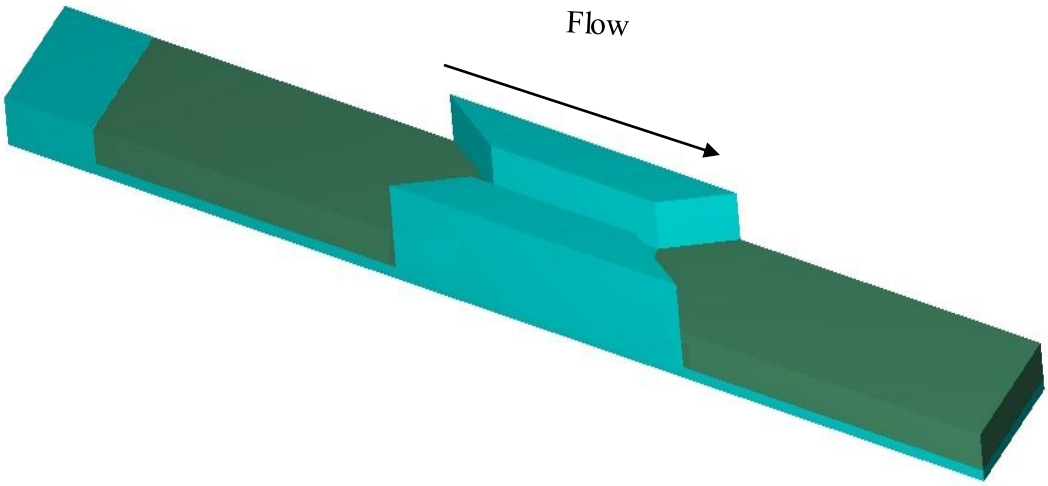

Figure 3.10 Culvert geometry in Flow-3D

3.5 Meshing

CFD applies numerical methods called discretization to develop approximations of the governing equations of fluid mechanics in the fluid region of interest. Domain is discretized into a finite set of control volumes or cells. The discretized domain is called the grid or the mesh. The mesh is a subdivision of the flow domain into a relatively small parts of the CFD numerical model, and the minimum part of the divided called cells. Since the cell size of each block mesh can affect simulation time and accuracy of results, it is more important to minimize the cell numbers, including sufficient resolution and appropriate flow details. Since mesh processing is a very important step in CFD modeling, much attention is required

Mesh generation for modeling complex shapes is done by FAVOR^{TM} technique with orthogonal meshes defined in Cartesian coordinate system or cylindrical coordinate system available in flow 3D. Since only orthogonal meshes are allowed to simplify the development of the mesh region in Flow-3D, baffles and obstacles are embedded in the orthogonal mesh and allow mesh and geometry characterization, so the effect on mesh generation It does not give. In Flow-3D some different mesh block used, included:

- **Uniform mesh** in all directions have a uniform cell sizes. These may be generated by supplying only the cell size in each coordinate direction, the total number of cells, or only a specific number of cells.

- **Non-uniform meshes** in some cases, it may be beneficial for the mesh to stretch the cell in a particular direction. In order to create this more complex mesh, an intermediate mesh plane is defined. In these places you can adjust the spacing of the grid lines by specifying the cell size or number of cells between specific mesh faces.
- **Multi-block meshes** A single block mesh is not valid for very complex geometries because one block mesh contains too many cells (Flow-3D User Manual, 2012).

As shown in Figure 3.11 reveals that, for this study uniform mesh was used and 3D computational domain that is 550 cm long, 60.5 cm width and 43 cm high. For all-directions cell size was 2.0 cm. The number of cells in all blocks were 244004, uniform cells were used.

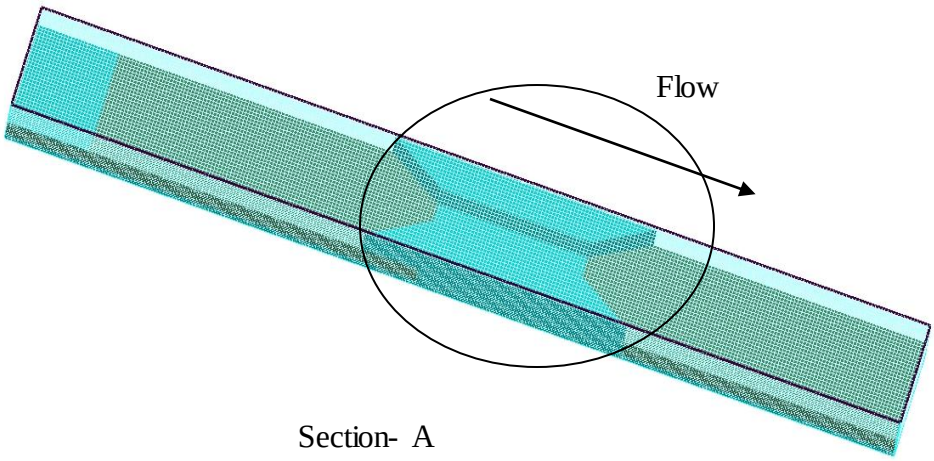

Section- A

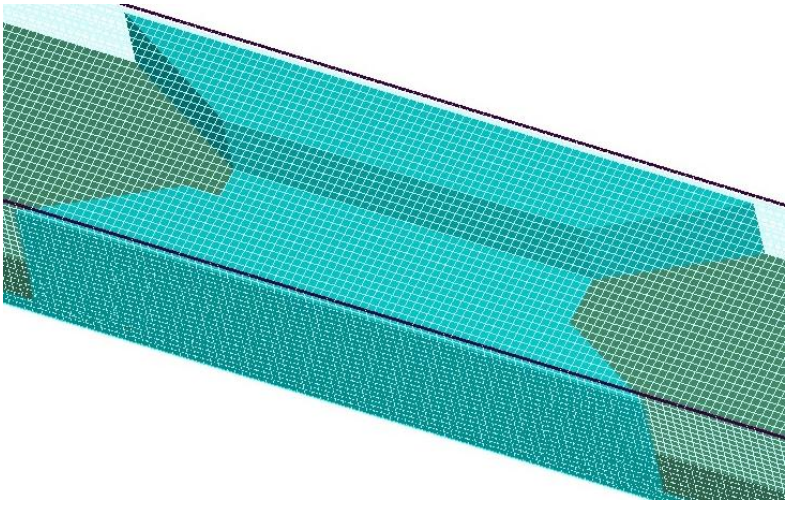

Figure 3.11 Representation of the geometry meshing of 3D model

3.5.1 Boundary Conditions

The equations governing the motion of the fluid flow are classified into categories of initial boundary value problem. In other words, the solution needs to be found at the first time and boundary. Therefore, it is very important that the solution assumed at the boundary is a good approximation at this position. The boundary condition is set for each mesh block in the boundary branch of the tree structure on the mesh operation panel.

Figure 3.12 shows the boundary condition types in Flow-3D. Each type is used for specific conditions of the model.

Figure 3.12 Type of boundary conditions in Flow-3D.

Figure 3.13 shows the boundary conditions on the x-y-z planes for the simulated model, as shown the maximum and minimum y direction was labeled as wall. The minimum z boundary of the bottom is designated as the wall boundary while the maximum z boundary is designated as the pressure boundary and the zero fluid fraction. The boundary condition in maximum x direction was designated outflow while in minimum x boundary specified the volume flow rate. In this study, the flow worked under unsteady conditions, mean that the flow rate changed with time. The stepwise hydrograph for tests must be imported in minimum x boundary condition for volume flow rate to obtained accurate result when compared with experimental result as shown in Figure 3.14.

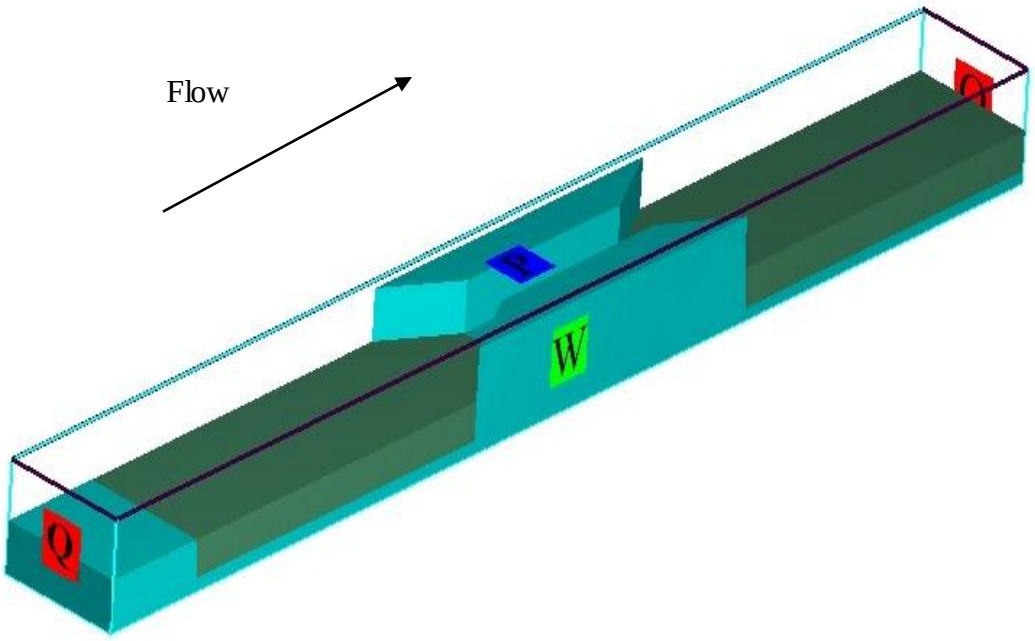

Figure 3.13 Configuration of boundary conditions

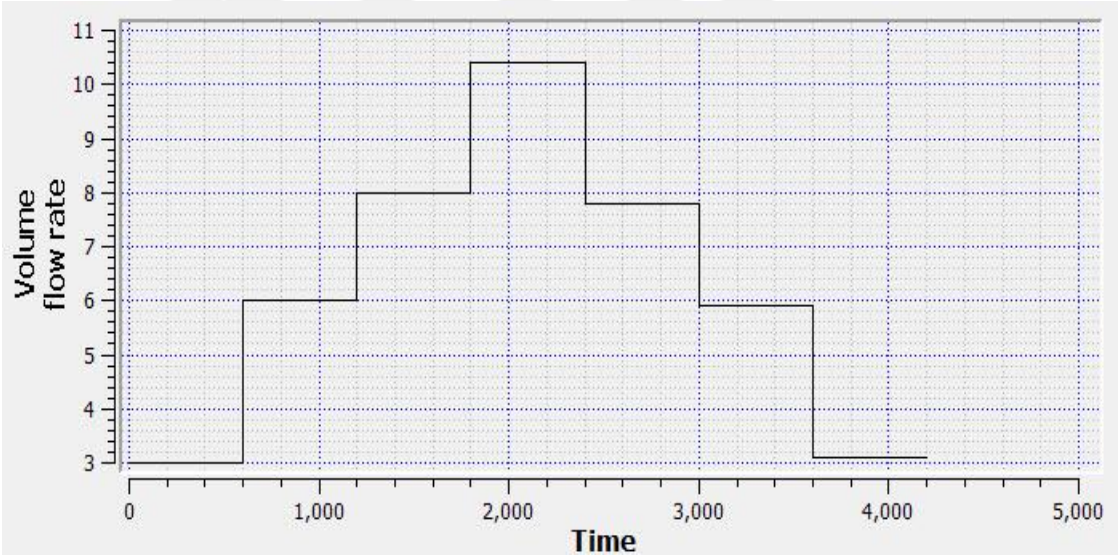

Figure 3.14 Stepwise hydrograph for tests in Flow-3D

CHAPTER 4

RESULTS AND DISCUSSION

4.1 General introduction

In this chapter, simulated results that obtained from Flow-3D software of box culvert model and formation of scour at the outlet are compared with laboratory results to evaluate the accuracy of the numerical model. Laboratory box culvert was carried out for two conditions; the non-blocked situation and the partially blocked condition with the blockage ratio of 40% for this destination used two different sizes of plates and the finer sediment was used in this study with the median grain size being 0.85 mm and 2.0 mm, the flow conditions in the laboratory were unsteady. It is mean that the flow rates during the time were changed. The performance of the numerical model based on renormalization group (RNG) and in the last case also used k-ε with RNG to comparing with experimental results. The aim of this investigation is to evaluate the numerical simulations based on the different percent of blockage and fine sediment sizes under unsteady conditions. In this section, results will be presented as the comparisons of the simulation and experimental results, scour hole creation at a different time with different flow rate. In this section, calculated the comparison between center line scour profile, maximum scour depth and location of maximum scour depth, in addition determining the water surface profile, location of vorticity and direction of vectors for both types of bed material.

4.2 Comparison between numerical and experimental results for first set (d_{50}=0.85 mm)

The comparison between the results attained from numerical work and experimental results presented in Table 4.1. In this section, the prosecution of the CFD model based on RNG and compared with experimental results. It shows that two tests were done US1B0 and US1B40 with the first type of fine sediment (d_{50}=0.85 mm) with the

different blockage ratio. Depend on using stepwise hydrographs for two-bed materials the value of flow rate proportionally changed with time. Each set was run in partially blocked and non-blocked conditions. In the first set with the finer sediment (d_{50}=0.85 mm), each time step takes 10 minutes and the different value of peak flow was change after this time as shown in Figure 4.1. Measuring of the scour hole was done for each time step and was conducted at the end of each time step. This means that after about 8 minutes of changing the flow rate the scour profile was recorded.

Table 4.1 Comparison results between numerical and physical model

Test	d_{50} (mm)	B (%)	Flow rate (Lt/s)	t (min)	X_{sm} (mm)	d_{sm} (mm)	X_{sm} (mm)	d_{sm} (mm)
					Experimental result		CFD result (RNG)	
US1B0	0.85	0	3	10	300	11.2	300	11.3
		0	6	20	200	20.5	200	20.6
		0	8	30	200	36.6	200	41.1
		0	10.4	40	250	49.3	250	58.4
		0	7.8	50	200	52.8	200	63.5
		0	5.9	60	300	56.2	300	70.5
		0	3.1	70	300	56	300	70
US1B40	0.85	40	3	10	150	38.7	150	59
		40	6	20	200	35.7	200	63
		40	8	30	200	41.4	200	71.5
		40	10.4	40	300	56.4	300	79
		40	7.8	50	350	55.7	350	82
		40	5.9	60	300	57.1	300	87
		40	3.1	70	300	56.5	300	85

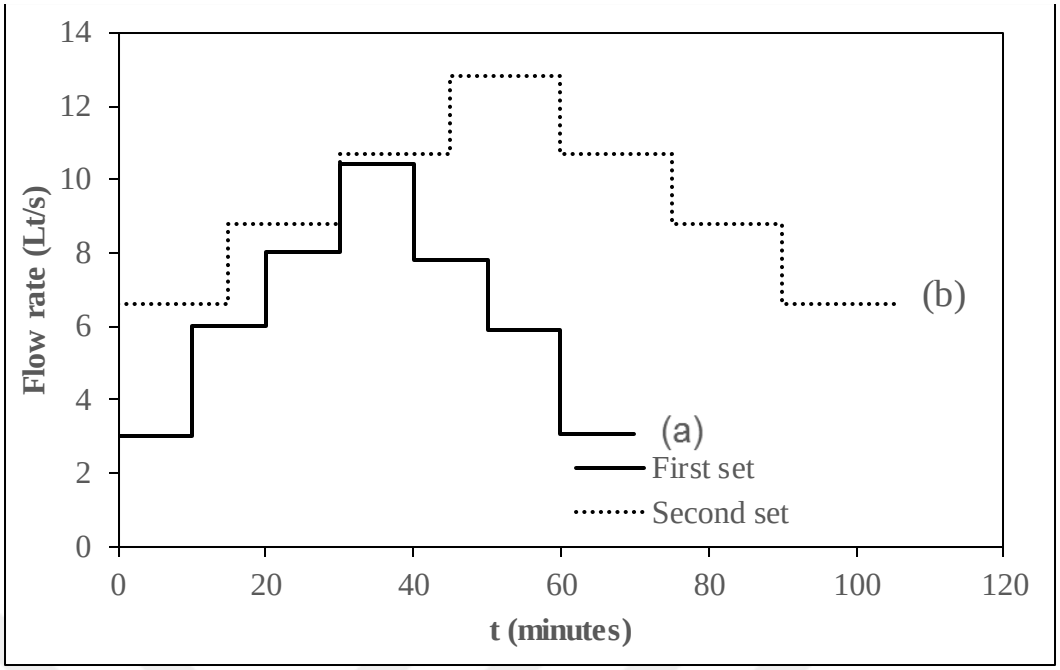

Figure 4.1 Stepwise hydrograph for tests both in partially blocked and non-blocked conditions; First set: hydrograph for material with d_{50}=0.85 mm, Second set: hydrograph for material with d_{50}=2.0 mm

4.2.1 Centerline profiles along horizontal axis

Figure 4.2a to Figure 4.2g show the creation of scouring profile under an unsteady flow in each step and compared the scour profile between CFD results and physical results, also they show that the Flow-3D results for bed profile at each time step in partially blocked and non-blocked conditions with the median grain size (d_{50}=0.85 mm) were compared with experimental work. In the first step of the hydrograph Figure 4-2a, the experimental measurement for scour depth in this point for the non-blocked condition is around 0 and for partially blocked around 20 mm while obtained these results by Flow-3D software around 0 for non-blocked condition and 31 mm for partially blocked condition. In the flow rate 6 Lt/s, the observed measurement for scour depth at the first point for non-blocked condition was around 5 mm and for partially blocked condition was about 21 mm, the various percent between both situations is about (76%), while numerical results for non-blocked situation was around 10 mm and for partially blocked condition was around 35 mm, the different percent between both conditions was about (71%). It is revealed that by increasing the rising limb, in another word by increasing the blockage ratio at culvert inlet the initiation of scouring happens in the initial steps of the hydrograph while for the non-blocked condition it still takes

a few more steps Figure 4.2b. Moreover, it is shown that the overall results from the Flow-3D close to the experimental results and comparison had a good agreement. Generally, the difference between the scour amounts in a non-blocked and a partially blocked culvert is more significant and causes for this phenomenon is that by increasing the blockage ratio the flow velocity is increased, it is mean that velocity proportionally changes with scouring amount.

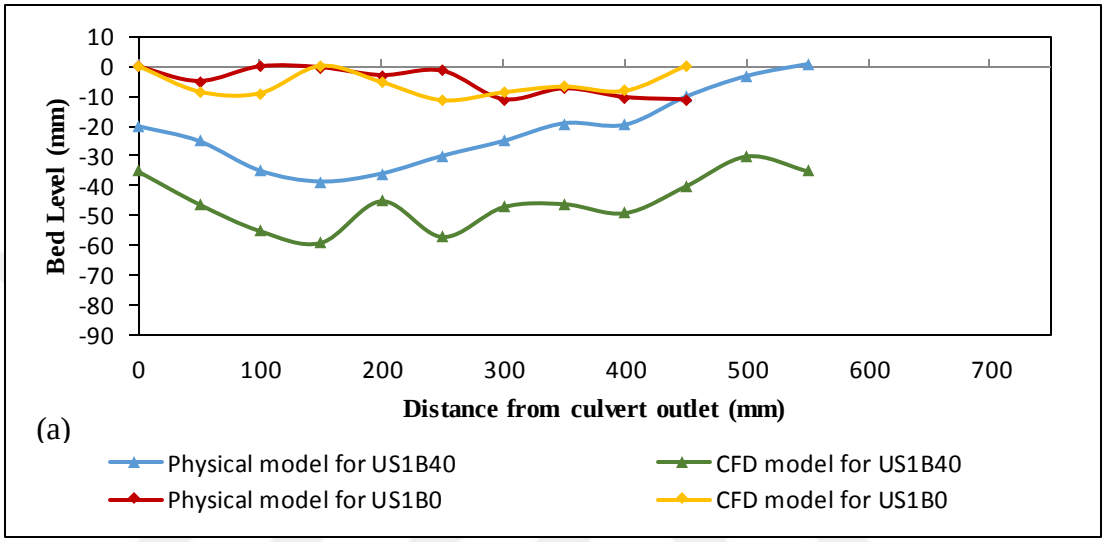

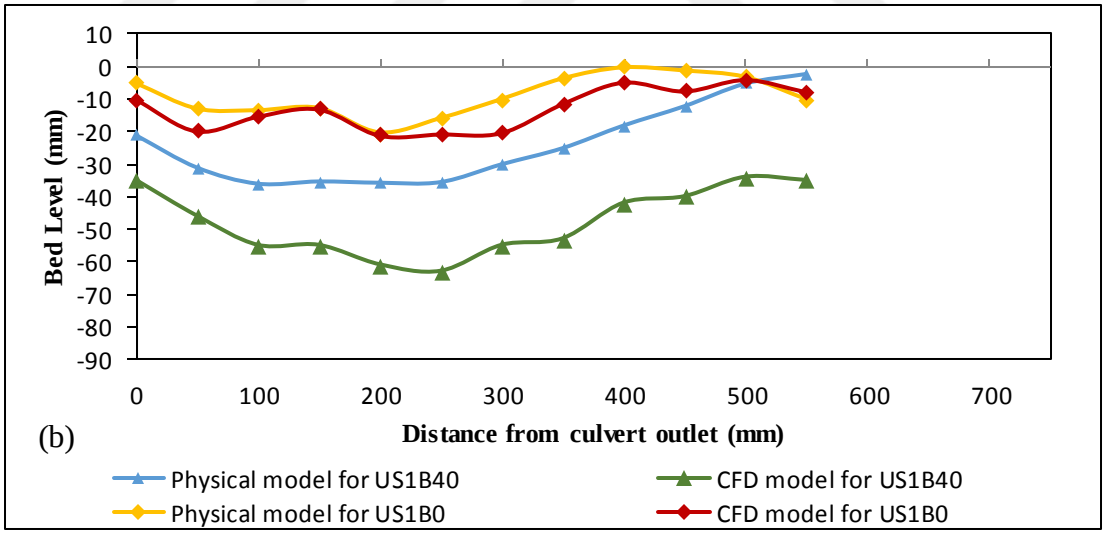

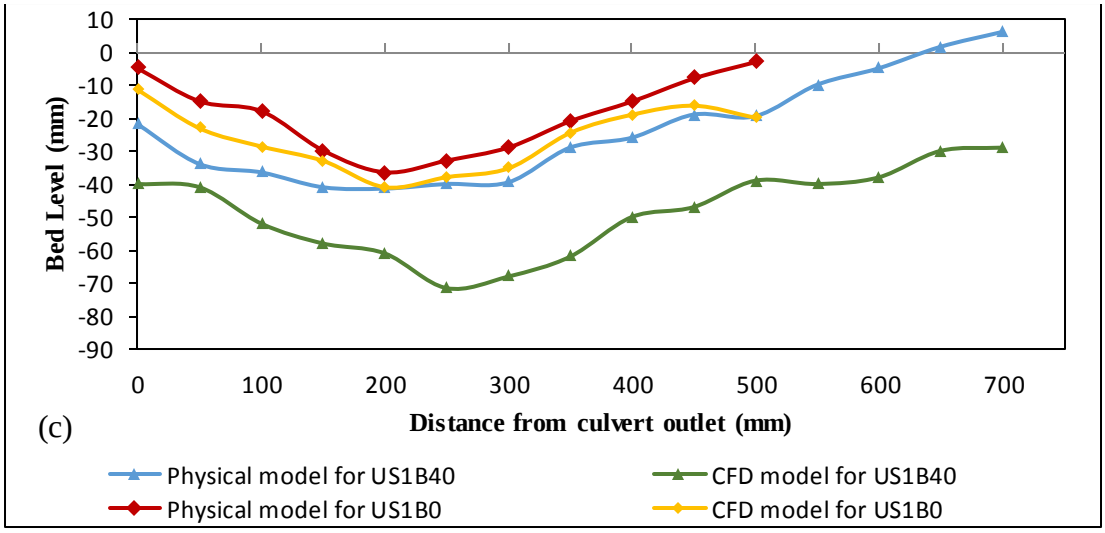
Bed Level (mm)
10
0
-10
-20
-30
-40
-50
-60
-70
-80
-90
0
100
200
300
400
500
600
700
Distance from culvert outlet (mm)
Physical model for US1B40
CFD model for US1B40
Physical model for US1B0
CFD model for US1B0

(c)

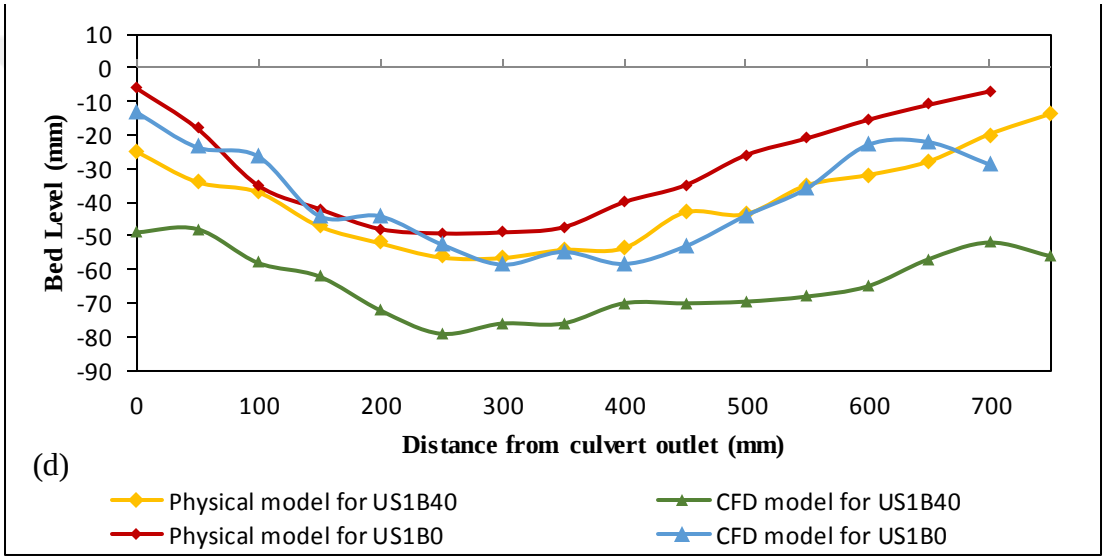
Bed Level (mm)
10
0
-10
-20
-30
-40
-50
-60
-70
-80
-90
0
100
200
300
400
500
600
700
Distance from culvert outlet (mm)
Physical model for US1B40
CFD model for US1B40
Physical model for US1B0
CFD model for US1B0

(d)

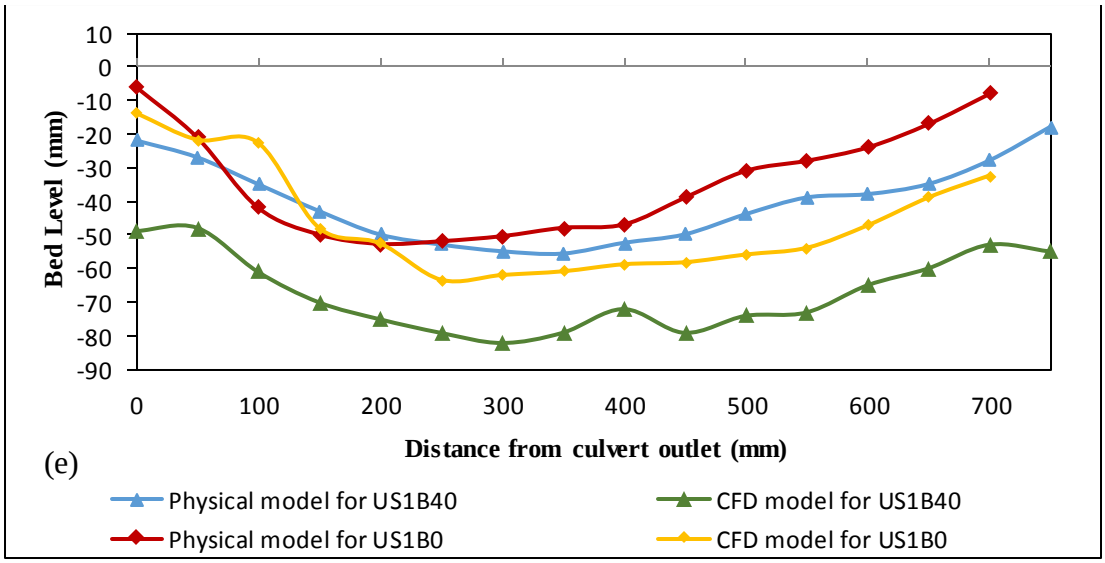
Bed Level (mm)
10
0
-10
-20
-30
-40
-50
-60
-70
-80
-90
0
100
200
300
400
500
600
700
Distance from culvert outlet (mm)
Physical model for US1B40
CFD model for US1B40
Physical model for US1B0
CFD model for US1B0

(e)

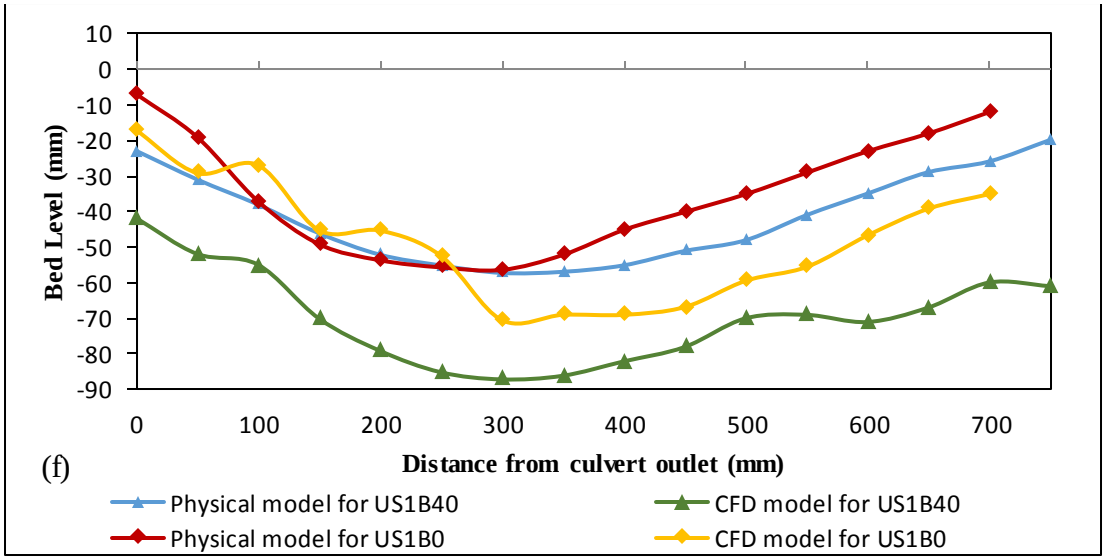

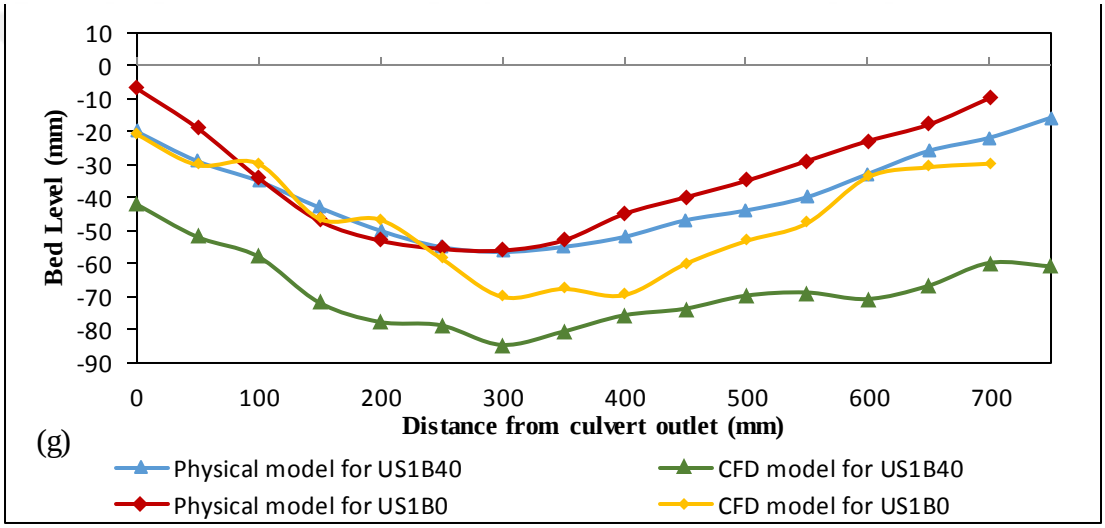

Figure 4.2 Comparison between CFD model and physical model for scour profile with the first set of fine sediment: (a) Flow rate is 3 Lt/s at 10 minutes (b) Flow rate is 6 Lt/s at 20 minutes (c) Flow rate is 8 Lt/s at 30 minutes (d) Flow rate is 10.4 Lt/s at 40 minutes (e) Flow rate is 7.8 Lt/s at 50 minutes (f) Flow rate is 5.9 Lt/s at 60 minutes (g) Flow rate is 3.1 Lt/s at 70 minutes

4.2.2 Maximum scour depth

In Table 4.1 shown that the maximum scour depth is developed in each step of the hydrograph. The results show that the progress of maximum scours depth when attained by Flow-3D and compared with experimental results. Figure4.3 shows that the evolution of normalized maximum scours depth with time for the first set.

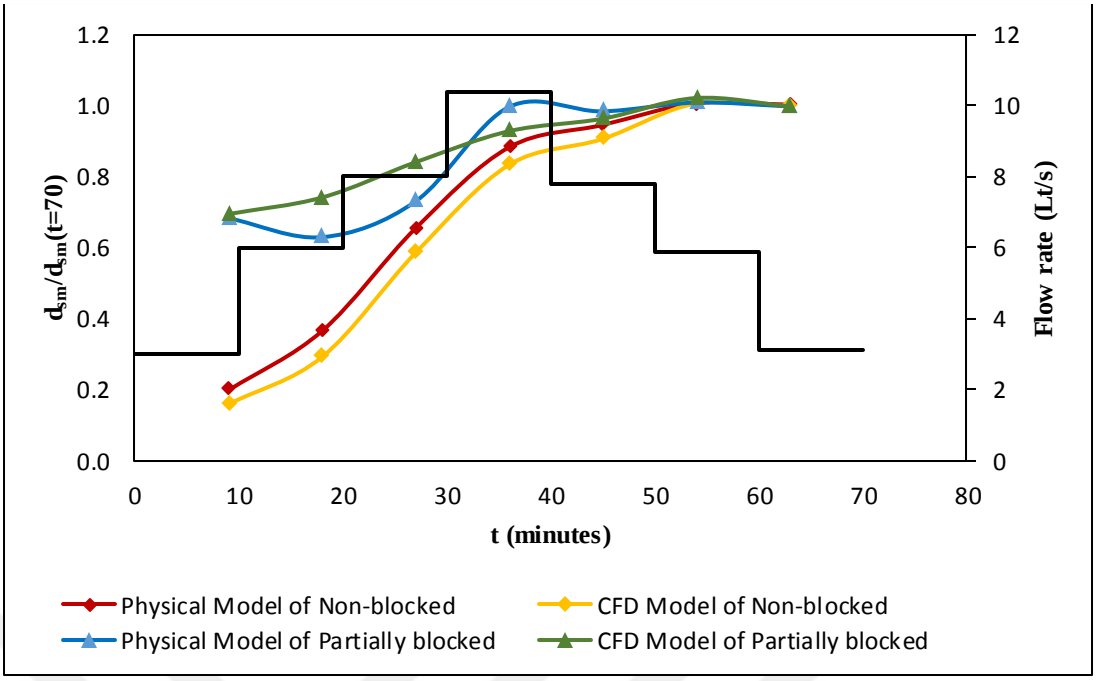

Figure 4.3 Comparison between CFD model and physical model for evolution of normalized maximum scour depth with time for the first set.

As was shown in the graph the numerical investigation contains several maximum scour depths while maximum scour depth of the hydrograph at each step is normalized with the maximum scour depth at the final step of hydrograph ($d_{sm}(t=70)$) and the same procedure was used for observed work. In both experimental and numerical investigation for all flow rates, it can be seen that during the time maximum scour depth happened withal the normalized scour depth of the non-blocked culvert had less significantly than the normalized scour depth of partially blocked. The procedure of starting the scour hole and reaching to the final depth of scouring ($d_{sm}(t=70)$) happens less progressively in the non-blocked culvert compared to the partially blocked culvert. For example, at the observed investigation for discharge 6 Lt/s it can saw that the maximum scour hole had formed in non-blocked condition is around 36% and the maximum scour hole had formed in partially blocked situation around 63%, as shown in the previous example whether compared to the Flow-3D model the maximum scour hole had formed in non-blocked condition is around 29% While the maximum scour hole had formed in partially blocked situation around 74%. In experimental work for peak flow 10.4 Lt/s, in the final step ($d_{sm}(t=70)$) was formed 88% the maximum scour depth for the non-blocked condition while maximum scour depth developed for peak flow was 98% for partially blocked condition at the final step. Despite these results

when compared with CFD model for peak flow, in non-blocked condition 83 % of the maximum scour depth at final step ($d_{sm}(t=70)$) was formed during the rising limb of hydrograph while in the partially blocked condition the growth of maximum scour depth at peak flow was 93 % of the maximum scour depth at the final step. Moreover, it is more important in this section when comparing the experimental with numerical study for founding maximum scouring amount in the outlet of the culvert. The maximum scour depth was recorded at flow rate 5.9 Lt/s for experimental and numerical model in both conditions as shown in Figure 4.1f. These comparisons are exhibited that the changed between cases are proportioned and the good agreement happened between experimental and numerical results. Finally, it showed that the amount of maximum scour proportionally changed with blockage ratio.

4.2.3 Location of maximum scour depth

Table 4.1 presented the comparison of the results for each experimental and numerical data for the location of maximum scour depth along the flow direction (X_{sm}) with hydrograph steps. It shows the location of maximum scour depth when obtained by Flow-3D and compared with experimental results. Depicted in Figure 4.4 is the location of maximum scour depth along the flow direction (X_{sm}) with hydrograph steps and shows the comparison between numerical and experimental result for partially blocked and non-blocked condition. As was depicted in the graph the experimental investigation contains several location of maximum scour depths while location of maximum scour depth of the hydrograph at each step is normalized with the location of maximum scour depth at the first step of hydrograph ($X_{sm}(t=0)$) and the same procedure was used for numerical work. The ratio $\frac{Xsm(t=40)}{Xsm(t=0)}$ was used for obtaining the exact location of maximum scour. For example, in experimental work for peak flow rate 10.4 Lt/s, in non-blocked condition is 0.83, and for partially blocked condition is 2, while observed in numerical work for non-blocked condition is 1.2, and for partially blocked condition is 1.7. It is indicating the results of Flow-3D is close to the experimental results, and proportionally changed was occurs between them. It is shown that the distance of maximum scour depth from the culvert outlet (X_{sm}) in blocked situation increases. It means that position of the maximum scour hole moves to the culvert outlet during the rising limb of hydrograph. In other words, by increasing

the ratio of blockage and flow rate for partially blocked condition the location of maximum scour hole increased. On the other hand, by increasing the rising limb of hydrograph, culvert outlet and the distance of maximum scour depth were increased.

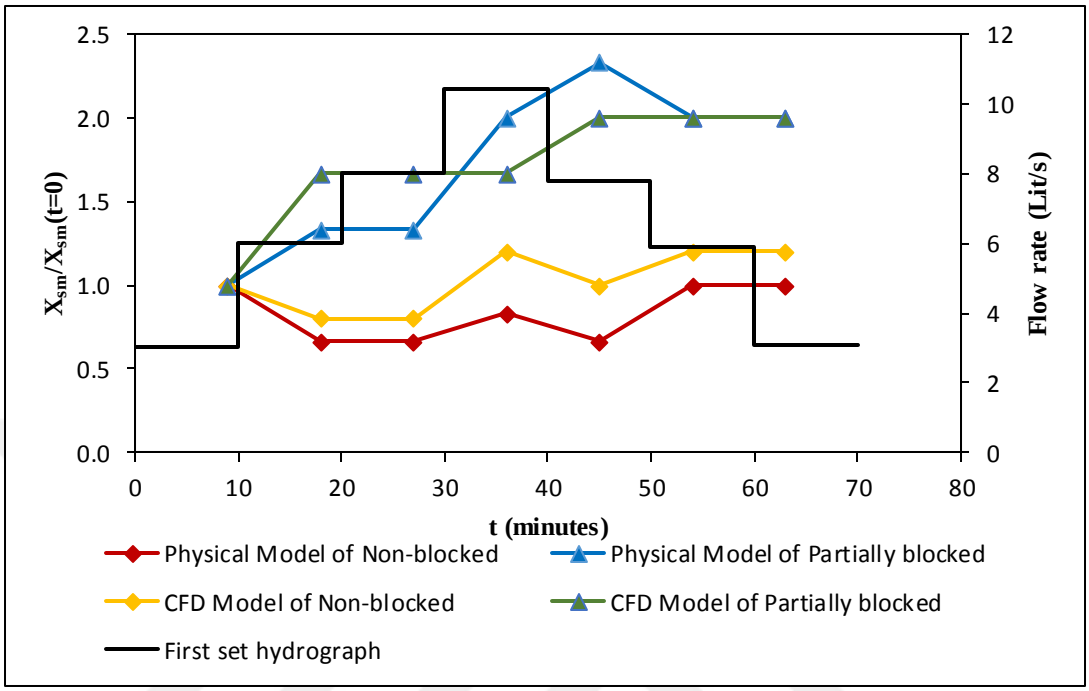

Figure 4.4 Comparison between CFD model and physical model for normalized location of maximum scour depth with hydrograph for the first set

4.3 Comparison between numerical and experimental results for Second set (d_{50}=2.0 mm)

In table 4.2 reveals the comparison between observed results with this results achieved from numerical work. In this part, the application of the CFD model based on RNG was compared to the experimental work, but in the last case used RNG and k-ε for achieved maximum scour depth and compared with experimental results. It shows that two tests were done US2B0 and US2B40 with the second type of fine sediment (d_{50}=2.0 mm) with the different blockage ratio. By using stepwise hydrographs for two-bed materials the worth of discharge changed with time. Each set was run in partially blocked and non-blocked conditions. In the second set, (d_{50}=2.0 mm) each step takes 15 minutes and with the prior set, measuring was done in the last few minutes of each step Figure 4.1. Measuring of the scour hole procedure was done for both numerical and physical model.

Table 4.2 Comparison results between numerical and physical model

Test	d_{50} (mm)	B (%)	Flow rate (Lt/s)	t (min)	X_{sm} (mm)	d_{sm} (mm)	X_{sm} (mm)	d_{sm} (mm)	d_{sm} (mm)
					Experimental result		CFD result (RNG)		CFD result (k-ε)
US2B0	2	0	6.6	15	350	1.3	250	14.6	
		0	8.8	30	350	2.2	200	15.4	
		0	10.7	45	350	7.9	200	18.1	
		0	12.8	60	300	48.8	300	50	
		0	10.7	75	300	49.4	250	63	
		0	8.8	90	300	51.6	300	62	
		0	6.6	105	300	51.1	300	60	
US2B40	2	40	6.6	15	100	0.6	150	13	25
		40	8.8	30	100	8.5	250	23	37
		40	10.7	45	100	31.6	250	42	58
		40	12.8	60	250	43.2	250	64	78
		40	10.7	75	250	48.9	300	69	83
		40	8.8	90	300	48.8	300	68	83
		40	6.6	105	300	48.4	300	68	82

4.3.1 Centerline profiles along horizontal axis by using empirical equation (RNG)

Figure 4.5a to Figure 4.5g reveals the scour profile formation under unsteady flow conditions in each step. In this section, by using numerical simulation from Flow-3D three-dimensional model based on RNG at each time step in non-blocked and partially blocked conditions the results were found and compared to the observed formation of scouring profile. From Figure 4.5a to Figure 4.5b, it depicted that a first and second flow rate of the hydrograph was insufficient to start a movement in sediment for a

physical model in non-blocked condition but for partially blocked situation similarly for first discharge when for second discharge some motion in the sediment was seen, while these results compared to the Flow-3D was exposes the scour happened after 200 mm at outlet of culvert. The noticeable difference of scour was happening in the third step of the hydrograph around 50 mm from culvert outlet. For third flow rate 10.7 Lt/s with fine sediment (d_{50}=2.0 mm) at 50 mm after outlet of culvert, the scour depth at this point for non-blocked condition was around 4 mm and for partially blocked situation was about 25 mm while these results achieved by Flow-3D for non-blocked condition was around 2 mm and for partially blocked condition was about 29 mm as shown in Figure 4.5c. Depicted in Figure 4.5a to Figure 4.5g, the occurrence of scour in centerline along horizontal axis for both numerical and experimental work and indicate the comparison between them. However, the Flow-3D results are not quite similar to the experimental but it gives the closed conclusion for these models.

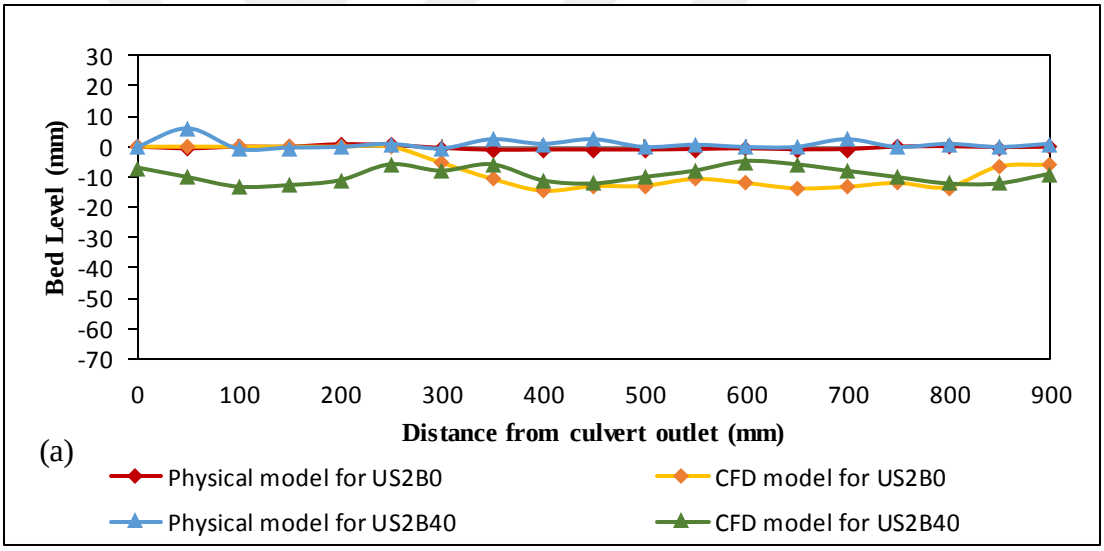

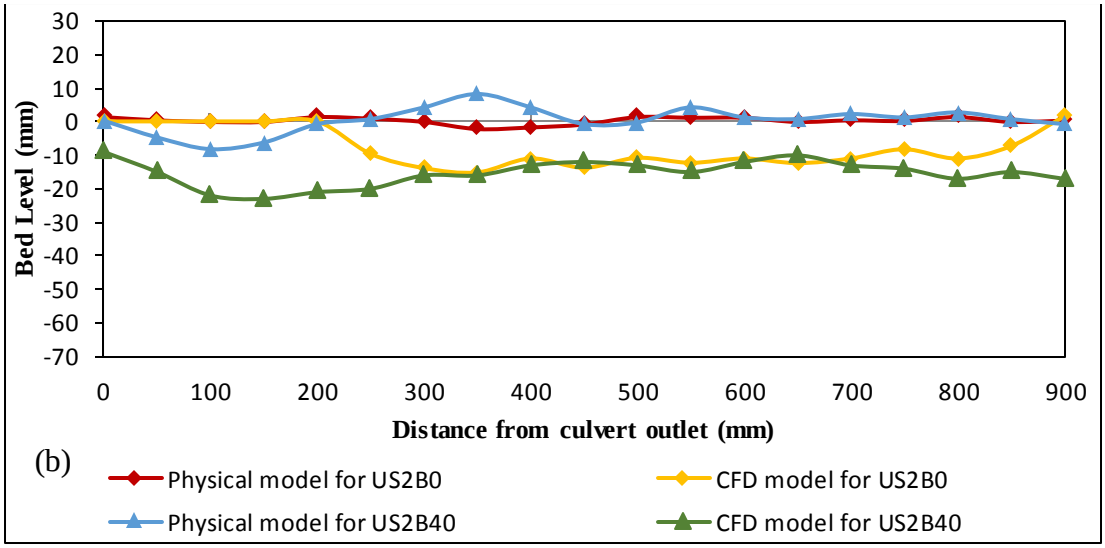
30
20
10
0
-10
-20
-30
-40
-50
-60
-70
Bed Level (mm)
0
100
200
300
400
500
600
700
800
900
Distance from culvert outlet (mm)
(b)
Physical model for US2B0
CFD model for US2B0
Physical model for US2B40
CFD model for US2B40

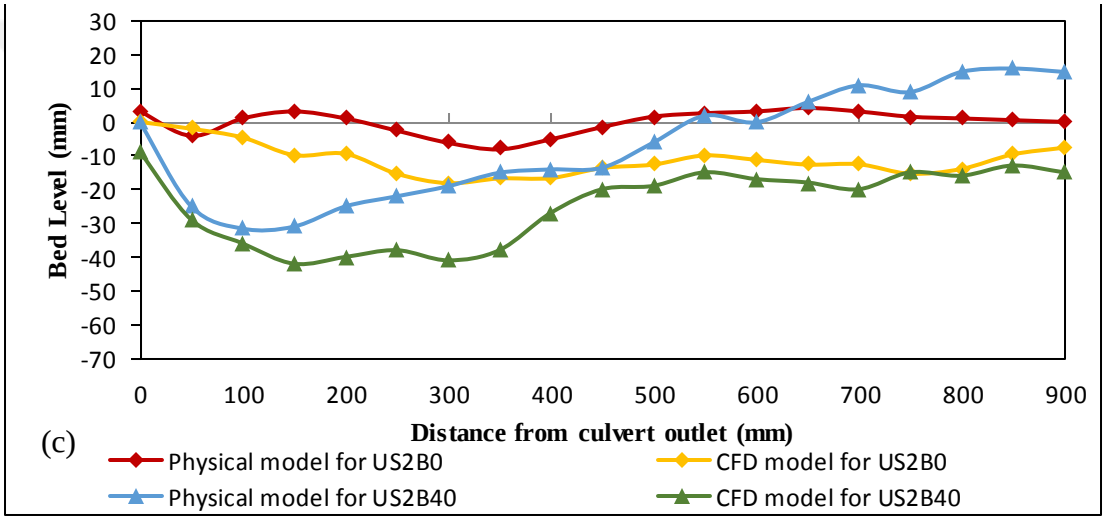
30
20
10
0
-10
-20
-30
-40
-50
-60
-70
Bed Level (mm)
0
100
200
300
400
500
600
700
800
900
Distance from culvert outlet (mm)
(c)
Physical model for US2B0
CFD model for US2B0
Physical model for US2B40
CFD model for US2B40

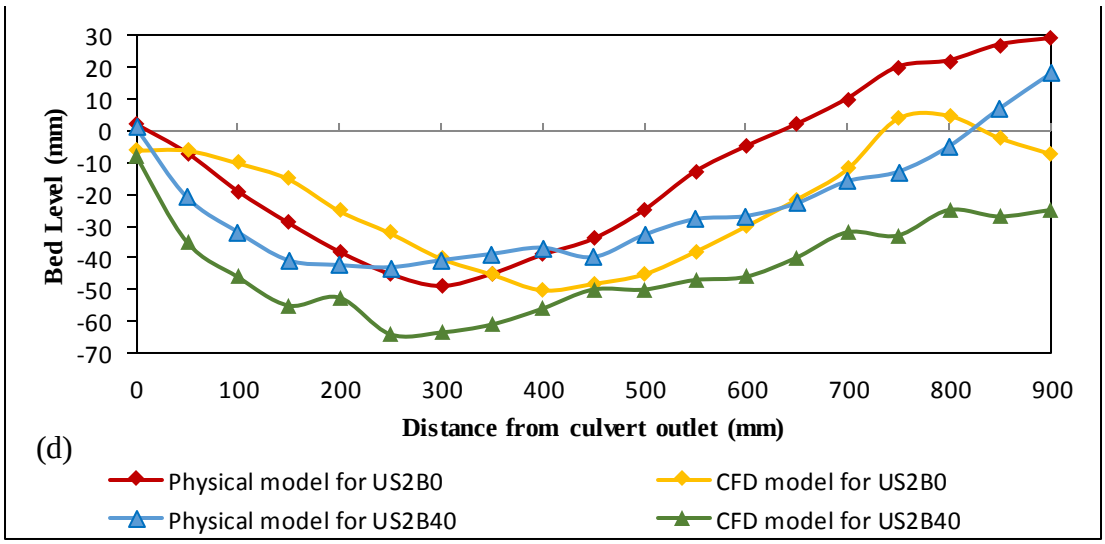
30
20
10
0
-10
-20
-30
-40
-50
-60
-70
Bed Level (mm)
0
100
200
300
400
500
600
700
800
900
Distance from culvert outlet (mm)
(d)
Physical model for US2B0
CFD model for US2B0
Physical model for US2B40
CFD model for US2B40

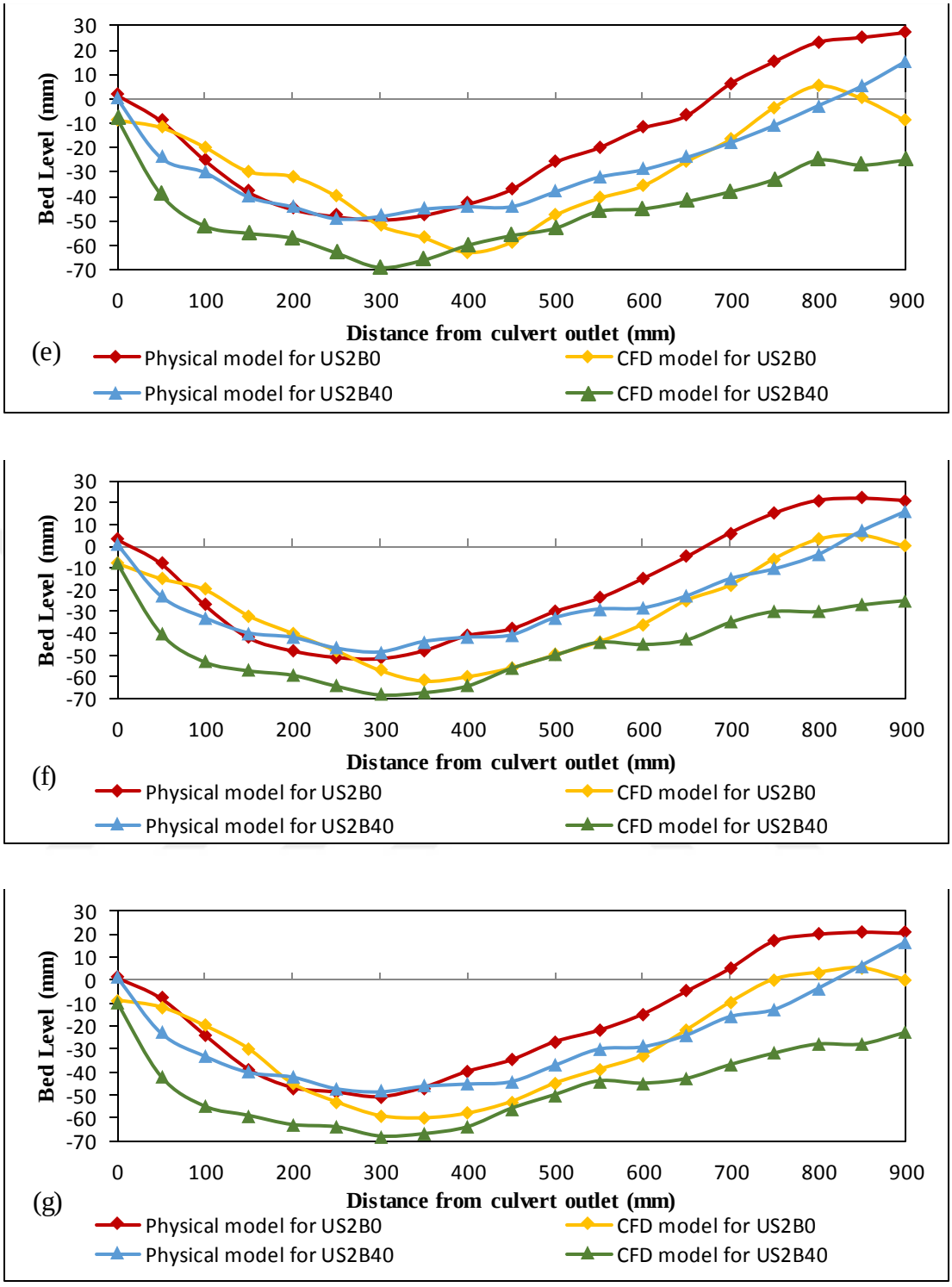

Figure 4.5 Comparison between CFD model and physical model for scour profile with the second set of fine sediment: (a) Flow rate is 6.6 Lt/s at 15 minutes (b) Flow rate is 8.8 Lt/s at 30 minutes (c) Flow rate is 10.7 Lt/s at 45 minutes (d) Flow rate is 12.8 Lt/s at 60 minutes (e) Flow rate is 10.7 Lt/s at 75 minutes (f) Flow rate is 8.8 Lt/s at 90 minutes (g) Flow rate is 6.6 Lt/s at 105 minutes

4.3.2 Centerline profiles along horizontal axis by using empirical equation (k-ε)

As it showed in a previous case for fine sediment (d_{50}=2.0 mm), the empirical equation RNG used in Flow-3D and compared with experimental work. In Table 4.2 presented that in the last case empirical equation k-ε used to achieve maximum scour depth and compared with results that obtained from empirical equation RNG with experimental results. By using stepwise hydrographs for two-bed materials the value of discharge changed with time. It also shown that the results obtained for each time step under partially blocked conditions were run by using k-ε. These results have significant value to attained the different percentage between CFD models for both empirical equations (RNG, k-ε) and compared with experimental work. Figure 4.6a to Figure 4.6g exposes the scour profile development under unsteady flow conditions in each step. In this section, by using numerical simulation from Flow-3D by selecting RNG and k-ε at each time step in partially blocked conditions the results were found and compared to the detected formation of scouring profile. They also depicted that for all steps of the hydrograph flow velocity sufficient to start sediment motion in the early stage of culvert outlet by using k-ε. it is mean that centerline profile along horizontal axis for all steps indicate that, the percentage of maximum scour depth with the movement of sediment particles obtained by choosing k-ε is greater than these percentages achieved based on RNG in the closes point of culvert outlet. Overall results can say that the Flow-3D has a good agreement and results in the acceptable range but RNG closer to experimental if comparing with k-ε.

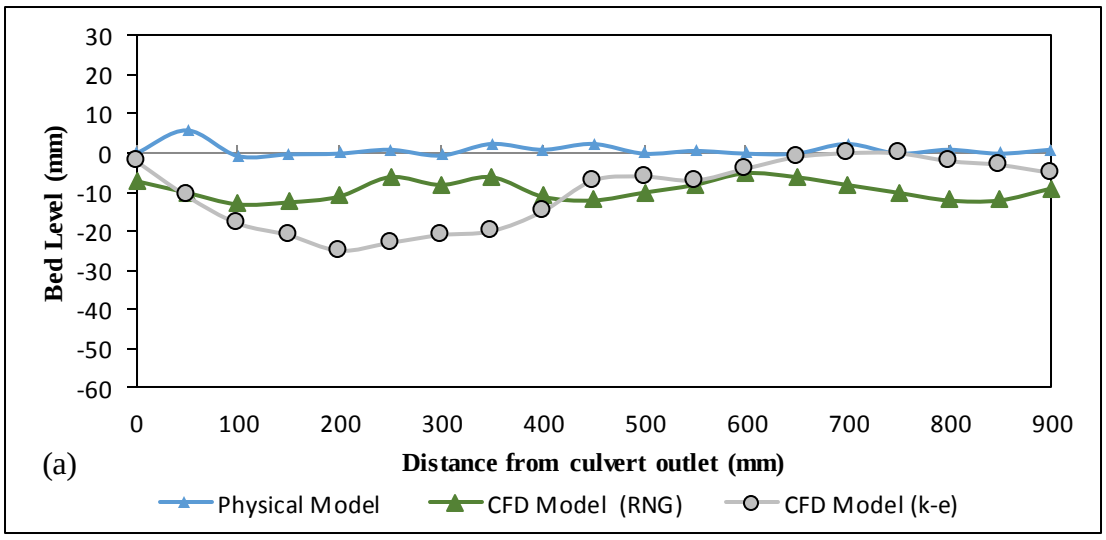

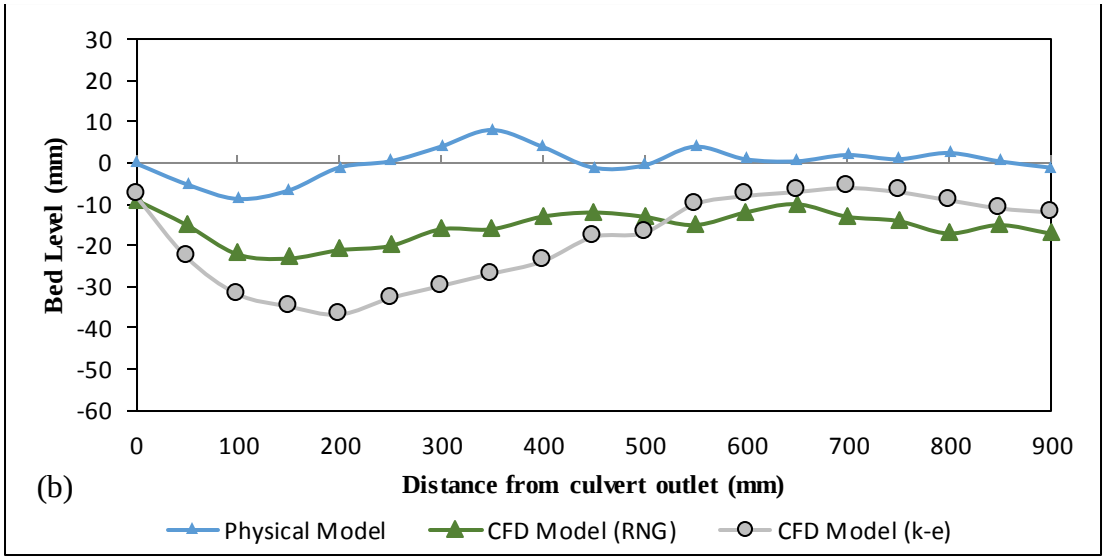
30
20
10
0
-10
-20
-30
-40
-50
-60
Bed Level (mm)
0
100
200
300
400
500
600
700
800
900
Distance from culvert outlet (mm)
Physical Model
CFD Model (RNG)
CFD Model (k-e)

(b)

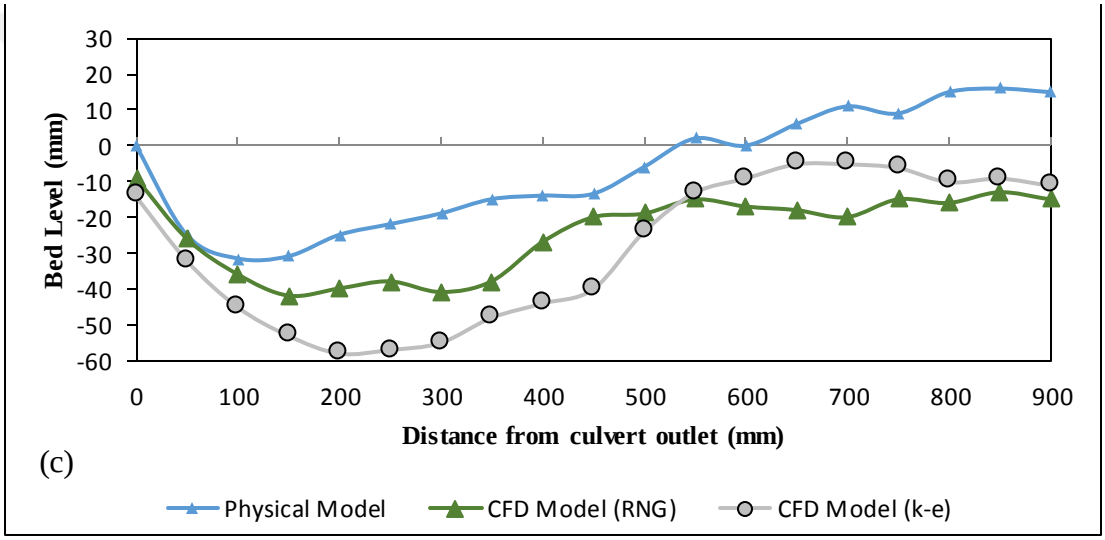
30
20
10
0
-10
-20
-30
-40
-50
-60
Bed Level (mm)
0
100
200
300
400
500
600
700
800
900
Distance from culvert outlet (mm)
Physical Model
CFD Model (RNG)
CFD Model (k-e)

(c)

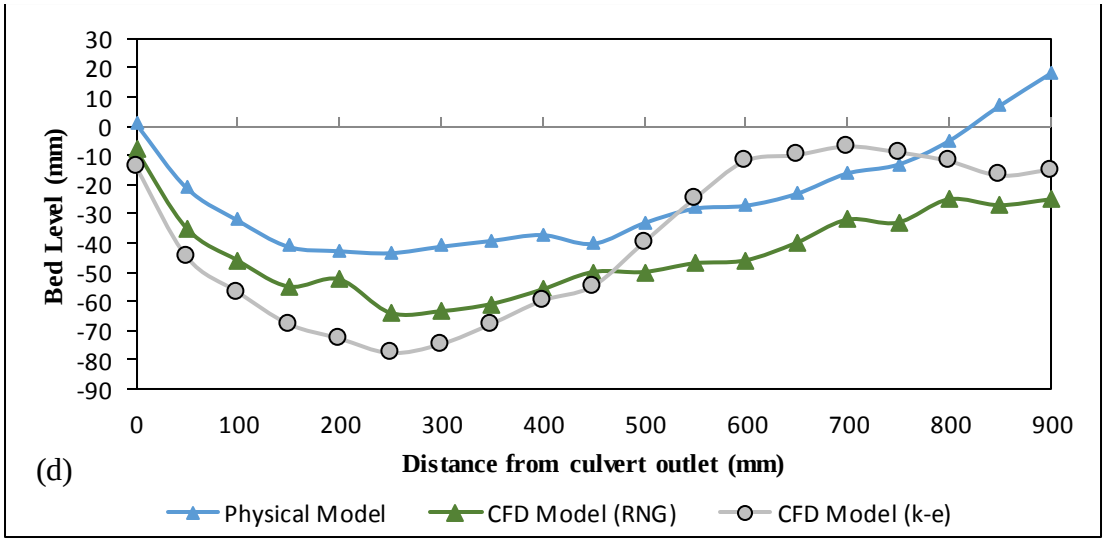
30
20
10
0
-10
-20
-30
-40
-50
-60
-70
-80
-90
Bed Level (mm)
0
100
200
300
400
500
600
700
800
900
Distance from culvert outlet (mm)
Physical Model
CFD Model (RNG)
CFD Model (k-e)

(d)

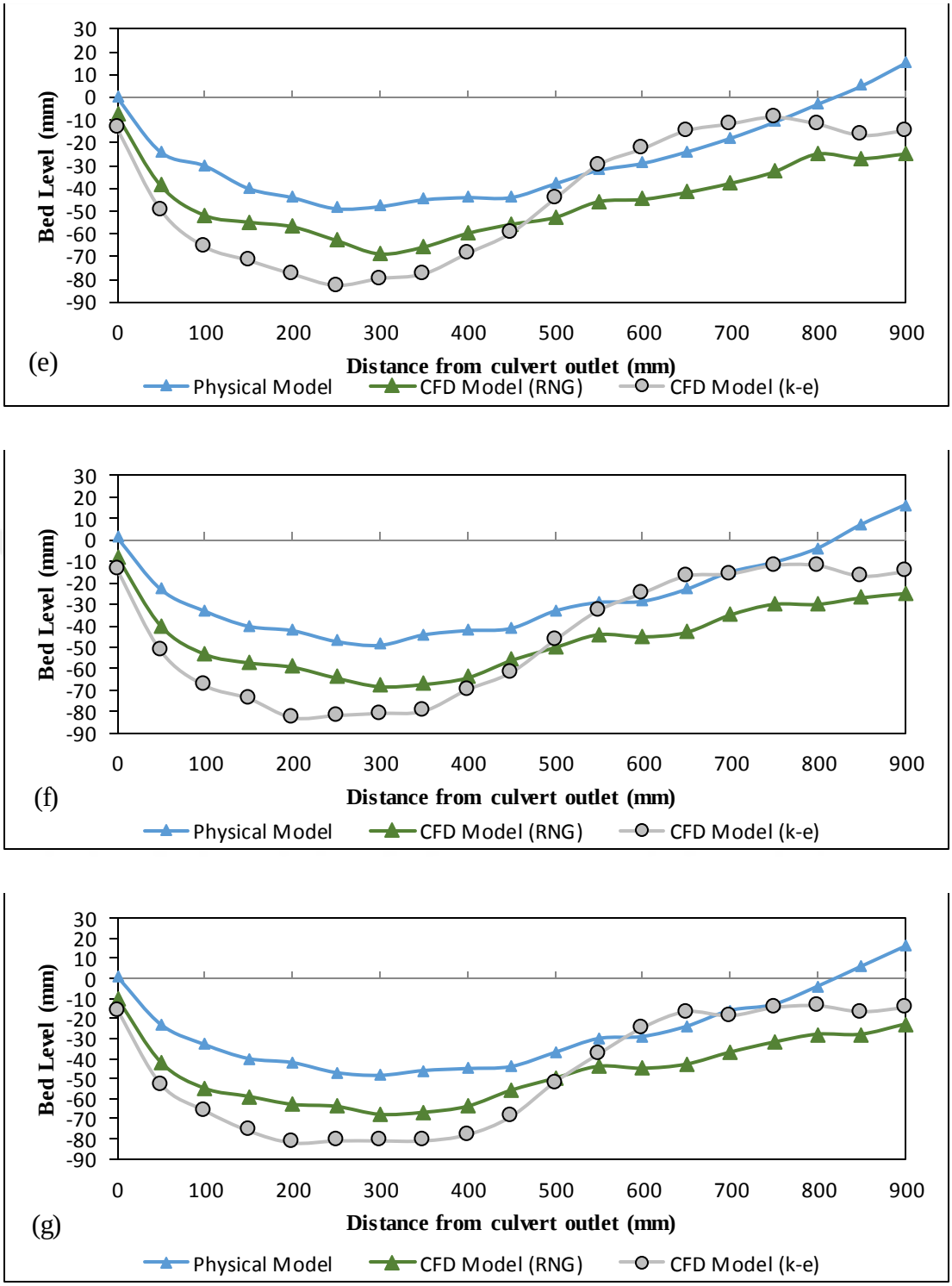

Figure 4.6 Comparison between CFD model and physical model for scouring profile with the second set of fine sediment by using RNG and k-ε: (a) Flow rate is 6.6 Lt/s at 15 minutes (b) Flow rate is 8.8 Lt/s at 30 minutes (c) Flow rate is 10.7 Lt/s at 45 minutes (d) Flow rate is 12.8 Lt/s at 60 minutes (e) Flow rate is 10.7 Lt/s at 75 minutes (f) Flow rate is 8.8 Lt/s at 90 minutes (g) Flow rate is 6.6 Lt/s at 105 minutes

4.3.3 Maximum scour depth

In Table 4.2 shown that the formation maximum scour depth in each step of the hydrograph. In the second set, two different tests were used US2B0, US2B40 with specific blockage ratio. For the first test US2B0 by using empirical equation RNG the maximum scour depth was achieved when in the second test US2B40 was selected RNG and $k-\varepsilon$ for obtained maximum scour depth and compare with experimental work. From first and second test in Figure 4.7, similar to the fine sediment (d_{50}=0.85 mm), the major part of forming scour hole for non-blocked and partially blocked situations, same as the earlier set was occurred by increasing limb of the hydrograph. Although, at the first step of hydrograph for non-blocked and partially blocked conditions start from around 0 for physical model and in CFD model similarly for both conditions was about 0, the creation of maximum scour depth at the following steps of the hydrograph in non-blocked condition was slower than partially blocked condition. In experimental investigation for both tests, the maximum scours depth in non-blocked condition was about 51.6 mm and for partially blocked condition was around 48.9 mm, while the numerical value for same tests in non-blocked condition was about 63 mm and for partially blocked condition was around 69 mm. it is mean that the Flow-3D results are not same with experimental but it gives acceptable agreement. From Figure 4.7 depicted that the comparison between both empirical equations (RNG, k-ε) with experimental work for maximum scour depth. In experimental study for this tests the maximum scour depth partially blocked condition was around 48.9 mm, while the numerical value for same tests by selecting RNG was about 69 mm and also for k-ε was around 83 mm. This variability indicates that by using RNG. The overall results tell us, by using RNG and value of this empirical equation is closer than k-ε when compared with experimental work.

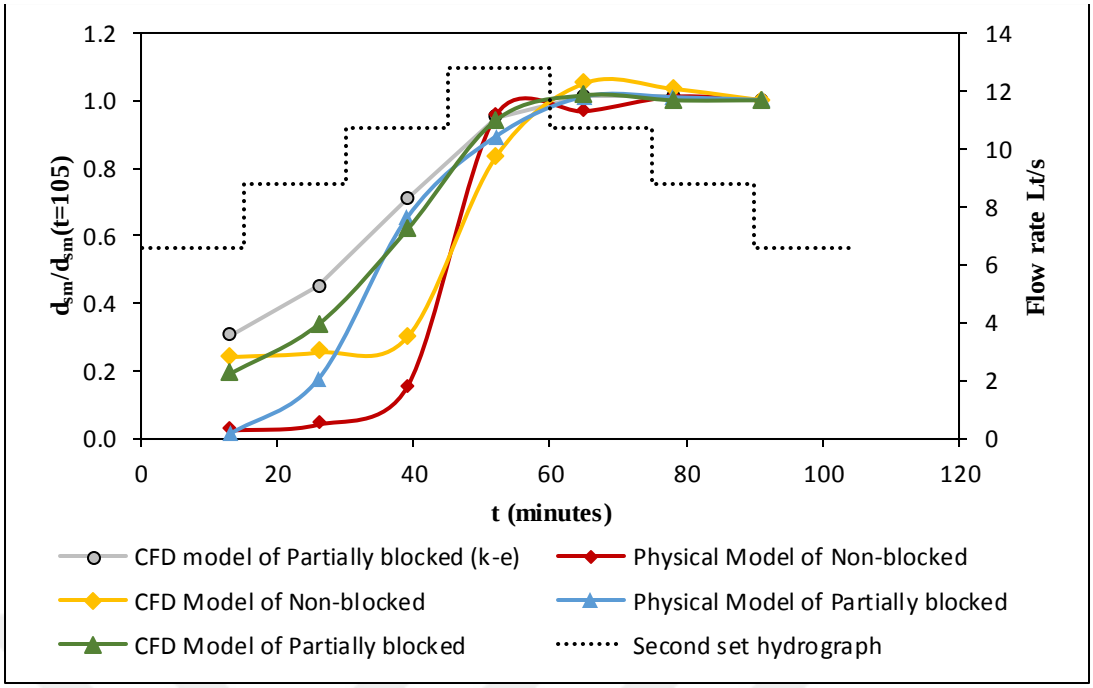

Figure 4.7 Comparison between CFD model by using (RNG, k-ε) and physical model for evolution of normalized maximum scour depth with time for the second set

4.3.4 Location of maximum scour depth

These results obtained for comparison of maximum scour position between CFD and the physical model was presented in Table 4-2. This comparison when used the Flow-3D only selected the empirical equation RNG for partially blocked and non-blocked condition. The ratio $\frac{Xsm(t=40)}{Xsm(t=0)}$ was used for achieved the accurate place of maximum scour. Shown in Figure 4-8 was the maximum scour depth position from the culvert outlet along flow direction (Xsm) for the second set with hydrograph steps. As shows in the Figure 4.8, for the first three steps of the hydrograph the position of maximum scour depth for both partially blocked and non-blocked tests stays unchanged for experimental work, whereas for numerical conditions indicate that, this phenomenon progressively changed. However, it showed a great variance at the peak flow rate where the ratio of was 2.5 for partially blocked situations and 0.85 for non-blocked condition. While at the peak flow rate Flow-3D model found this value for partially blocked condition was about 2.5 and for non-blocked condition was around 1. For this set at final stage, when CFD model compared with physical model, the place of maximum scour hole at the final stage becomes closer to the culvert outlet in non-blocked condition while in partially blocked condition it is almost 3 times further than

the location it was at the first stage as shown in Figure 4.8. Overall results tell us, these values attained by Flow-3D has good agreement when compared with experimental work.

This section is the last part to indicate a comparison between experimental and numerical work. Finally, these comparisons tell us overall numerical results are in the maximum scour depth greater than experimental work for all cases. According to the

Flow-3D for both sets when compared with experimental work, it has some difference in process of work as shown below:

1. In the laboratory, for both sets, two different sediment size was used with sieve analysis, while for Flow-3D in the physical section can determine the exact size of sediment.
2. In the laboratory, after sieve analysis may be some percent of silt and clay remaining on the sieves with both sets were mixed and used in tests. While in Flow-3D does not allow to mix any percent of silt and clay with sets.
3. Before laboratory test was started, sediment was saturated slowly from upstream and downstream sides. While in Flow-3D does not do the same process.
4. The tests were under unsteady flow conditions, with hydrograph was designed for each set and in exact time the flow rate was changed. In the laboratory tests, this process
5. was done by hand, and depend on the opening the valve. While this process in Flow-3D was done automatically may be faster than experimental
6. in the laboratory during tests time may be the changing of temperature occurred on the runs, while in Flow-3D can be used fixed degree.

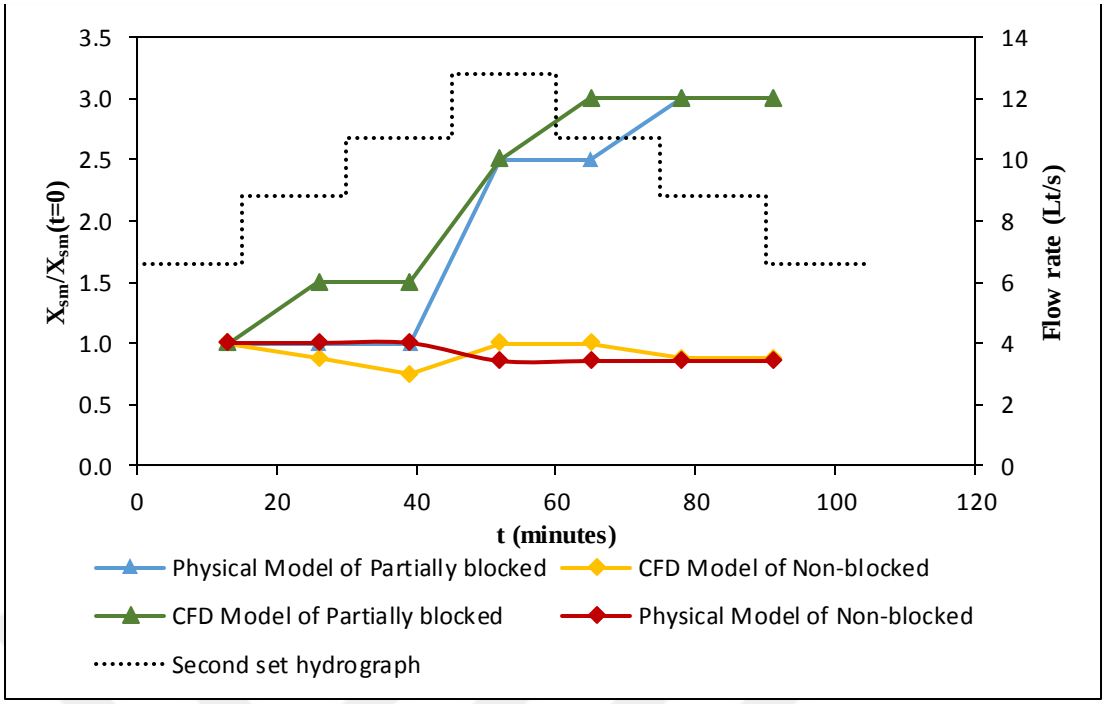

Figure 4.8 Comparison between CFD model and physical model for normalized location of maximum scour depth with hydrograph for the second set

4.4 Water surface profile for both sets

The water surface profile within a culvert can be classified with hydraulic slope, which is based on the slope of the culvert bottom and hydraulic curve, which is based on the relationship of the water depth relative to critical depth and normal depth. Hydraulic curve classifications are used to describe the shape of the water surface profile at a specific flow. In Figure 4.9a to Figure 4.9d, was shows these changes occurred in water surface elevation when found by Flow-3D for both sets. Water surface profile continuously changed in upstream and downstream of box culvert because of that the flow conditions were under unsteady and the flow rates were changed in each step of the hydrograph. For both tests US1B0 and US2B0, the ratio of blockage was 0, the elevation water surface profile slowly increased until peak flow of hydrograph after that gradually decreased. it is indicating that the scouring process occurred slightly with hydraulic jump as shown in Figure 4.9a to Figure4.9c.

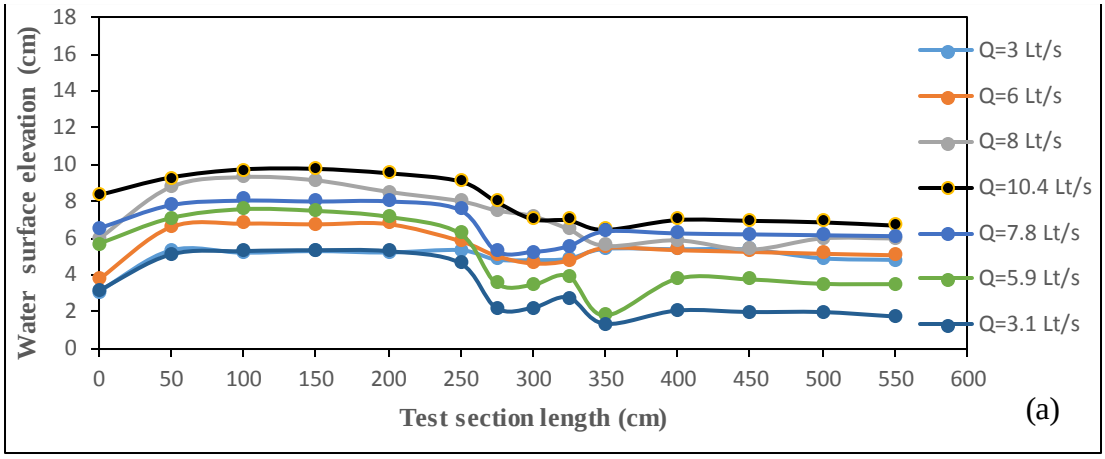

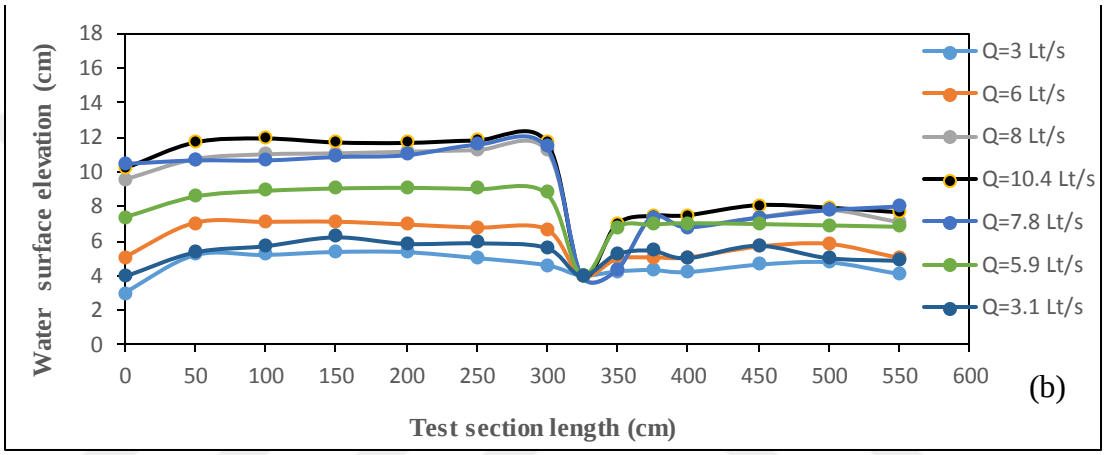

While, for test US1B40 and US2B40, the ratio of blockage 40% at the inlet of the culvert and the elevation of water surface was raised because of the blockage ratio. it is indicating that the scouring process occurred more than other tests. In the position of blockage, the water level in both tests passed beneath the blockage plate and it did not overflow the plate. It is disclosing that water was a transition from subcritical to supercritical and in the outlet of a culvert in consequence of scour observed, again the flow is provides a transition to subcritical from supercritical to creating a hydraulic jump Figure 4.9b to Figure 4.9d.

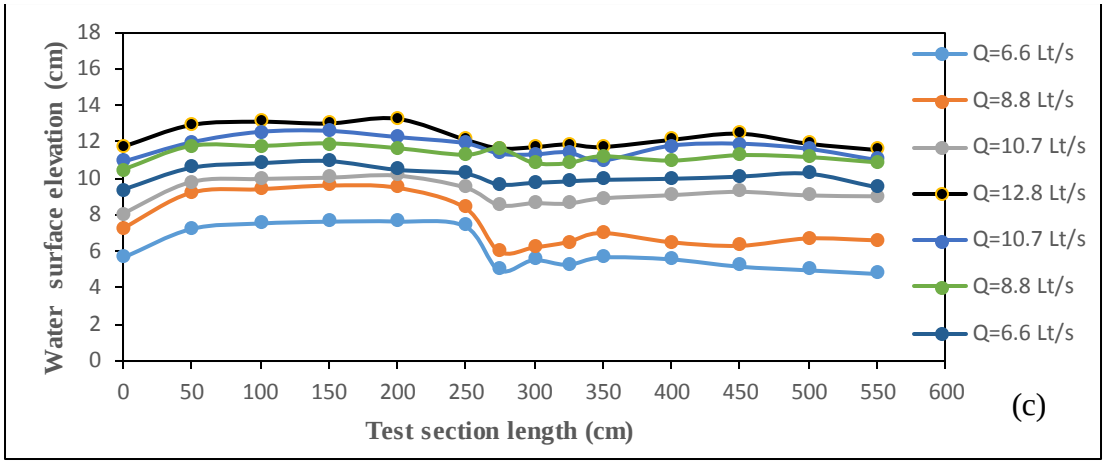

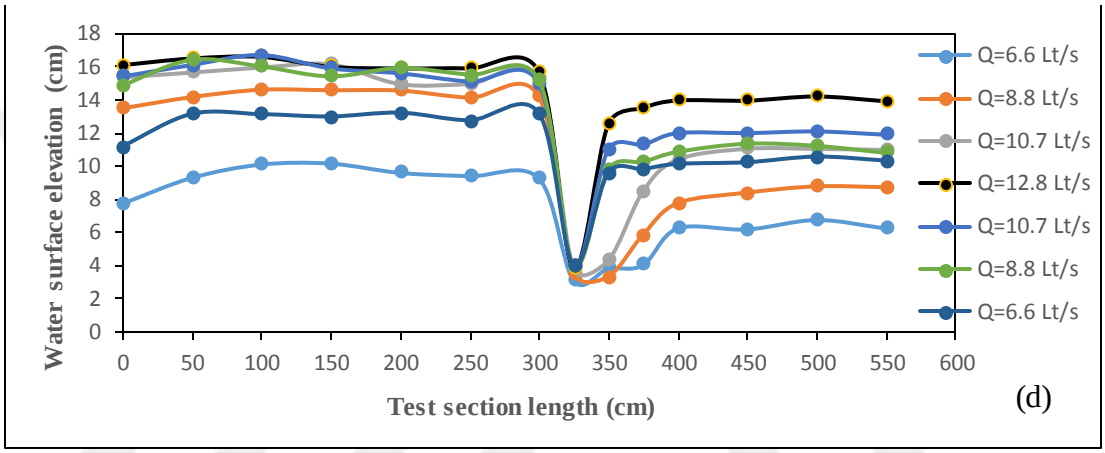

Figure 4.9 Water surface profile for both sediment types: (a) US1B0 (b) US1B40 (c)US2B0 (d) US2B40

4.5 Vortex

In fluid dynamics, vorticity is a vector quantity and it tells us the tendency of a fluid particle to rotate or circulate at a particular point. It is mathematically defined as the curl of velocity and also relates it to the circulation of a fluid, which is the line integral of the velocity along a closed curve.

4.5.1 Effect of vortex on scouring

Scouring downstream of culvert outlets is a common problem that can lead to damage to the culvert structure and neighboring land. In this section, indicate the flow structure within scour holes downstream of box culvert outlets with a different percentage blockage ratio under unsteady flow condition. In Figure 4.11a to Figure 4.11e, shows the direction of flow with flow vectors and the scour hole formation for peak flow in

all cases. The vortices direction led to a foundational understanding of the flow structure in scour holes. Prediction of scour depths downstream of such structures can be determined from a selection of empirical equations Breusers and Raudkivi (1991), Ruff et al. (1982), with some diversity over the key parameters for determining to scour depth. As depicted in Figure 4.11a to Figure 4.11e, the vortex is happening in the culvert outlet by increasing the scour phenomenon, the vorticity in these positions were increased and the flow rotation clearly appearance.

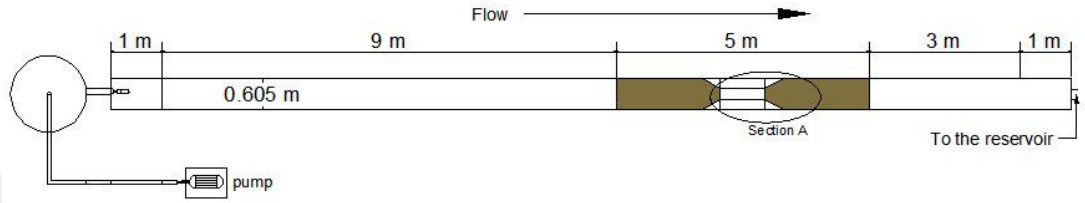

Figure 4.10 Model set up, top view

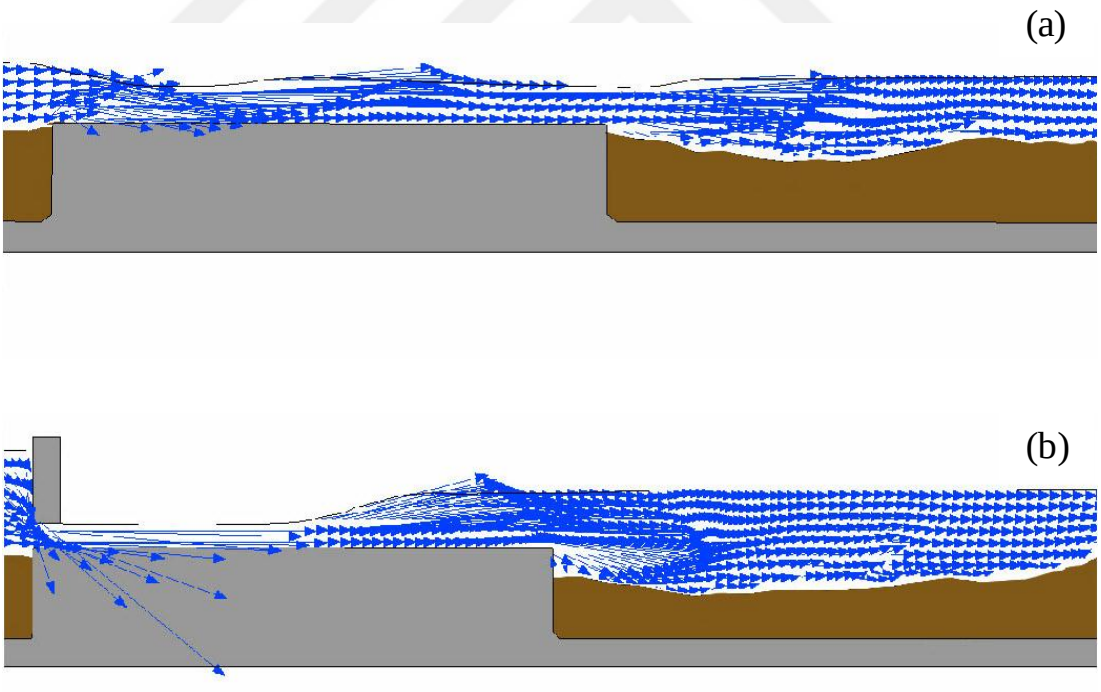

(c)

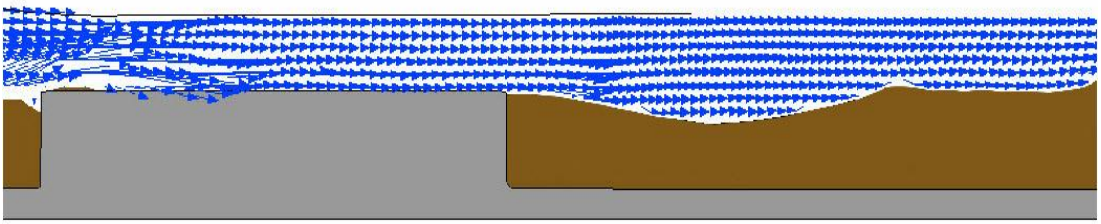

(d)

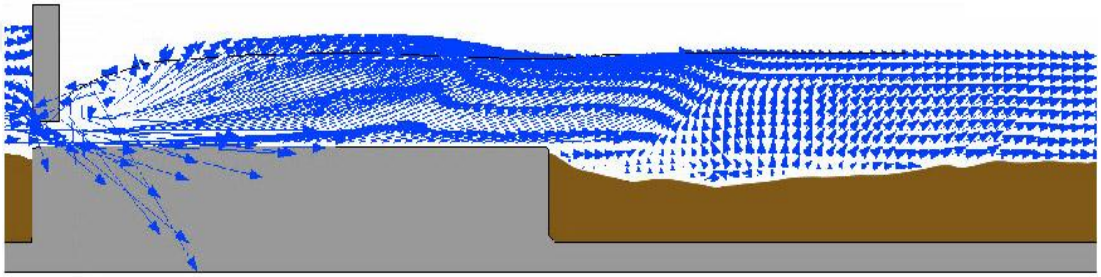

(e)

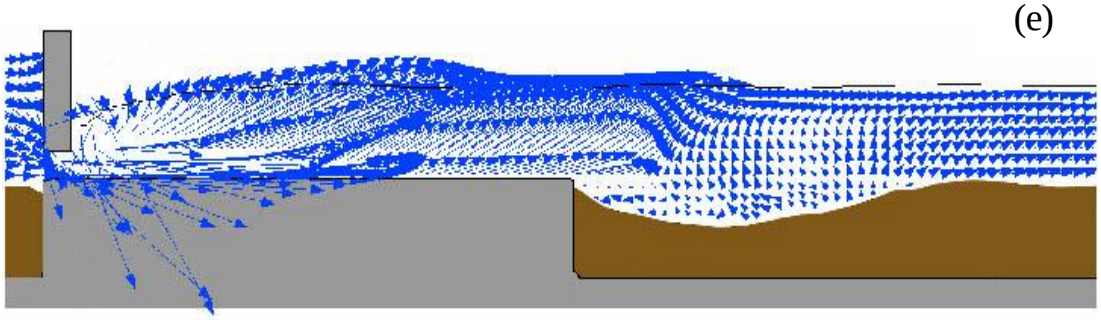

Figure 4.11 section (A): (a) Case US1B0, flow rate is 10.4 Lt/s (b) Case US1B40, flow rate is 10.4 Lt/s (c) Case US2B0, flow rate is 12.8 Lt/s (d) Case US2B40, flow rate is 12.8 Lt/s (d) Case US2B40, flow rate is 12.8 Lt/s by using k-ε.

4.6 Scour formation using CFD model

To realize the scour formation and indicate the scour location in box culvert outlet by using Flow-3D are shown in Figure 4.12. It is exposed that the scour had occurred for both sets with additional case of k-ε.

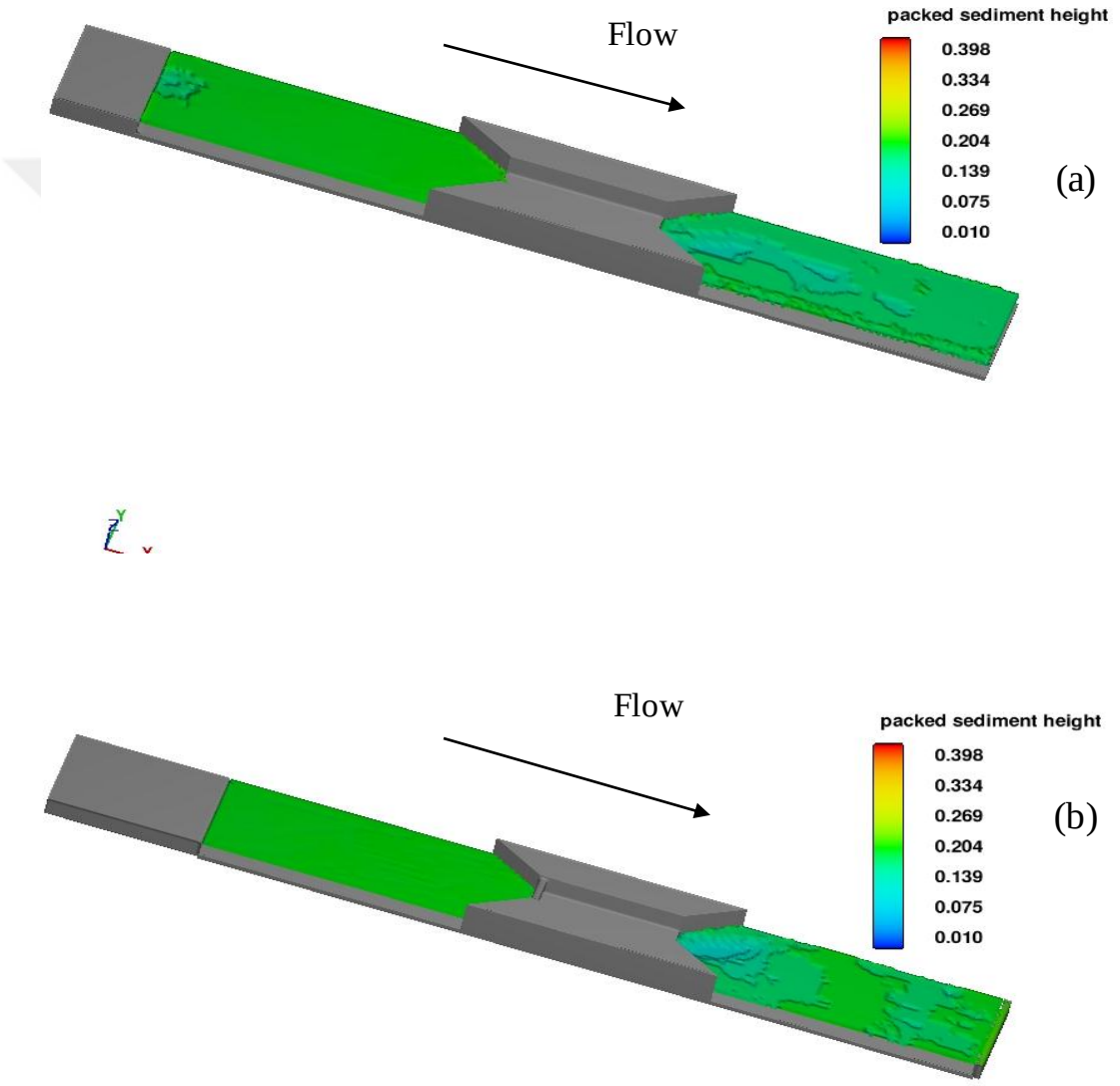

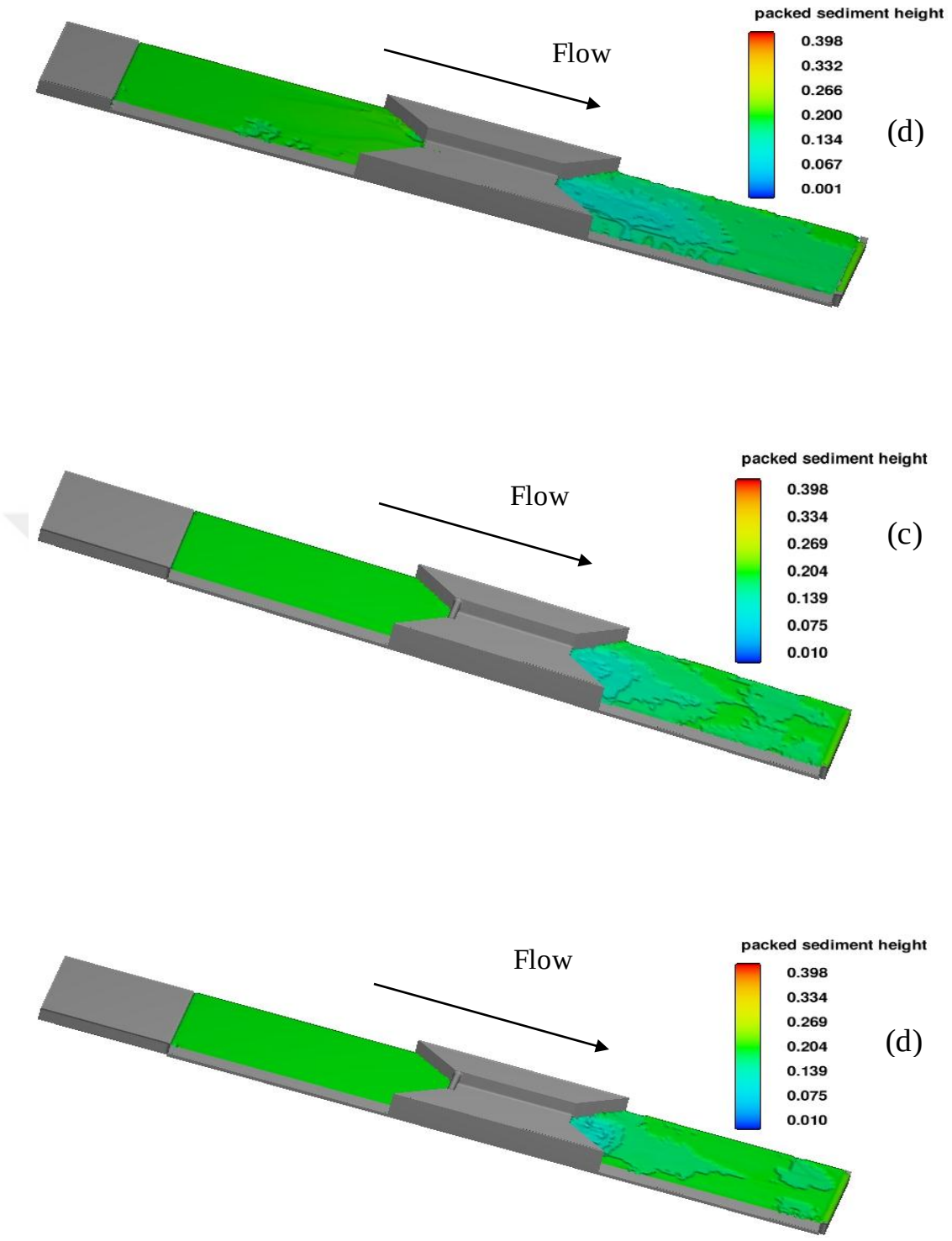

Figure 4.12 3D Plots of scour formation for both sets (a) case US1B0, flow rate is 10.4 Lit/s (b) case US1B40, flow rate is 10.4 Lit/s (c) case US2B0, flow rate is 12.8 Lit/s (d)case US2B40, flow rate is 12.8 Lit/s (d) case US2B40, flow rate is 12.8 Lit/s for k-ε.

CHAPTER 5

CONCLUSIONS AND RECOMMENDATIONS

5.1 Conclusions

This study work was an attempt to examine hydraulic parameters and characteristics that reduce scour based on the general experimental study and also CFD modeling used for scour prediction. In this chapter, simulated results that obtained from Flow-3D software of box culvert model and formation of scour at the outlet are compared with laboratory results to evaluate the accuracy of the numerical model. Laboratory box culvert was carried out for two conditions; the non-blocked situation and the partially blocked condition with the blockage ratio of 40% for this destination used two different sizes of plates and the finer sediment was used in this study with the median grain size being 0.85 mm and 2.0 mm, the flow conditions in the laboratory were unsteady. It is mean that the flow rates during the time were changed. The performance of the numerical model based on renormalization group (RNG) and in the last case also used k-ε with RNG to comparing with experimental results. For evaluate the numerical simulations based on the different percent of blockage and fine sediment sizes under unsteady conditions.

Most important results and conclusions from the study are present bellows:

- For first set (d_{50}=0.85 mm), centerline profile along horizontal axis, in the flow rate 6 Lt/s, the observed measurement for scour depth at the first point for non-blocked condition was around 5 mm and for partially blocked condition was about 21 mm, the various percent between both situations is about (76%), while numerical results for non-blocked situation was around 10 mm and for partially blocked condition was around 35 mm, the different percent between both conditions was about (71%). It is revealed that by increasing the rising limb, in another word by increasing the blockage ratio at culvert inlet the initiation

of scouring happens in the initial steps of the hydrograph while for the non-blocked condition it still takes a few more steps.

- For first set (d_{50}=0.85 mm), at the observed investigation for discharge 6 Lt/s, it can saw that the maximum scour hole had formed in non-blocked condition is around 36% and for partially blocked situation around 63%, whether compared to the Flow-3D model the maximum scour hole had formed in non-blocked condition is around 29% While the maximum scour hole had formed in partially blocked situation around 74%.
- For first set (d_{50}=0.85 mm), location of maximum scour depth in experimental work for peak flow rate 10.4 Lt/s, in non-blocked condition is 0.83, and for partially blocked condition is 2, while observed in numerical work for non-blocked condition is 1.2, and for partially blocked condition is 1.7. It is indicating the results of Flow-3D in all tests are close to the experimental results, and proportionally changed was occurs between them.
- By using empirical equation(RNG) for centerline profile along horizontal axis the noticeable difference of scour was happening in the third step of the hydrograph around 50 mm from culvert outlet. For third flow rate 10.7 Lt/s with fine sediment (d_{50}=2.0 mm) at 50 mm after outlet of culvert, the scour depth at this point for non-blocked condition was around 4 mm and for partially blocked situation was about 25 mm while these results achieved by Flow-3D for non-blocked condition was around 2 mm and for partially blocked condition was about 29 mm.
- For second set (d_{50}=2.0 mm), In experimental study for this tests the maximum scour depth partially blocked condition was around 48.9 mm, while the numerical value for same tests by selecting RNG was about 69 mm and also for k-ε was around 83 mm. This variability indicates that by using RNG. The overall results tell us, by using RNG and value of this empirical equation is closer than k-ε when compared with experimental work.
- Flow-3D program ability has been confirmed by simulating existing experimental study and comparing the numerical results with experimental outcomes.
- In an observed laboratory with numerical results, the maximum scour depth was more in the partially blocked condition in all steps of the hydrograph. Flow

3D is a powerful tool to complement experimental investigation. However, in order to accurately verify the capabilities of the model, long-term simulation is necessary. Special attention is required for mesh resolution and the characteristics of the turbulence model that may affect the results.

5.2 Recommendations

- In this study, to simulate blockage at the inlet 2 plates with different sizes were used. At the inlet of the culvert, plates were installed. To obtain different ranges of blockage the height of the plates was varied. In the physical model Instead of plates, wooden materials or sticks can be used. In that case, the possible form of the blockage caused by the accumulation of debris at the inlet for future studies is recommended.
- This study was conducted for a box culvert; however, there are many different forms of culverts. Therefore, for a better understanding of the shape effect in the case of occlusion, experimental tests with different culvert shapes can be studied.
- In this study, the length of the culvert and the horizontal slope were fixed. However, in practice, the length and slope may change based on the morphology and topography of the location where they are going to be built. It can be useful to investigate the effect of blockage on the length and slope of the different culvert.
- In this research, uniform and non-cohesive sediment used as bed material. Although it is more important to scour with uniform sediments, in reality, the sediments are largely well graded. Also, the mechanism of scour in non-cohesive sand can be different with cohesive sediment. It is proposed that well-graded sediment and cohesive are used for future studies in partially blocked culverts.
- Under clear water conditions, the experimental test of this research was done. During flood events and rainy seasons in practice culvert sites experience has different flow conditions. For future research, it is recommended to perform successfully designed physical tests considering living bed conditions, due to partially blocked drains.From the results of both studies, it became clear that engineers can consider the durability of hydraulic structure and the best model of scouring reduction proposal.

very powerful research tool is a Flow-3D, but the Flow-3D model is a very sensitive procedure, for the model that best describes the nature of problem it need prices and accurate parameter, may huge change in the results occur when any tine changes in the parameters, so it is very important for every researcher to specialize in the fundamentals of computational fluid dynamics and Flow-3D software before use it.

REFERENCES

FLOW-3D (2012) "User Manual", Flow Science, Inc.

Sorourian, S. (2015). Study of blockage effects on scouring pattern downstream of box culverts, Doctoral dissertation.

Sorourian, S., Keshavarzi, A., Ball, J., Samali, B. (2013). Study of Blockage Effect on Scouring Pattern Downstream of a Box Culvert under Unsteady Flow, *Australian Journal of Water Resorces*.

Sorourian, S., Keshavarzi, A., Ball, J. E. (2015). Scour at partially blocked box-culverts under steady flow, In *Proceedings of the Institution of Civil Engineers-Water Management*, **169(6)**, 247-259.

Abida, H., Townsend, R. D. (1991). Local scour downstream of box-culvert outlets, *Journal of irrigation and drainage engineering*, **117(3)**, 425-440.

Williams, R. J., Watford, F. A. (1997). Identification of structures restricting tidal flow in New South Wales, Australia. *Wetlands Ecology and Management*, **5(1)**, 87-97.

Rigby, E. H., Boyd, J., Roso, S., Silveri, P., Davis, A. (2002). Causes and effects of culvert blockage during large storms, In *Global solutions for urban drainage*, **pp**, 1-16.Weeks, W., Witheridge, G., Rigby, E., Barthelmess, A. (2013). Project 11: blockage of hydraulic structures.

Ebraim, N., heydarenjad, M., (2014). Experimental Investigation of the Effect of Flow Angle of Attack on the Rate of Scour around the Slotted Bridge Pier at Different Level of River Bend, *IJRASET-International* for Research in Applied Science and Engineering Technology, **2(12)**, 276-282

Moody, J. A., Smith, D., & Ragan, W. (2005). Critical shear stress for erosion of cohesive soils subjected to temperatures typical of wildfires, *Journal of Geophysical Research: Earth Surface*, 110 (F1).

Pitt, R., Clark, S. E., Lake, D. W. (2007). Construction Site Erosion and Sediment Controls: Planning, Design and Performance. DEStech Publications, Inc.

Wu, S., Rajaratnam, N. (1996). Transition from hydraulic jump to open channel flow, *Journal of hydraulic engineering*, **122(9)**, 526-528.

Chen, Y. H. (1970). Scour at outlets of box culverts, Doctoral dissertation, Colorado State University.

Smith, G. L. (1957). An analysis of scour below culvert outlets, Doctoral dissertation, Colorado State Univ.

Simons, D. B., Stevens, N. A. (1971). Scour control in rock basins at culvert outlets, River Mechanics, **2(24)**, edited by HW Shen.

Wu, W., Vieira, D. A., Wang, S. S. (2004). One-dimensional numerical model for nonuniform sediment transport under unsteady flows in channel networks, *Journal of Hydraulic Engineering*, **130(9)**, 914-923.

Ferguson, R., Church, M. (2009). A critical perspective on 1-D modeling of river processes: Gravel load and aggradation in lower Fraser River, *Water Resources Research*, **45(11)**.

Sumer, B. M., Whitehouse, R. J., Torum, A. (2001). Scour around coastal structures: a summary of recent research, *Coastal Engineering*, **44(2)**, 153-190.

Wu, W., Marsooli, R., He, Z. (2011). Depth-averaged two-dimensional model of unsteady flow and sediment transport due to noncohesive embankment break/breaching, *Journal of Hydraulic Engineering*, **138(6)**, 503-516.

Smith, H. D., Foster, D. L. (2005). Modeling of flow around a cylinder over a scoured bed, *Journal of waterway, port, coastal, and ocean engineering*, **131(1)**, 14-24.

Liu, X., García, M. H. (2008). Three-dimensional numerical model with free water surface and mesh deformation for local sediment scour, *Journal of waterway, port, coastal, and ocean engineering*, **134(4)**, 203-217.

Ruether, N., Olsen, N. R. B. (2006). Towards the prediction of free-forming meander formation using 3D computational fluid dynamics, In *Proceedings of Annual Conference on Hydraulic Engineering: Flow Simulation in Hydraulic Engineering*, **pp**, 31-38.

Nitatwichit, C., Khunatorn, Y., Tippayawong, N. (2008). Computational analysis and visualisation of wind-driven naturally ventilated flows around a school building, *Maejo international journal of science and technology*, **2(1)**, 240-254.

Dey, S., Raikar, R. V. (2007). Scour below a high vertical drop. *Journal of Hydraulic Engineering*, **133(5)**, 564-568.

Bormann, N. E., Julien, P. Y. (1991). Scour downstream of grade-control structures, *Journal of Hydraulic Engineering*, **117(5)**, 579-594.

Papanicolaou, T. N., Elhakeem, M., Krallis, G., Prakash, S., Edinger, J. (2008). Sediment transport modeling review-current and future developments, *Journal of Hydraulic Engineering*, **134(1)**, 1-14.

VRIES, D. (1973). Application of physical and mathematical models for river problem, *in general reports, discussions, lectures*.

Barthelmess, A. J., Rigby, E. H. (2011). Estimating Culvert and Bridge Blockages-a Simplified Procedure, *In Proceedings of the 34th World Congress of the International Association for Hydro-Environment Research and Engineering: 33rd Hydrology and Water Resources Symposium and 10th Conference on Hydraulics in Water Engineering* (p. 39). Engineers Australia.

Rigby, E. H., Barthelmess, A. J. (2011). Culvert Blockage Mechanisms and Their Impact On Flood Behavior-Are All Blockages Created Equal?', In *34th World Congress of the International Association for Hydro-Environment Research and Engineering, Engineers Australia, Brisbane, Australia*, **pp**, 380-7.

Weeks, W., Barthelmess, A., Rigby, E., Witheridge, G., Adamson, R. (2009). Australian rainfall and runoff revision project 11: blockage of hydraulic structures.

Bradley, J. B., Richards, D. L., Bahner, C. C. (2005). Debris control structures: Evaluation and countermeasures. US Department of Transportation, Federal Highway Administration.

Rigby, E. H., Boyd, M. J., Roso, S., Silveri, P., Davis, A. (2002). Causes and effects of culvert blockage during large storms, In *Global solutions for urban drainage* **pp**, 1-16.

Norman, J.M., Houghtalen, R.J. Johnson, W.J. (2001). Hydraulic Design of Highway Culverts, *Second Edition*, no. FHWA-NHI-01-020,HDS.

Breusers, H. N. C., Raudkivi, AJ. (1991). Scouring.

Raudkivi, A. J. (1998). Loose boundary hydraulics, CRC Press.

Özalp, M. C., Bozkuş, Z. (2013). Experimental investigation of local scour around bridge pier groups, Doctoral dissertation, M. Sc. thesis, Department of Civil Engineering, *the graduate School of Natural and Applied Sciences of Middle East Technical University*.

Stevens, M. (1968). 'Scouring of Riprap at Culvert Outlets', PhD. Dissertation, Department. Of Civil Engineering, Colorado State University, Fort Collins, CO.

Rouse, H. (1939). Experiments on the mechanics of sediment suspension.

Laursen, E. M. (1952). Observations on the nature of scour, In *Proceedings of the Fifth Hydraulics Conference, State University of Iowa, Iowa City, Iowa*, **pp**, 179-197.

Opie, T. R. (1968). Scour at culvert outlets, Doctoral dissertation, Colorado State University. Libraries.

Chiew, Y. M., Lim, S. Y. (1996). Local scour by a deeply submerged horizontal circular jet. *Journal of Hydraulic Engineering*, **122(9)**, 529-532.

Abt, S. R., Ruff, J. F., Doehring, F. K., Donnell, C. A. (1987). Influence of culvert shape on outlet scour, *Journal of Hydraulic engineering*, **113(3)**, 393-400.

Abt, S. R., Ruff, J. F., Doehring, F. K. (1985). Culvert slope effects on outlet scour, *Journal of Hydraulic Engineering*, **111(10)**, 1363-1367.

Rajaratnam, N., Diebel, M. (1981). Erosion below culvert-like structures, In Sixth Canadian Hydrotechnical Conference, **pp**, 469-484.

Lim, S. Y. (1995). Scour below unsubmerged full-flowing culvert outlets, *Proceedings of the Institution of Civil Engineers-Water Maritime and Energy*, **112(2)**, 136-149.

Elsabaie, I. H. (2013). An Experimental Study of Local Scour around Circular Bridge Pier in Sand Soil, *International Journal of Civil and Environmental Engineering IJCEE-IJENS*, **13(01).**

Lança, R. M., Fael, C. S., Maia, R. J., Pêgo, J. P., Cardoso, A. H. (2013). Clear-water scour at comparatively large cylindrical piers, *Journal of Hydraulic Engineering*, **139 (11)**, 1117-1125.

Uyumaz, A. (1988). Scour downstream of vertical gate, *Journal of Hydraulic Engineering*, **114(7)**, 811-816.

Morales, R., Ettema, R. (2012). Insights from depth-averaged numerical simulation of flow at bridge abutments in compound channels, *Journal of Hydraulic Engineering*, **139(5)**, 470-481.

Prinos, P. (1990). Turbulence modeling of main channel-floodplain flows with an algebraic stress model, In *Proc. Conf. River Flood Hydraulics*, **pp**, 173-185.

Krishnappan, B. G., Lau, Y. L. (1986). Turbulence modeling of flood plain flows, *Journal of hydraulic engineering*, **112(4)**, 251-266.

Pezzinga, G. (1994). Velocity distribution in compound channel flows by numerical modeling, *Journal of Hydraulic Engineering*, **120(10)**, 1176-1198.

Naot, D., Nezu, I., Nakagawa, H. (1993). Hydrodynamic behavior of compound rectangular open channels, *Journal of Hydraulic Engineering*, **119(3)**, 390-408.

Yakhot, V., Orszag, S. A. (1986). Renormalization-group analysis of turbulence, *Physical review letters*, **57(14)**, 1722.

Soulsby, R. (1997). Dynamics of marine sands: a manual for practical applications, Thomas Telford.

Julien, P. Y. (2010). Erosion and sedimentation, Cambridge University Press.

N. H. Brooks. (1958). Mechanics of streams with movable beds of fine sands, *Trans. ASCE*,**123**, 525-549.

Bormann, N. E., Julien, P. Y. (1991). Scour downstream of grade-control structures. *Journal of Hydraulic Engineering*, **117(5)**, 579-594.

Lane, E. W. (1953). Progress report on studies on the design of stable channels by the Bureau of Reclamation, In *Proceedings of the American Society of Civil Engineers*, **79(9)**,1-31.

Engelund, F., Fredsøe, J. (1976). A sediment transport model for straight alluvial channels, *Hydrology Research*, **7(5)**, 293-306.

Meyer-Peter, E., Müller, R. (1948). Formulas for bed-load transport, In IAHSR 2nd meeting, Stockholm, appendix *2*. IAHR.

Nielsen, P. (1992). Coastal bottom boundary layers and sediment transport, World Scientific Publishing Co Inc.

Mehnifard, M., Dalfardi, S., Baghdadi, H., Seirfar, Z. (2015). Simulation of local scour caused by submerged horizontal jets with Flow-3D numerical model, *Desert*, **20(1)**, 47-55.

Li, G., Lang, L., Ning, J. (2013). 3D Numerical Simulation of Flow and Local Scour around a Spur Dike, In IAHR World Congress, **pp**, 1-9.

Richardson, J. E., Panchang, V. G. (1998). Three-dimensional simulation of scour-inducing flow at bridge piers, *Journal of Hydraulic Engineering*, **124(5)**, 530-540.

Olsen, N. R., Melaaen, M. C. (1993). Three-dimensional calculation of scour around cylinders, *Journal of Hydraulic Engineering*, **119(9)**, 1048-1054.

Olsen, N. R., Kjellesvig, H. M. (1998). Three-dimensional numerical flow modeling for estimation of maximum local scour depth, *Journal of Hydraulic Research*, **36(4)**, 579-590.

Zhang, H., Nakagawa, H., Ishigaki, T., Muto, Y. (2005). Prediction of 3D flow field and local scouring around spur dykes, *proceedings of hydraulic engineering*, **49**, 1003-1008.

Roulund, A., Sumer, M., Fredsoe, J., Michelsen, J. (2005). Numerical and experimental investigation of flow and scour around a circular pile, *Journal of Fluid Mechanics*, **534**, 351-401.

Liu, X., García, M. H. (2008). Three-dimensional numerical model with free water surface and mesh deformation for local sediment scour, *Journal of waterway, port, coastal, and ocean engineering*, **134(4)**, 203-217.

Olsen, N. R. B. (2003). Three-dimensional CFD modeling of self-forming meandering channel, *Journal of Hydraulic Engineering*, **129(5)**, 366-372.

Esmaeili, T. (2009). Hydraulic and geometric numerical simulation of scouring around concrete bridge piers, Doctoral dissertation, MS thesis, Dept. Hydr. Eng., Islamic Azad Univ-South Tehran *Branch*.

Koken, M., Gogus, M. (2010). Effect of Abutment Length on the Bed Shear Stress and the Horseshoe Vortex System.

Asano, T. (1991). Two-phase flow model on oscillatory sheet-flow. In *Coastal Engineering*, **pp**, 2372-2384.

Li, L. (1995). Multi-phase model on sediment transport in sheet flow regime under oscillatory flow, *Coastal Eng. in Japan*, **38(2)**, 157-178.

Ali, K. H., Karim, O. A., O'Connor, B. A. (1997). Flow patterns around bridge piers and offshore structures, In *ASCE*.

Wu, W., Wang, S. S. (1999). Movable bed roughness in alluvial rivers, *Journal of Hydraulic Engineering*, **125(12)**, 1309-1312.

Dou, X. (1997). Numerical simulation of three-dimensional flow field and local scour at bridge crossings, Doctoral dissertation, University of Mississippi.

Jia, Y., Kitamura, T., Wang, S. S. (2001). Simulation of scour process in plunging pool of loose bed-material, *Journal of hydraulic engineering*, **127(3)**, 219-229.

Teklemariam, E., Korbaylo, B. W., Groeneveld, J. L., Fuchs, D. M. (2002). Computational fluid dynamics: Diverse applications in hydropower project's design and analysis, In Proceedings of the CWRA 55th Annual Conference, Winnipeg, **pp**, 11-14.

Kumcu, S. Y. (2016). Steady and unsteady pressure scour under bridges at clear-water conditions, *Canadian Journal of Civil Engineering*, **43(4)**, 334-342.

Sharifi, N., Amiri, B. M. (2014). The Comparative Impact of Recast and Prompt on EFL Learners' Autonomy and Motivation, *Procedia-Social and Behavioral Sciences*, **98**, 1754-1761.

Shahheydari, H., Nodoshan, E. J., Barati, R., Moghadam, M. A. (2015). Discharge coefficient and energy dissipation over stepped spillway under skimming flow regime, *KSCE Journal of Civil Engineering*, **19(4)**, 1174-1182.

Gacek, J. D. (2007). Numerical simulation of flow through a spillway and diversion structure, Doctoral dissertation, McGill University.

Tabbara, M., Chatila, J., Awwad, R. (2005). Computational simulation of flow over stepped spillways, *Computers and structures*, **83(27)**, 2215-2224.

An, S., Ku, H., Julien, P. Y. (2015). Numerical modelling of local scour caused by submerged jets, *Maejo International Journal of Science and Technology*, **9(3)**, 328.

Pati, V. V. R. (2010). CFD modeling and analysis of flow through culverts, Doctoral dissertation, Northern Illinois University.

Yakhot, V., Orszag, S. A. (1986). Renormalization-group analysis of turbulence, *Physical* review letters, **57(14)**, 17-22.

Anu, A. and Jennifer, G. D. (2011). Experimental study and numerical simulation of flow and sediment transport around a series of super dikes, PhD thesis, university of Arizona, Arizona, USA.

Hirt, C. W., Nichols, B. D. (1981). Volume of fluid (VOF) method for the dynamics of free boundaries, *Journal of computational physics*, **39(1)**, 201-225.

Abdulnaser A., Mustafa G. Hamid H. (2015). Investigating of local scour and Discharge Characteristics of Single Step Broad Crested Weir, (ICCESEN 2015), Antalya, Turkey.

Mueller, D. S., Wagner, C. R. (2002). Analysis of pier scour predictions and real-time field measurements, In First International Conference on Scour of Foundations.

Abdelaziz, S., Bui, M. D., Rutschmann, P. (2010). Numerical simulation of scour development due to submerged horizontal jet, In River Flow. Process of the International Conference on Fluvial Hydraulics, **pp**, 8-10.

Breusers, H. N. C., Raudkivi, A. J. (1991). Scouring, hydraulic structures design manual, *IAHR, AA Balkema, Rotterdam*.

Ruff, J. F., Abt, S. R., Mendoza, C., Shaikh, A., Kloberdanz, R. (1982). Scour at culvert outlets in mixed bed materials, **66(11)**,82-11.

Vasquez, J. A., Walsh, B. W. (2009). CFD simulation of local scour in complex piers under tidal flow, In *33rd IAHR Congress:* Water Engineering for a Sustainable Environment.

Zhang, H., Nakagawa, H., Kawaike, K., Yasuyuki, B. A. B. A. (2009). Experiment and simulation of turbulent flow in local scour around a spur dyke, *International Journal of Sediment Research*, **24(1)**, 33-45.

Jahangirzadeh, A., Basser, H., Akib, S., Karami, H., Naji, S., Shamshirband, S. (2014). Experimental and numerical investigation of the effect of different shapes of collars on the reduction of scour around a single bridge pier, *PloS one*, **9(6)**, 98-592.

Pagliara, S., Hassanabadi, L., Kurdistani, S. M. (2015). Clear water scour downstream of log deflectors in horizontal channels, *Journal of Irrigation and Drainage Engineering*, **141(9)**, 1401-5007.

APPENDICES

APPENDIX

Figures of two-dimensional affect vortex on scouring for both sediment bed materials

A. For US1B0

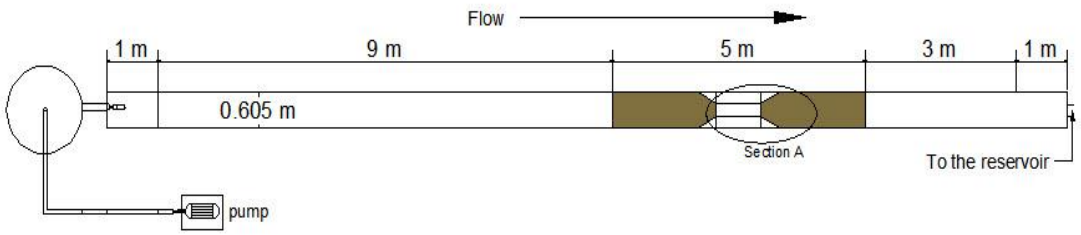

Section A:

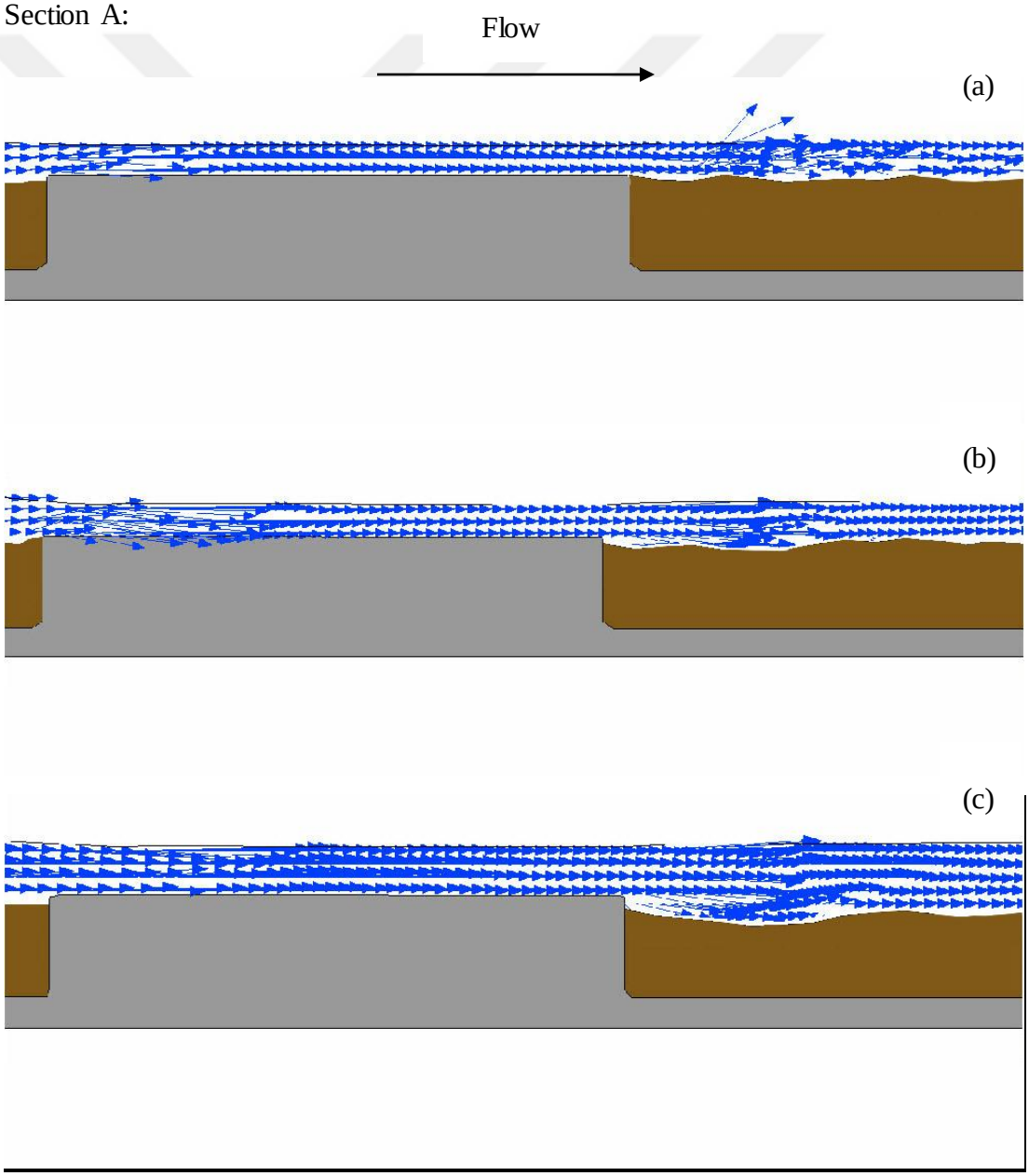

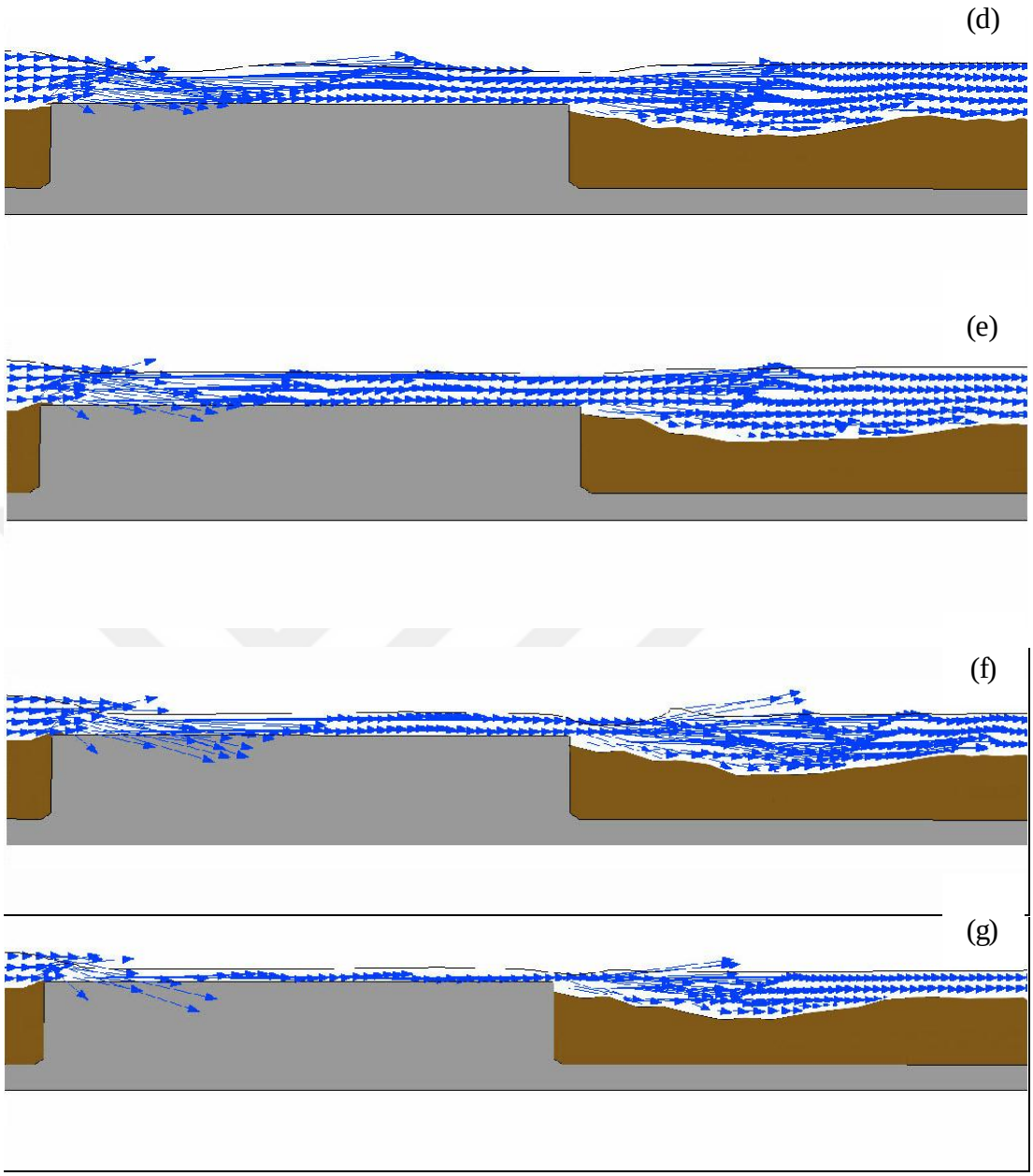

Figure A.1 Affect vortex on scouring for case USIB0: (a) Flow rate is 3 Lt/s at 10 munities (b) Flow rate is 6 Lt/s at 20 munities (c) Flow rate is 8 Lt/s at 30 munities (d) Flow rate is 10.4 Lt/s at 40 munities (e) Flow rate is 7.8 Lt/s at 50 munities (f) Flow rate is 5.9 Lt/s at 60 munities (g) Flow rate is 3.1 Lt/s at 70 munities

B. For US1B40

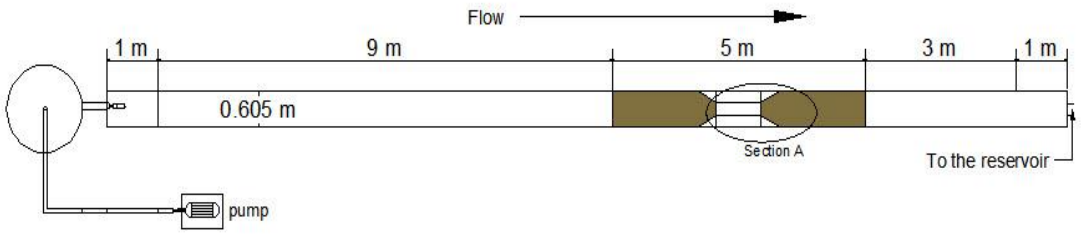

Section A:

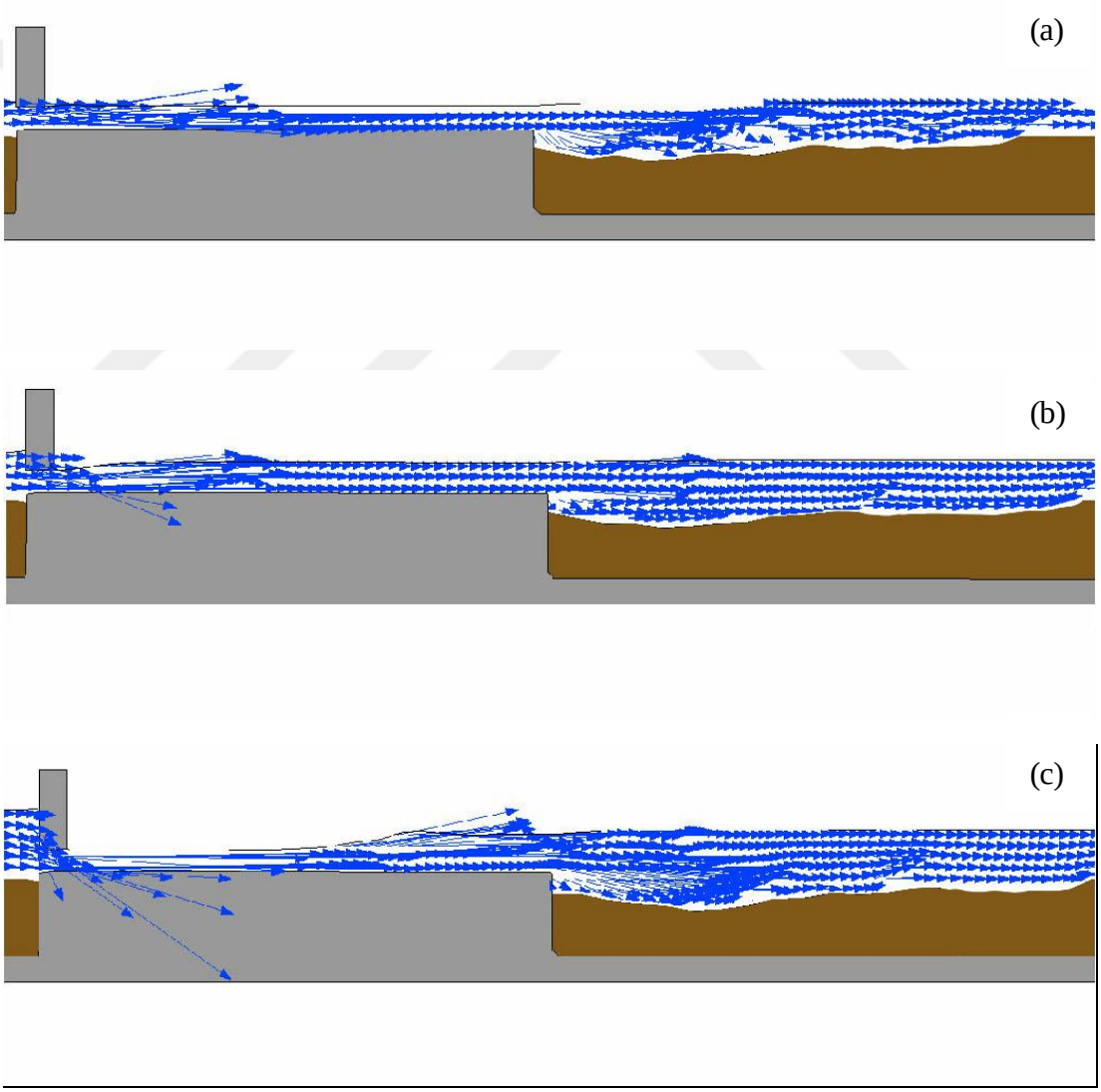

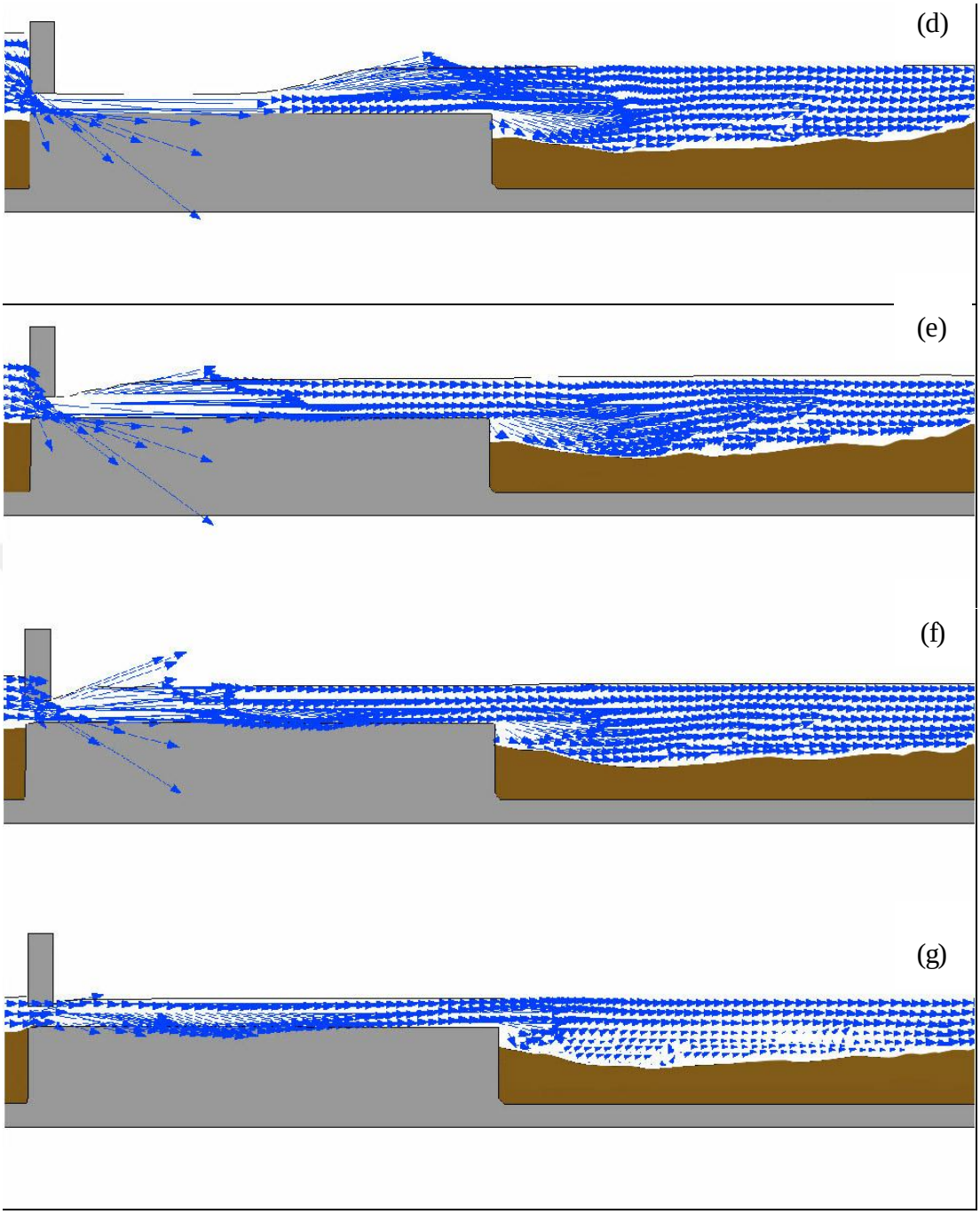

Figure B.1 Affect vortex on scouring for case USIB40: (a) Flow rate is 3 Lt/s at 10 munities (b) Flow rate is 6 Lt/s at 20 munities (c) Flow rate is 8 Lt/s at 30 munities (d) Flow rate is 10.4 Lt/s at 40 munities (e) Flow rate is 7.8 Lt/s at 50 munities (f) Flow rate is 5.9 Lt/s at 60 munities (g) Flow rate is 3.1 Lt/s at 70 munities

C. For US2B0

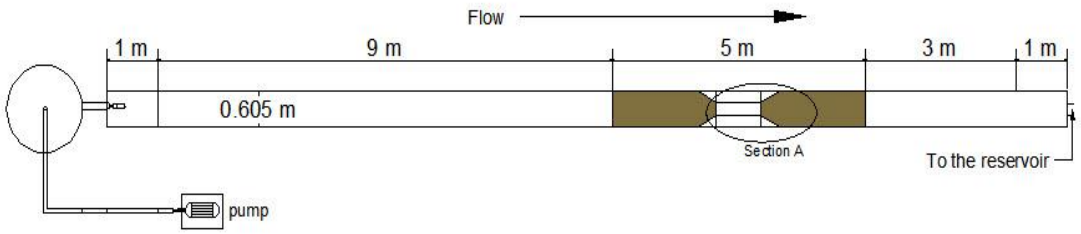

Section A:

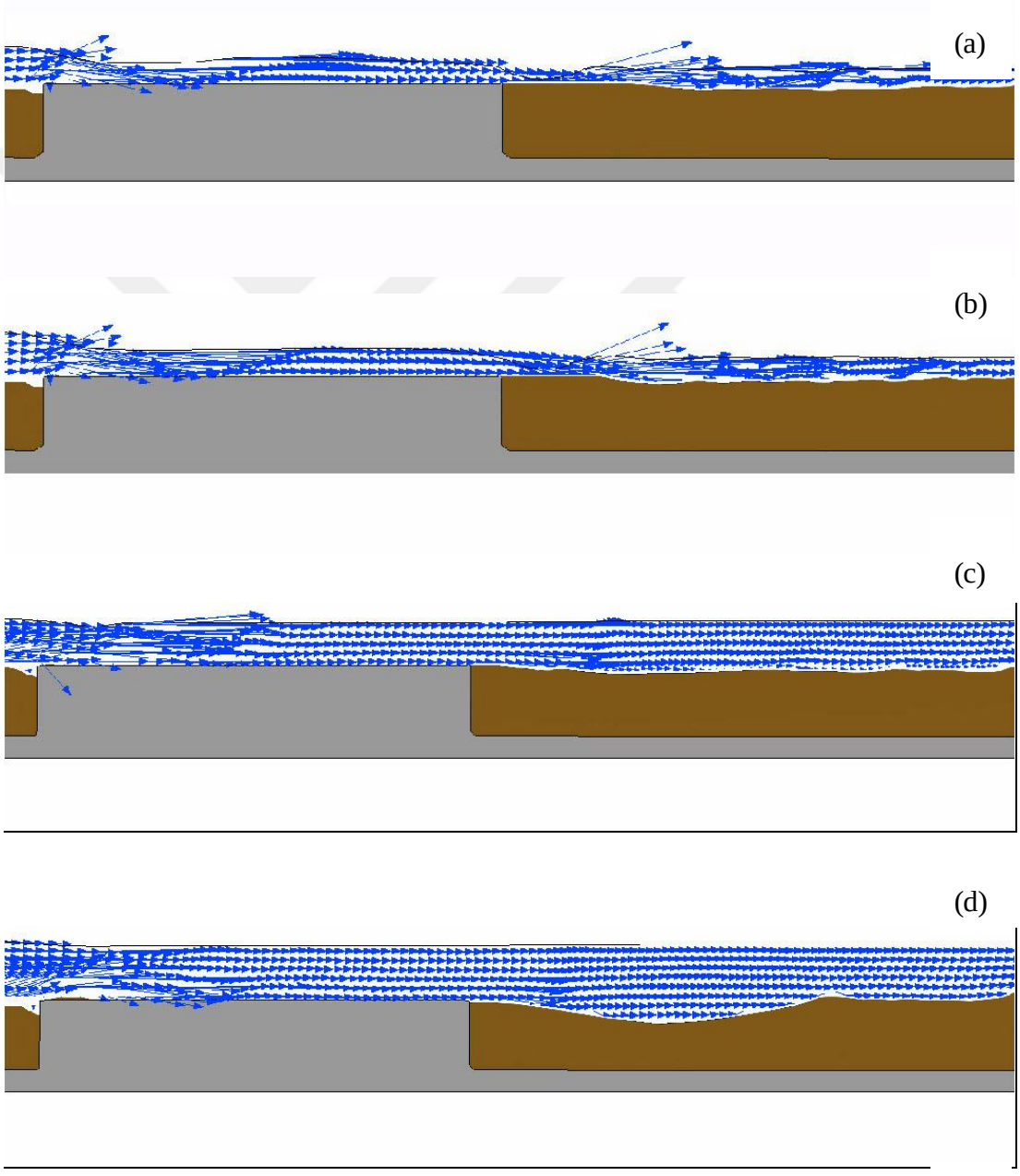

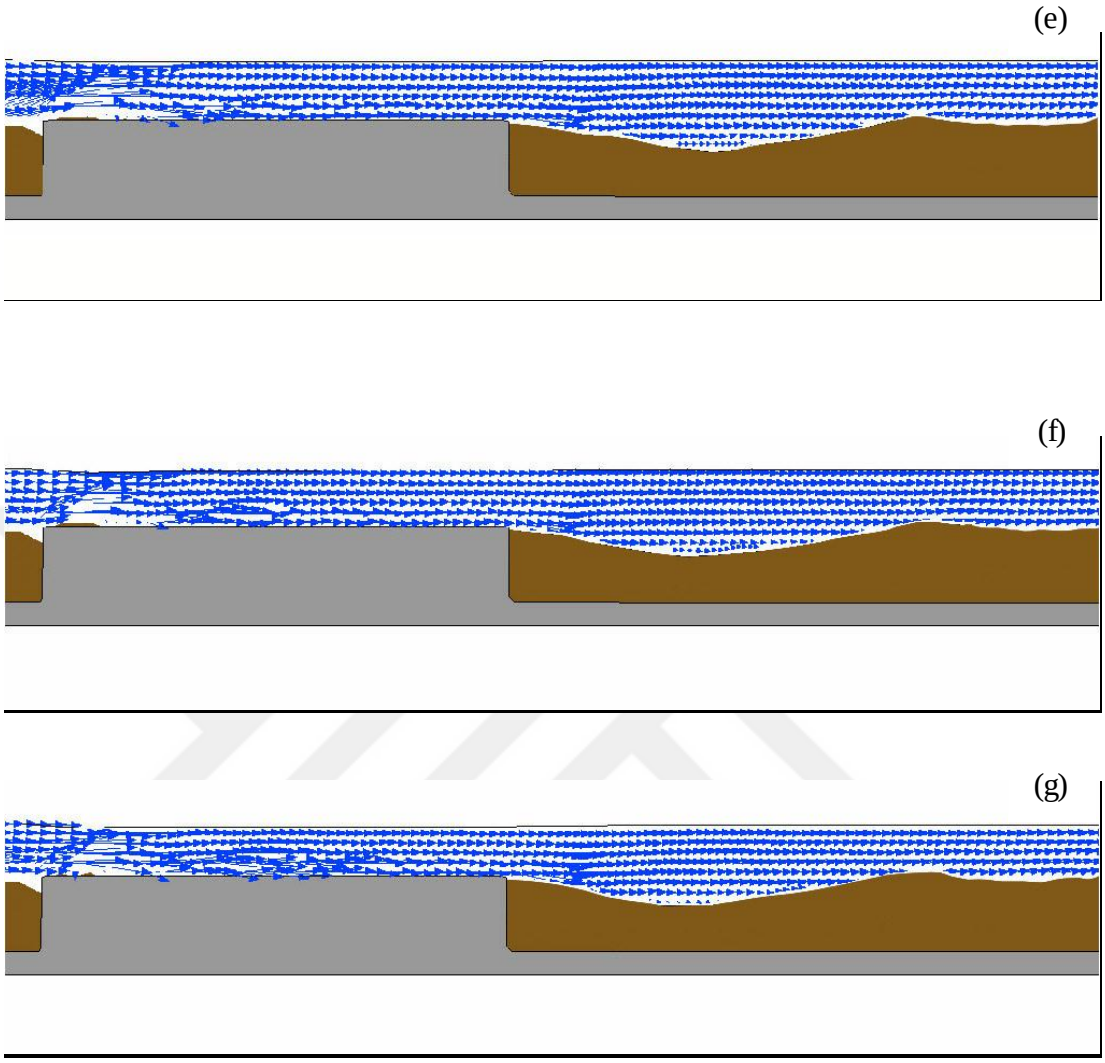

Figure C.1 Affect vortex on scouring for case US2B0: (a) Flow rate is 6.6 Lt/s at 15 munities (b) Flow rate is 8.8 Lt/s at 30 munities (c) Flow rate is 10.7 Lt/s at 45 munities (d) Flow rate is 12.8 Lt/s at 60 munities (e) Flow rate is 10.7 Lt/s at 75 munities (f) Flow rate is 8.8 Lt/s at 90 munities (g) Flow rate is 6.6 Lt/s at 105 munities

D. For US2B40

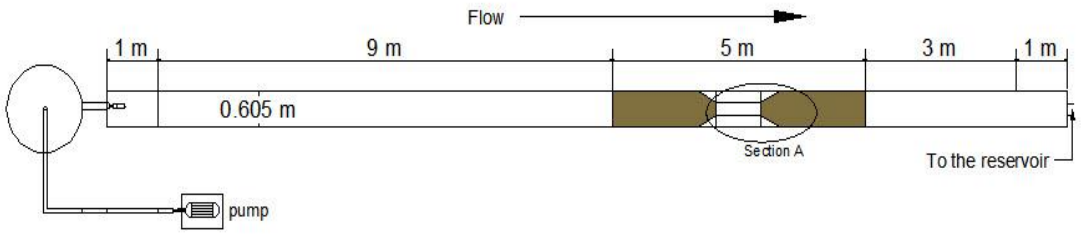

Section A:

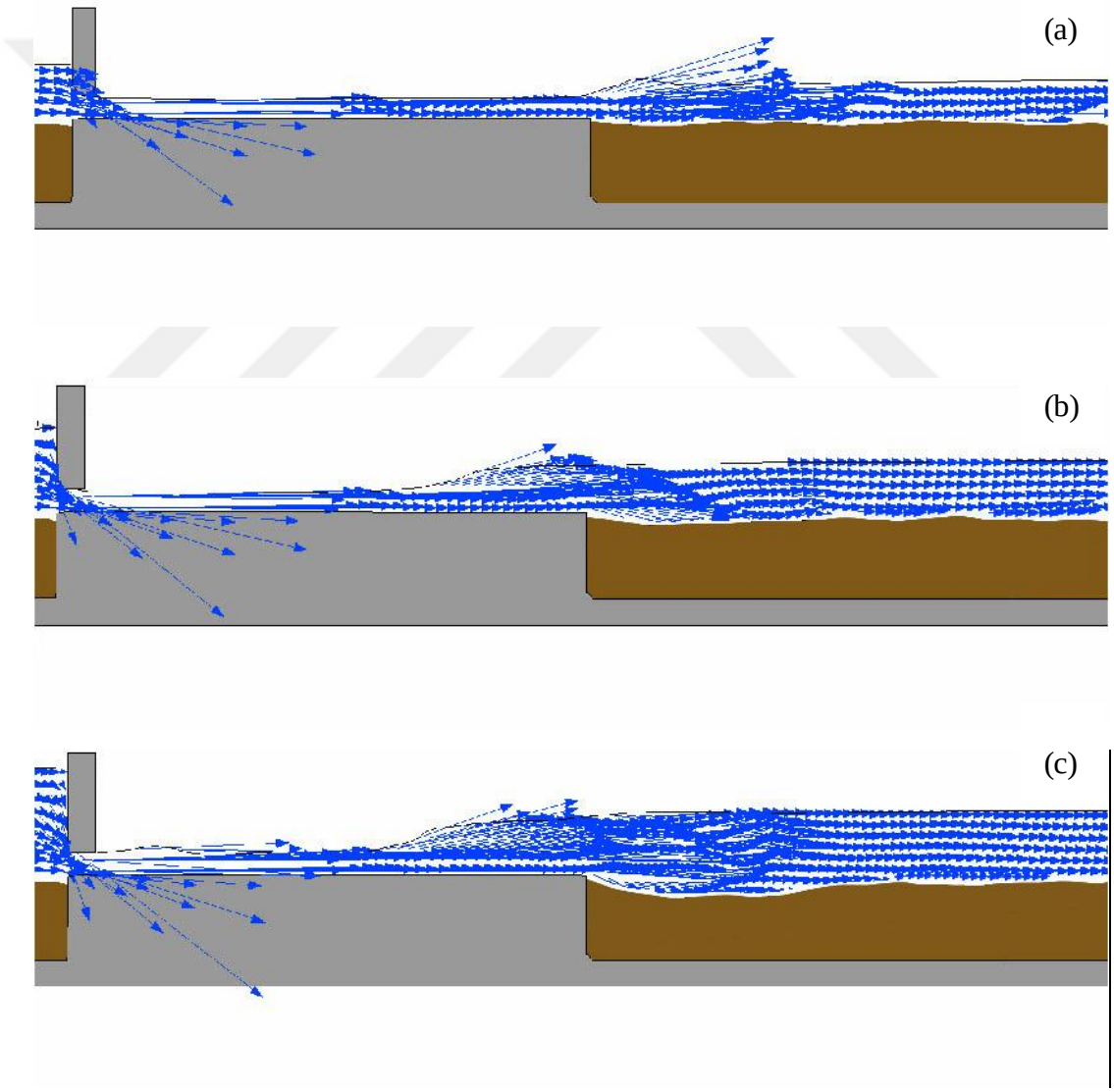

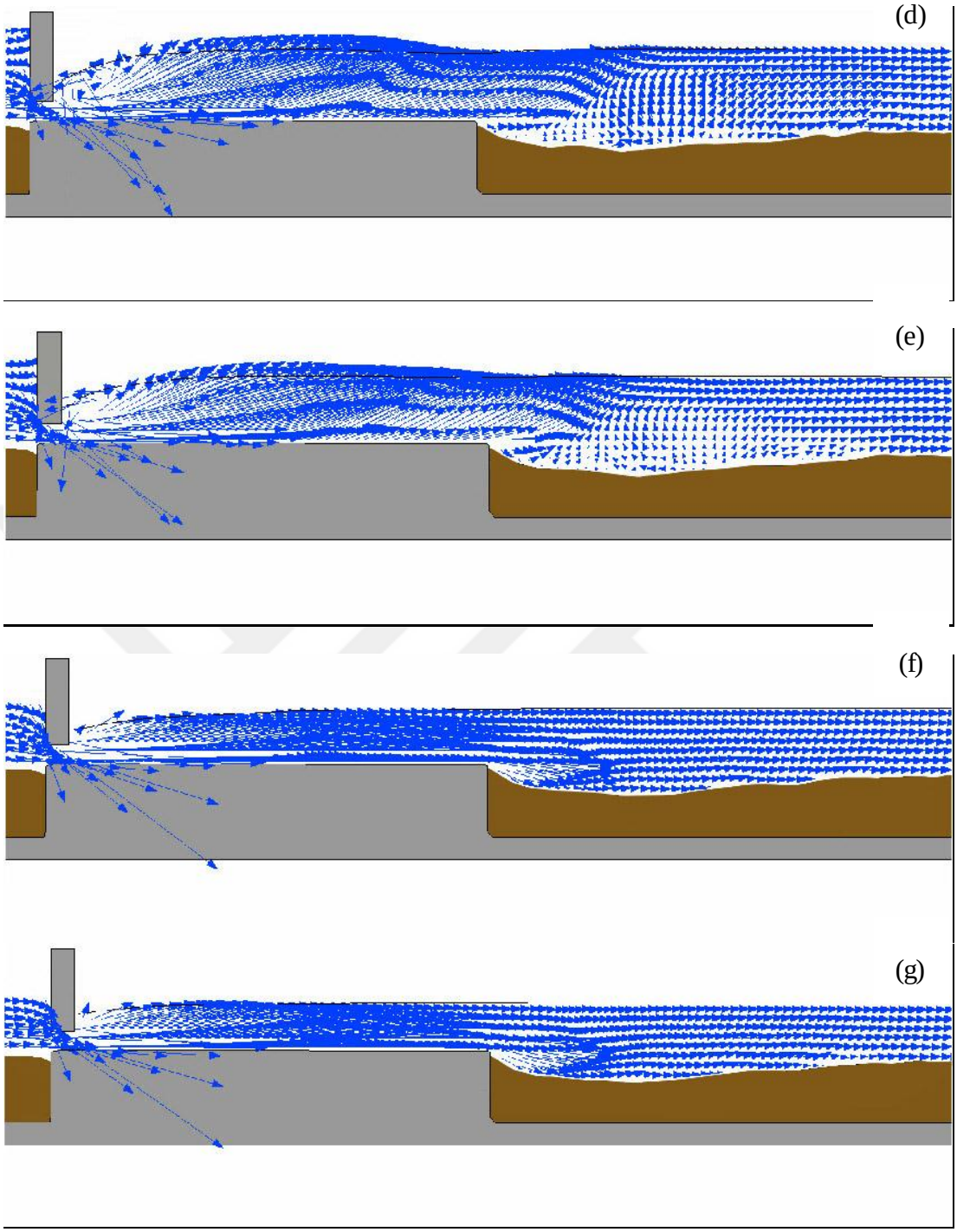

Figure D.1 Affect vortex on scouring for case US2B40: (a) Flow rate is 6.6 Lt/s at 15 munities (b) Flow rate is 8.8 Lt/s at 30 munities (c) Flow rate is 10.7 Lt/s at 45 munities (d) Flow rate is 12.8 Lt/s at 60 munities (e) Flow rate is 10.7 Lt/s at 75 munities (f) Flow rate is 8.8 Lt/s at 90 munities (g) Flow rate is 6.6 Lt/s at 105 munities

E. For US2B40 by using k-ε

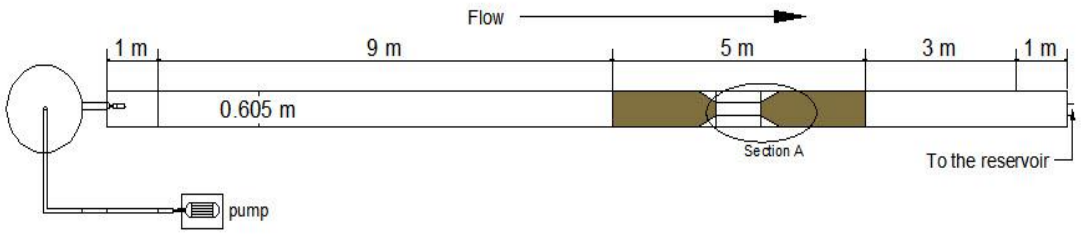

Section A:

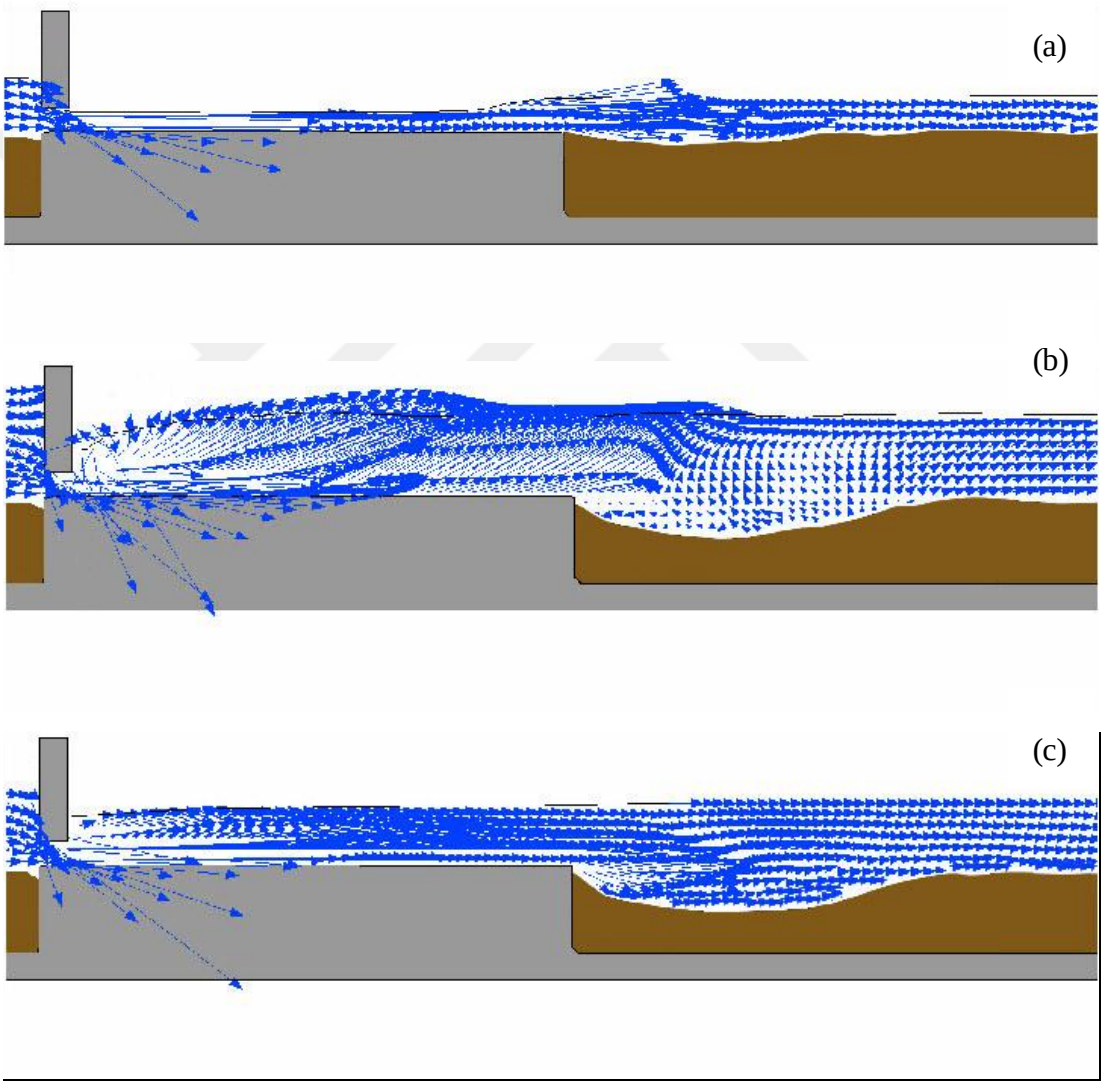

Figure E.1 Affect vortex on scouring for case US2B40 by using k-ε turbulent model: (a) Flow rate is 6.6 Lt/s at 15 munities (b) Flow rate is 12.8 Lt/s at 60 munities (c) Flow rate is 6.6 Lt/s at 105 munities

Figures of three-dimensional scour formation using CFD model for all cases

A. For US1B0

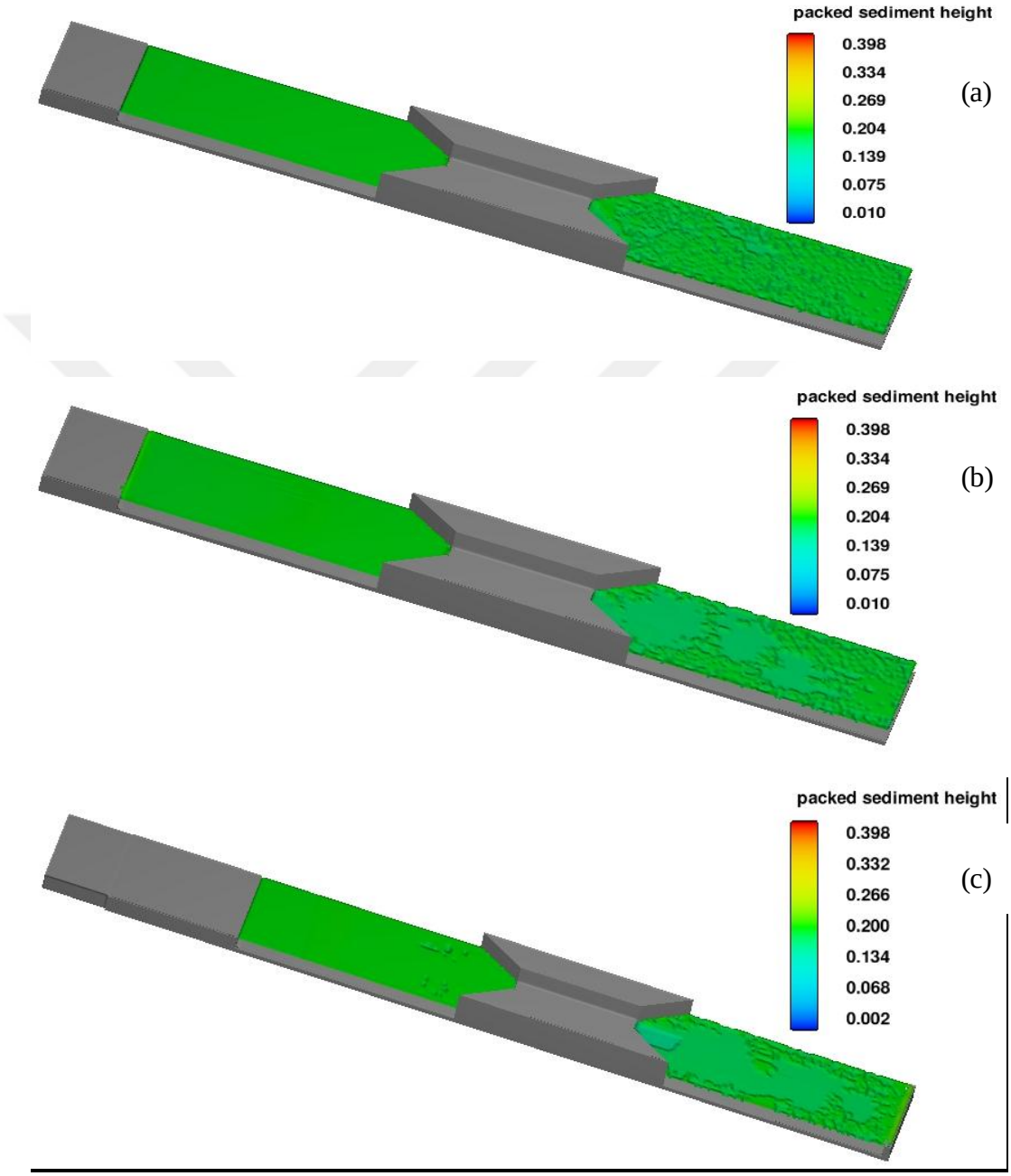

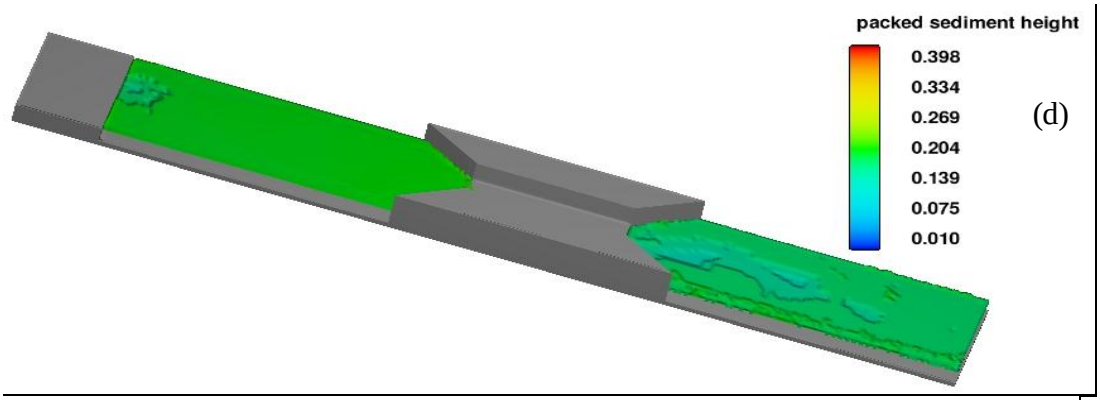
packed sediment height
0.398
0.334
0.269
0.204
0.139
0.075
0.010

(d)

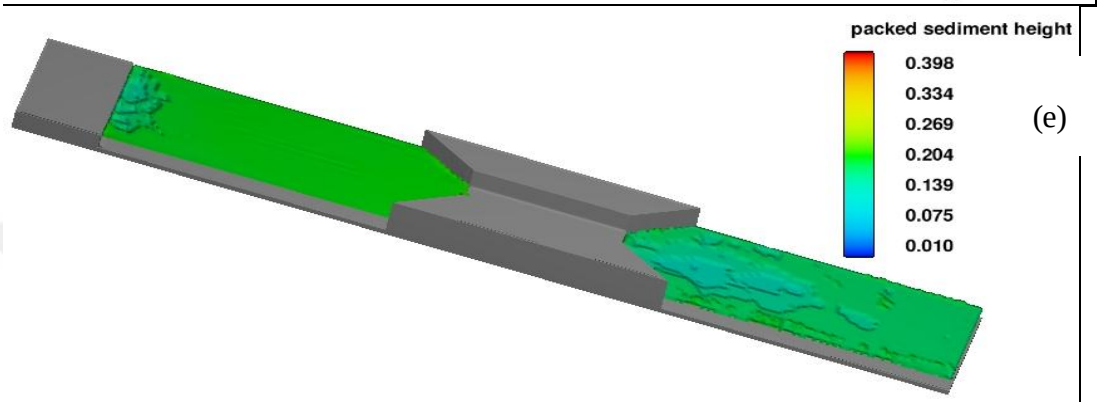
packed sediment height
0.398
0.334
0.269
0.204
0.139
0.075
0.010

(e)

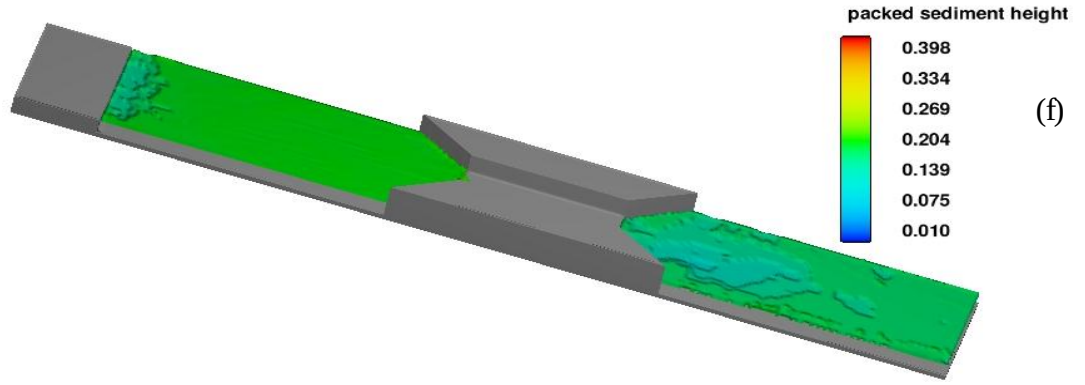
packed sediment height
0.398
0.334
0.269
0.204
0.139
0.075
0.010

(f)

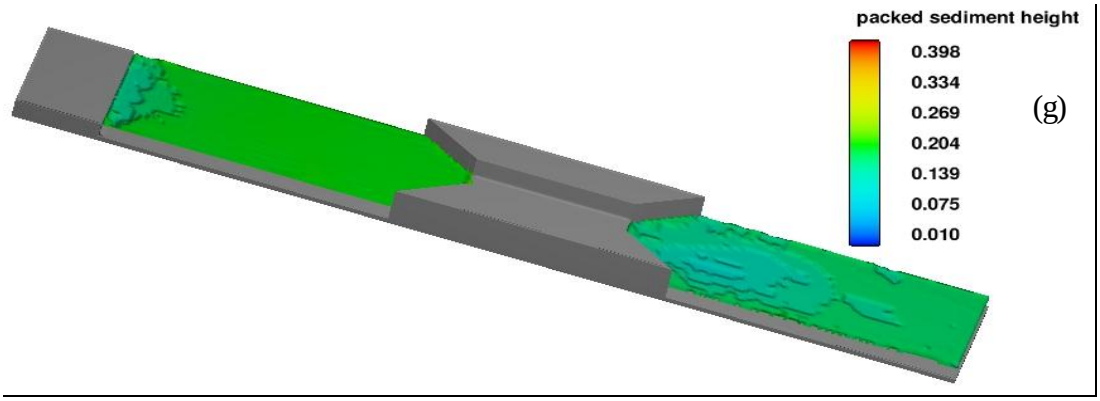
packed sediment height
0.398
0.334
0.269
0.204
0.139
0.075
0.010

(g)

Figure A.2 Scour formation using CFD model for case USIB0: (a) Flow rate is 3 Lt/s at 10 munities (b) Flow rate is 6 Lt/s at 20 munities (c) Flow rate is 8 Lt/s at 30 munities (d) Flow rate is 10.4 Lt/s at 40 munities (e) Flow rate is 7.8 Lt/s at 50 munities (f) Flow rate is 5.9 Lt/s at 60 munities (g) Flow rate is 3.1 Lt/s at 70 munities

B. For US1B40

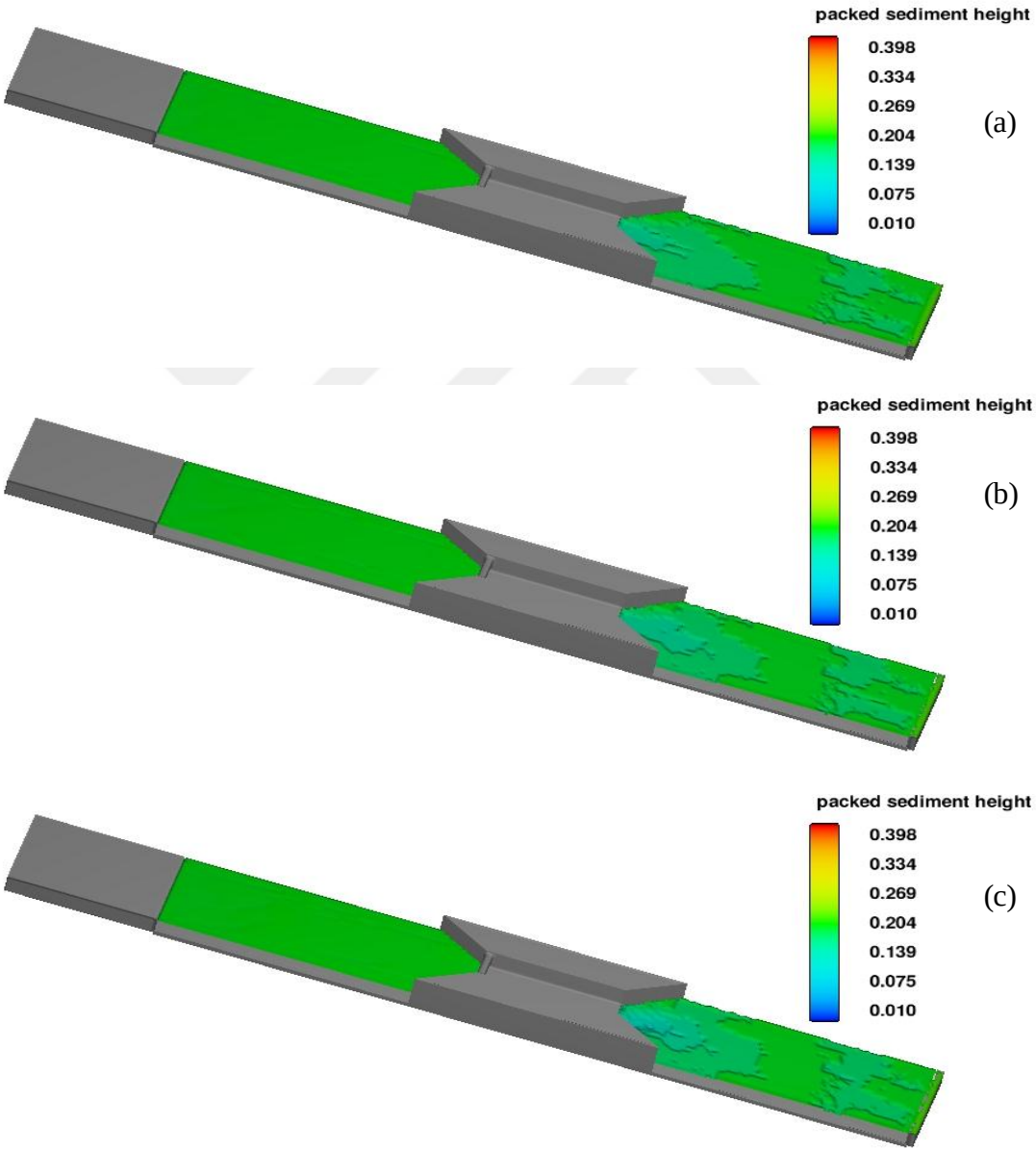

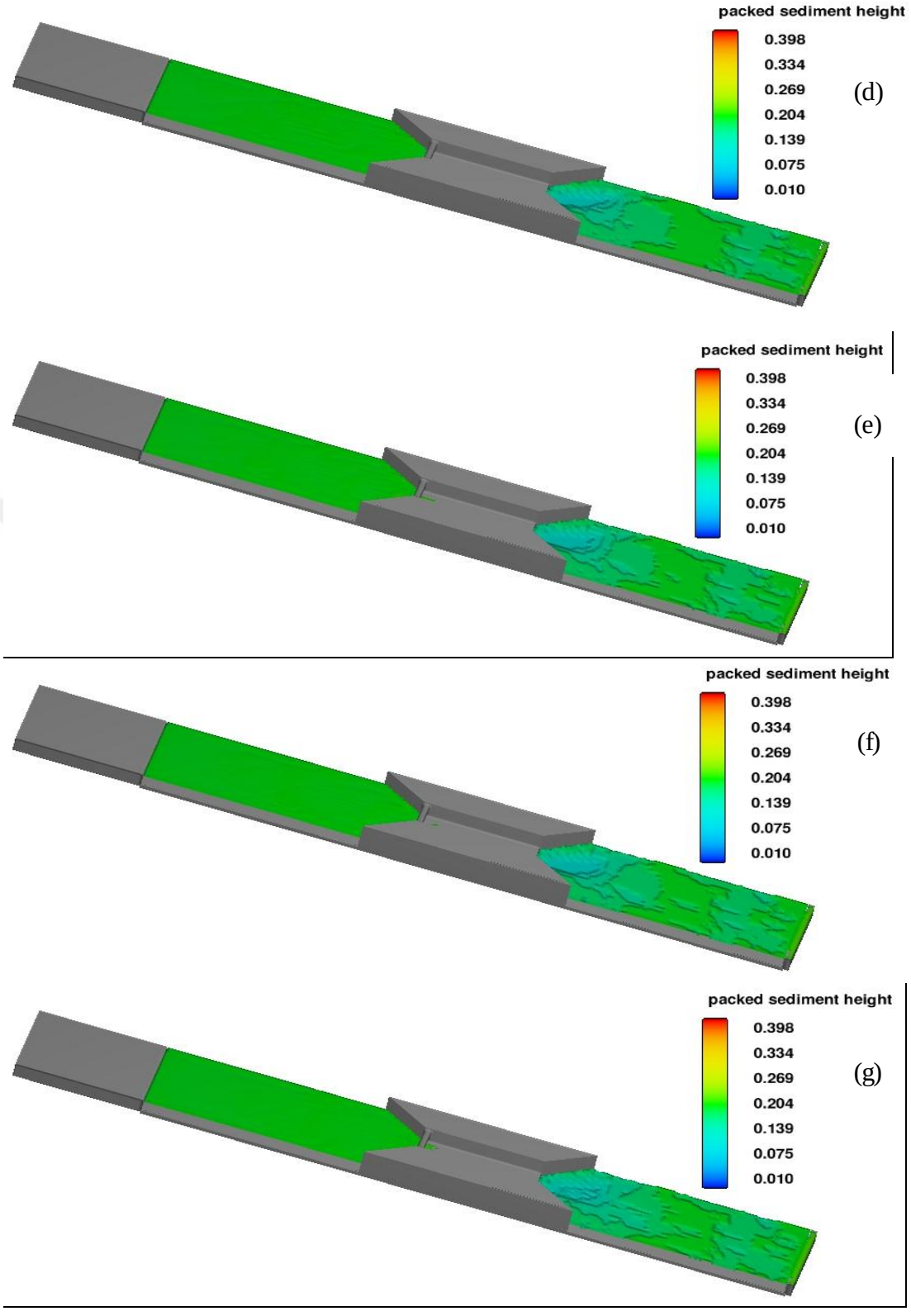

Figure B.2 Scour formation using CFD model for case USIB40: (a) Flow rate is 3 Lt/s at 10 munities (b) Flow rate is 6 Lt/s at 20 munities (c) Flow rate is 8 Lt/s at 30 munities (d) Flow rate is 10.4 Lt/s at 40 munities (e) Flow rate is 7.8 Lt/s at 50 munities (f) Flow rate is 5.9 Lt/s at 60 munities (g) Flow rate is 3.1 Lt/s at 70 munities

C. For US2B0

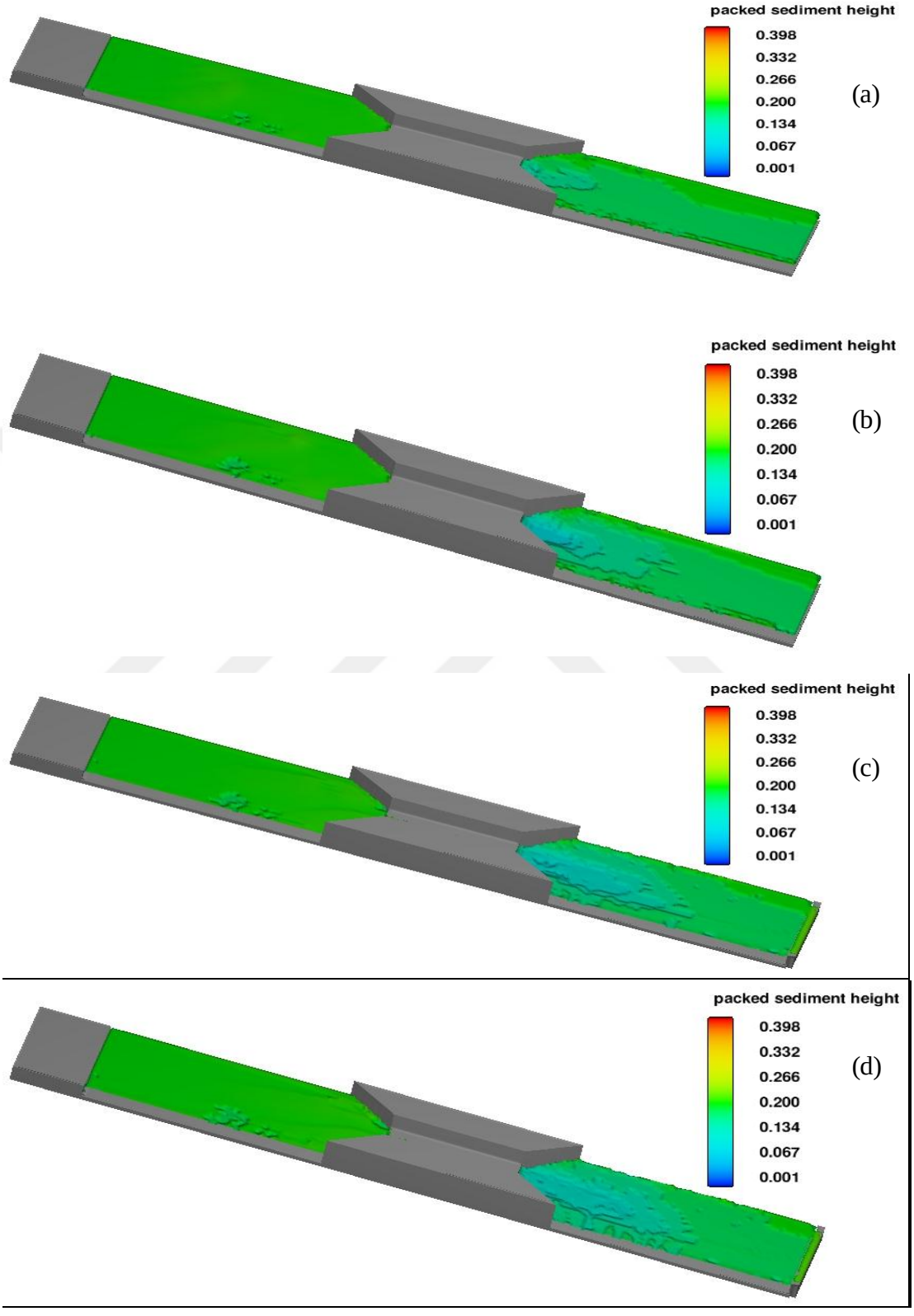
packed sediment height
0.398
0.332
0.266
0.200
0.134
0.067
0.001
(a)
packed sediment height
0.398
0.332
0.266
0.200
0.134
0.067
0.001
(b)
packed sediment height
0.398
0.332
0.266
0.200
0.134
0.067
0.001
(c)
packed sediment height
0.398
0.332
0.266
0.200
0.134
0.067
0.001
(d)

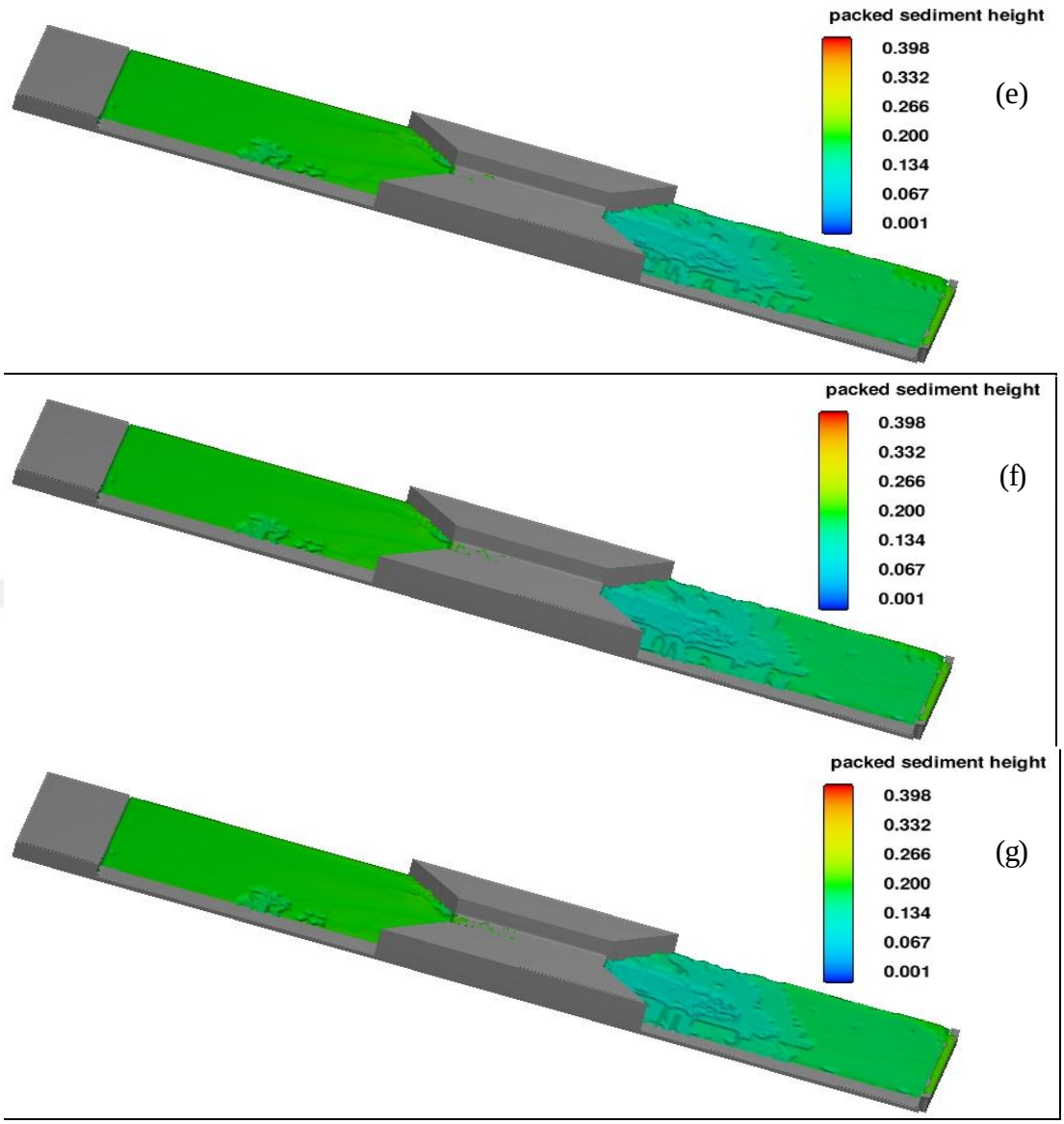

Figure C.2 Scour formation using CFD model for case US2B0: (a) Flow rate is 6.6 Lt/s at 15 munities (b) Flow rate is 8.8 Lt/s at 30 munities (c) Flow rate is 10.7 Lt/s at 45 munities (d) Flow rate is 12.8 Lt/s at 60 munities (e) Flow rate is 10.7 Lt/s at 75 munities (f) Flow rate is 8.8 Lt/s at 90 munities (g) Flow rate is 6.6 Lt/s at 105 munities

D. For US2B40

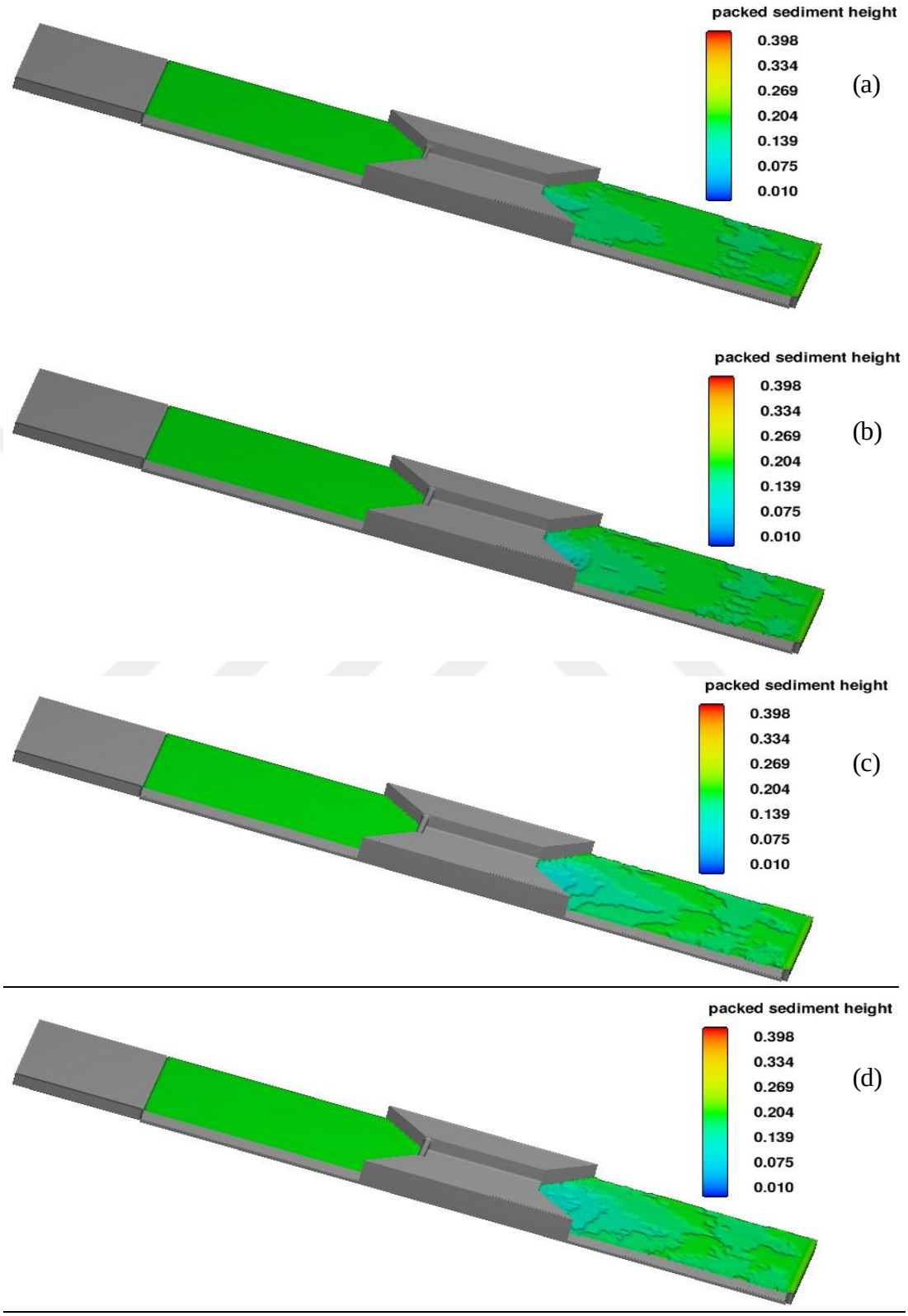
packed sediment height
0.398
0.334
0.269
0.204
0.139
0.075
0.010
(a)
packed sediment height
0.398
0.334
0.269
0.204
0.139
0.075
0.010
(b)
packed sediment height
0.398
0.334
0.269
0.204
0.139
0.075
0.010
(c)
packed sediment height
0.398
0.334
0.269
0.204
0.139
0.075
0.010
(d)

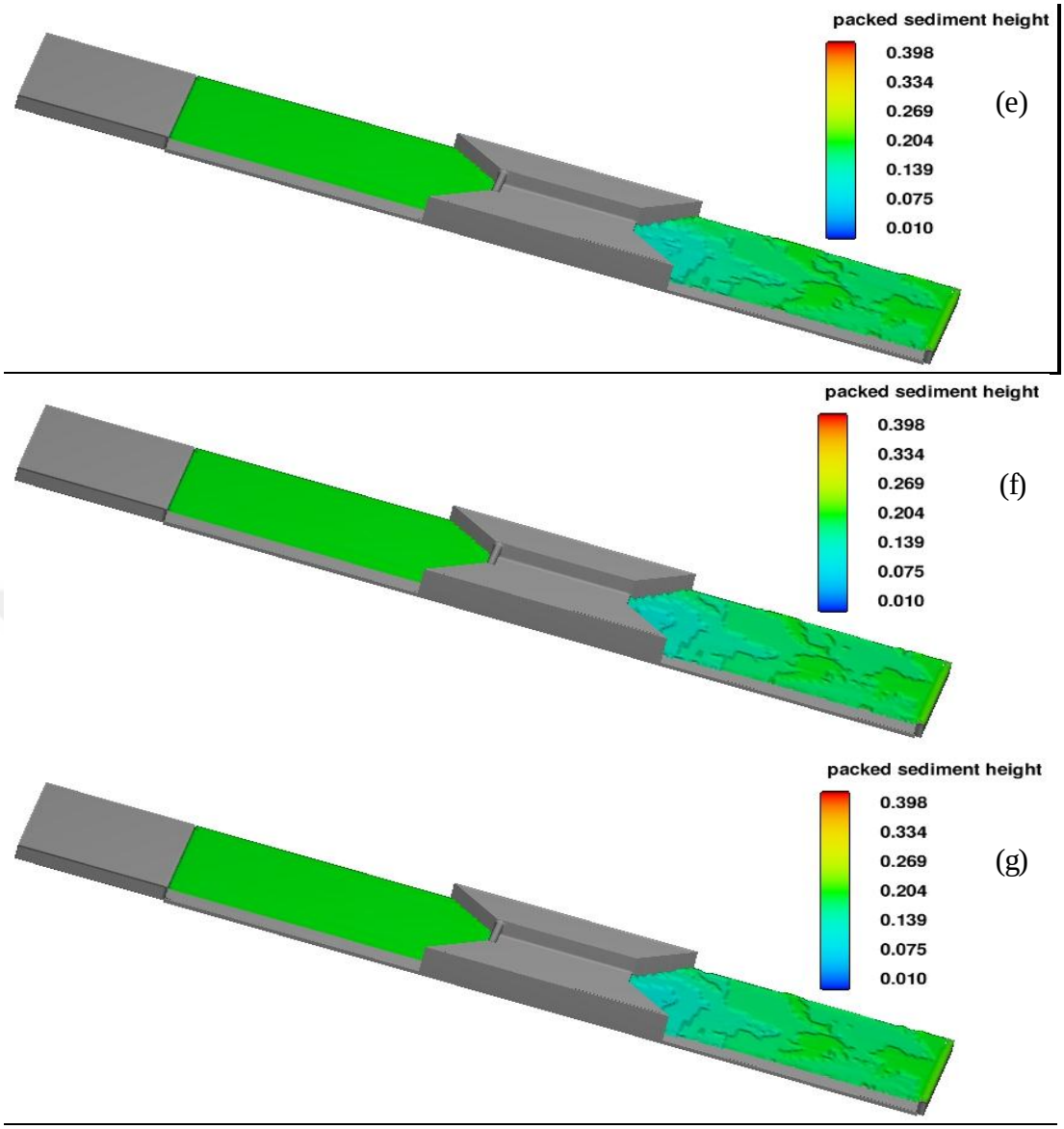

Figure D.2 Scour formation using CFD model for case US2B40: (a) Flow rate is 6.6 Lt/s at 15 munities (b) Flow rate is 8.8 Lt/s at 30 munities (c) Flow rate is 10.7 Lt/s at 45 munities (d) Flow rate is 12.8 Lt/s at 60 munities (e) Flow rate is 10.7 Lt/s at 75 munities (f) Flow rate is 8.8 Lt/s at 90 munities (g) Flow rate is 6.6 Lt/s at 105 munities

E. For US1B0 by using k-ε

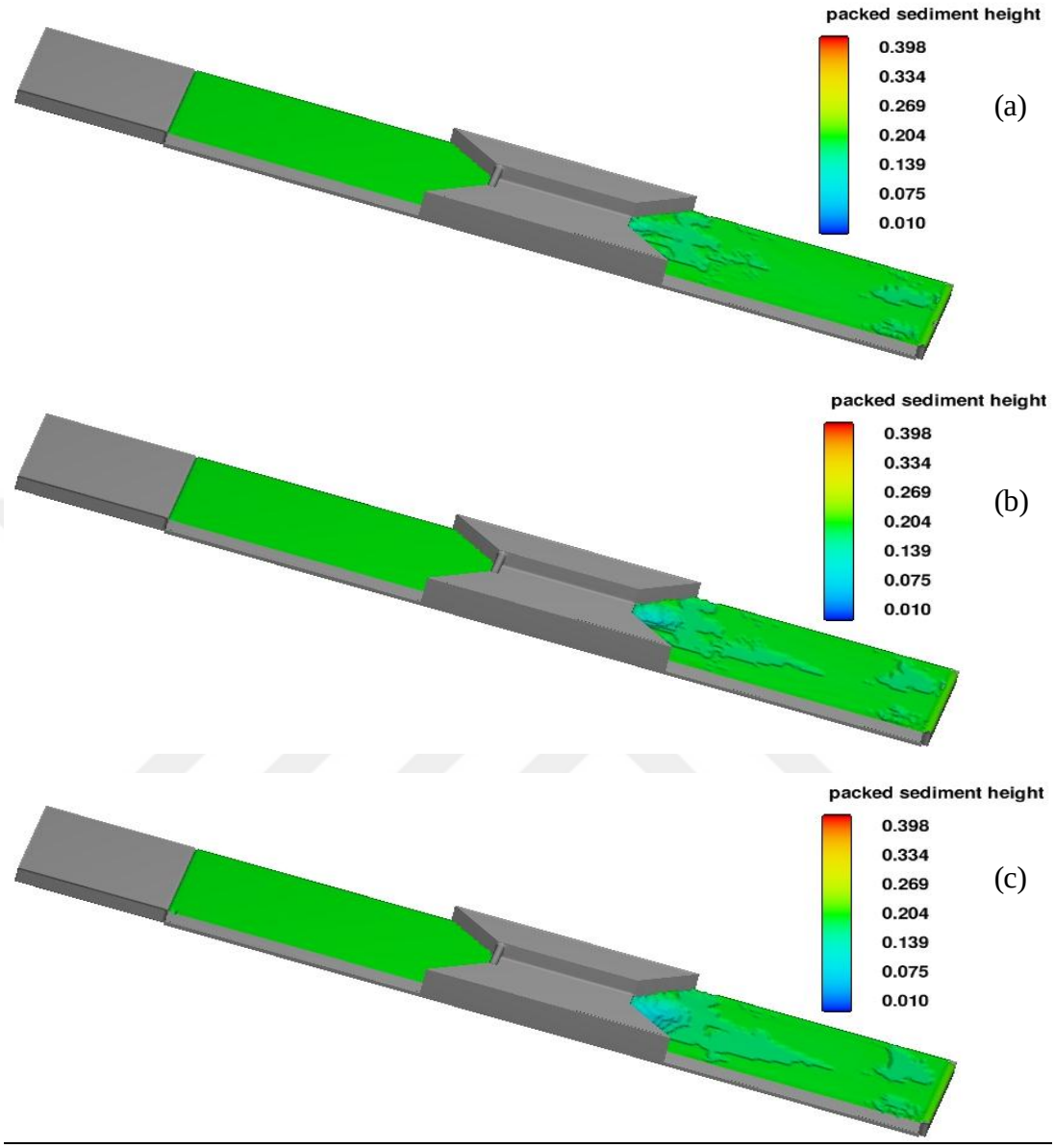

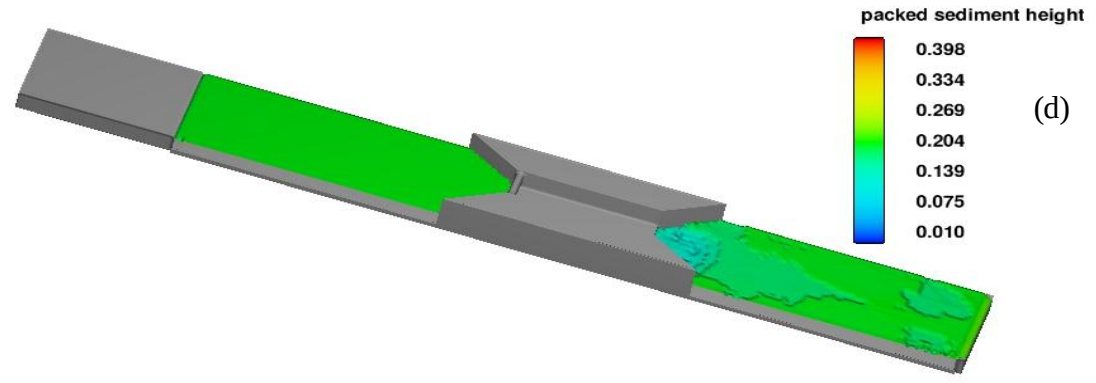

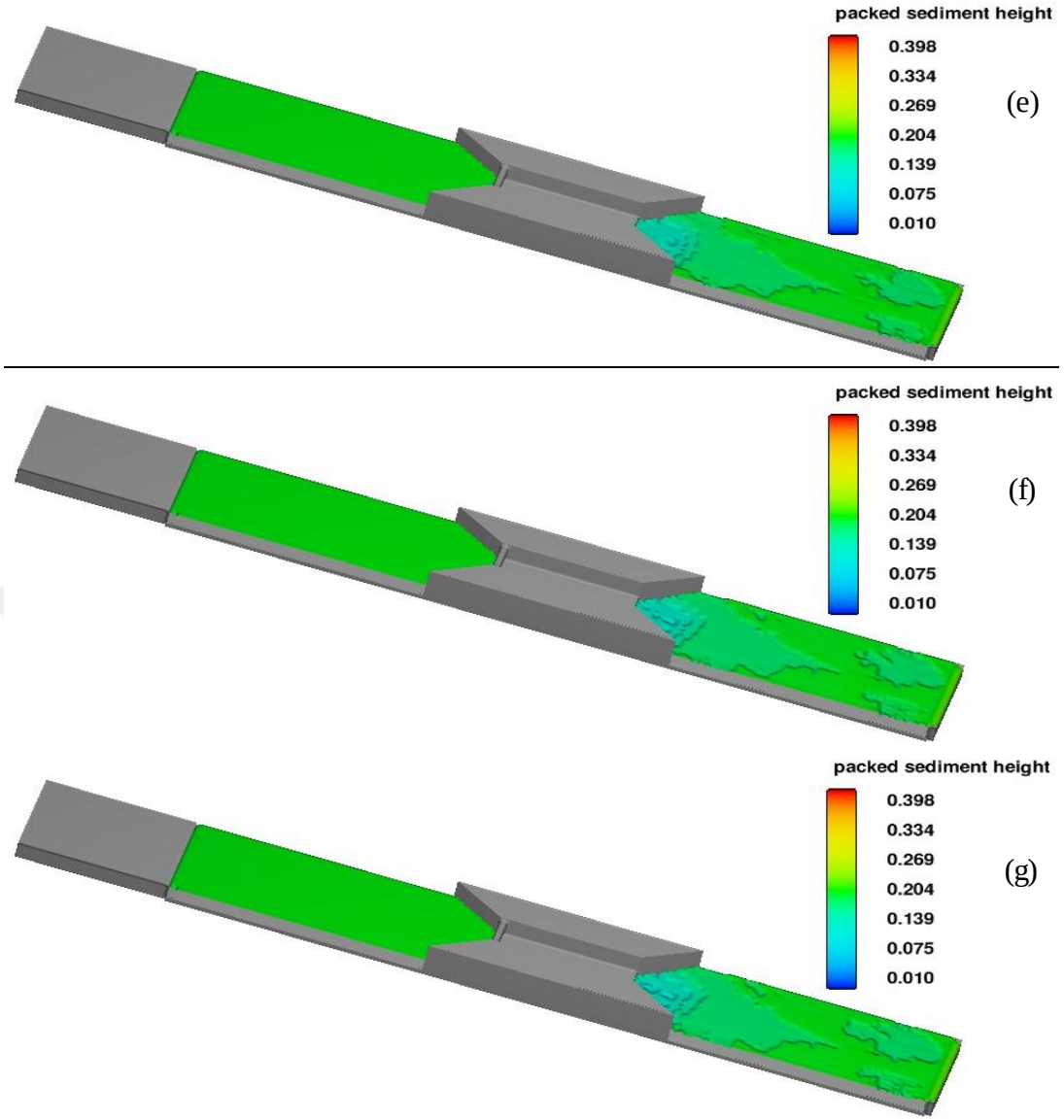

Figure E.2 Scour formation using CFD model for case US2B40: (a) Flow rate is 6.6 Lt/s at 15 munities (b) Flow rate is 8.8 Lt/s at 30 munities (c) Flow rate is 10.7 Lt/s at 45 munities (d) Flow rate is 12.8 Lt/s at 60 munities (e) Flow rate is 10.7 Lt/s at 75 munities (f) Flow rate is 8.8 Lt/s at 90 munities (g) Flow rate is 6.6 Lt/s at 105 munities